Fault sealing in the Krafla-Askja area south of Oseberg

Thomas Skålevik Foldnes

Master thesis in Geoscience

Geodynamics and Basin studies

Department of Earth Science

University of Bergen

June 2021

Abstract

Fault sealing is one of the key factors that control hydrocarbon accumulations. Faults in the subsurface can act as a conduit or a barrier to fluid flow and pressure communication. Understanding fault behavior is essential for hydrocarbon exploration, drilling, and development. There have been multiple studies with well-established workflows for carrying out a fault seal analysis based on clay content. The world is and will be dependent on oil and gas in years to come. With the rapidly growing climate problem, knowledge about fault sealing is crucial for carbon capture and storage (CCS). Fault plane maps, together with a horizon map and pressure data, are helpful when working on fault sealing, giving a three-dimensional view of fluid migration and trapping. The Krafla-Askja area consists of relatively new discoveries, with the first well drilled at Krafla in 2011 and Askja in 2013. Cross-fault spill points generally define the limit for hydrocarbon column heights. However, hydrocarbon columns which reach deeper than the spill points are common in the Krafla-Askja area.

This study aimed to investigate the geological constraints of fluids within the sands in the Brent Group in the Krafla-Askja area in the northern North Sea. A regional seismic interpretation of the Viking and Brent Groups was created based on 3D seismic data and published data from exploration wells. Detailed interpretation of 13 faults was conducted to map sand-sand juxtapositions along the faults, with a total of 77 juxtapositions being observed between Tarbert and Ness sands. Shale gouge ratio and across fault pressure differences in the juxtaposed areas were used with the intent to understand why these sets of structures behave in the way they do.

The Krafla-Askja area is heavily faulted with the structures being compartmentalized, varying in lateral communication. Migration routes are suggested to be closed with 13 faults working as fluid barriers. One fault north of Slemmestad, however, might be partially open in the water phase. Clay smear and seal by juxtaposition are suggested to be the main reason for sealing in the Krafla-Askja area. Five structures containing hydrocarbon are situated shallower than the oil and gas windows for the Draupne and Heather Formations suggesting that hydrocarbon migration has previously occurred in the area. WNW-ESE and E-W oriented faults perpendicular to the Viking Graben are critically stressed in the present-day stress field and are thought to be reactivated more recently, resulting in a lower across fault pressure difference.

Acknowledgments

The study is a part of my MSc degree in Geodynamics and Basin Studies at the Department of Earth Science at the University of Bergen and was made possible with guidance and feedback from several contributors.

First and foremost, I would like to thank my supervisor, Christian Hermanrud, for his help and guidance during this study and for setting up regular meetings, both with and without the PESTOH group. I would like to thank everyone in the PESTOH group: Aleksejs Fjodorovs and Amalie Sande Rødde for valuable discussions and feedback, and Philipp Müller for valuable discussions, feedback, and for helping me when I was struggling with Petrel.

I want to thank CGG Services AS and Equinor ASA for providing the seismic and well data necessary to complete this study and Leo Zijerveld for giving me remote access to the computer at the university so I could work on my dataset from home during the Covid-19 pandemic.

I want to express my gratitude to my fellow geology students, especially Mikail Farooqui, Vegard Solheim, Sebastian Aasheim, Nikolai Kvellestad, Jacob Sørli, and Erlend Godø, for all the great memories at the university, field trips, and other social gatherings during these five swift years.

I want to thank my family and friends for their support and encouragement through the years.

Finally, I want to thank Laura Då for proofreading the thesis and for being supportive and uplifting throughout the pandemic.

Thank you!

Bergen,

Thomas Skålevik Foldnes May 2021

Table of content

Chapter 1 - Introduction

Hydrocarbon exploration has taken place in the northern North Sea for several decades and is today regarded as a highly mature area. The typical hydrocarbon trap in the North Sea is tilted fault blocks with at least one fault sealing the hydrocarbon column. Faults can act as pressure barriers to subsurface fluids during the production of a field or as differential migration barriers to hydrocarbon over geological time. The probability of future discoveries of big hydrocarbon fields is unlikely, with the most apparent traps already drilled. However, better seismic resolution of the subsurface has allowed for interpretation of more complex geological structures resulting in discoveries of smaller structures. With hydrocarbons becoming harder to find and more expensive to extract, an understanding of the probability of faults acting as a migration barrier is therefore crucial for future exploration of smaller hydrocarbon traps. Many structures on the Norwegian Continental Shelf are filled to their structural spill point, but underfilled and overfilled traps do occur. Overfilled traps can be explained by fault sealing, while the dry and underfilled traps may result from limited charge or leakage. Understanding geological constraints on hydrocarbon columns are important for evaluating the remaining resources on the Norwegian Continental Shelf.

The geological constraints on the position of hydrocarbon-water contacts have lately gained traction with the attention to better estimate in-place hydrocarbon volumes and predict paleo and present-day migration. General knowledge of hydrocarbon trapping mechanisms has been available for a long time. A widely accepted model for realistic secondary migration is the “fill-spill” model by Gussow (1954). The spill point is the structurally deepest point in a trap that can hold hydrocarbons. Additional volumes would cause up-dip migration from the filled traps (Gussow, 1954). The shallowest spill point along a fault is the shallowest sand-sand juxtaposition. A structure is underfilled when the fluid contact is situated shallower than the spill point and overfilled when the hydrocarbon column reaches deeper than the spill point. When the column reaches deeper than the spill point, it could be due to the fault being open with hydrocarbon accumulating on both sides of the fault, or the fault is sealing the hydrocarbon column. Juxtaposition, clay smear, cataclasis, and diagenesis are some of the mechanisms that can lead to fault sealing and overfilled structures (Watts, 1987; Fristad et al., 1997; Yielding et al., 1997; Yielding, 2002; Færseth, 2006; Yielding et al., 2010).

The study area is located in block 30/11 on the Fensal Sub-basin near the Viking Graben in the west between the Oseberg Sør field to the northeast and the Frigg field to the southwest (Figure 1.1). NNE-SSW-striking normal faults parallel to the Viking Graben and ESE-WNW-striking normal faults perpendicular to the Viking Graben dominates the study area. Small scale rotated fault blocks, and a horst structure at Krafla make up the area's structures. The area generally shallows towards the northeast and Oseberg, and eastwards towards the Horda Platform (Figure 1.2 & 1.3). There are 11 structures containing hydrocarbons in one to three reservoir segments. The main reservoir is the sands in the Middle Jurassic Brent Group being the channel sand deposits within the upper and lower Ness Formation and the transgressive marine sands in the Tarbert Formation. The structures are charged by source rocks in the Draupne and Heather Formations, which also make up the Brent Group's top seal. The structures are overpressured, with hydrocarbons reaching deeper than the spill points.

Borge (2000) suggests that quartz cementation is the leading cause for overpressure generation in fault-bounded Jurassic reservoirs in the northern Viking Graben and that reduced overpressure and leakage from pressure compartments was due to hydraulic fracturing of cap rocks. More recent studies have shown that leakage is often caused by reactivation of faults due to stress changes (Wiprut & Zoback, 2002; Teige et al., 2002; Bolås & Hermanrud, 2003; Bolås et al., 2005). Evaluation of structural characteristics and current stress state is necessary to assess different leakage mechanisms.

This study aimed to investigate geological constraints of hydrocarbon column-heights and fault sealing of the Middle Jurassic Brent Group in the Krafla-Askja area. Sand-sand juxtapositions, fluid contacts, pressure regimes, and shale gouge ratio has been mapped in an attempt to get an understanding of how the structures behave the way they do.

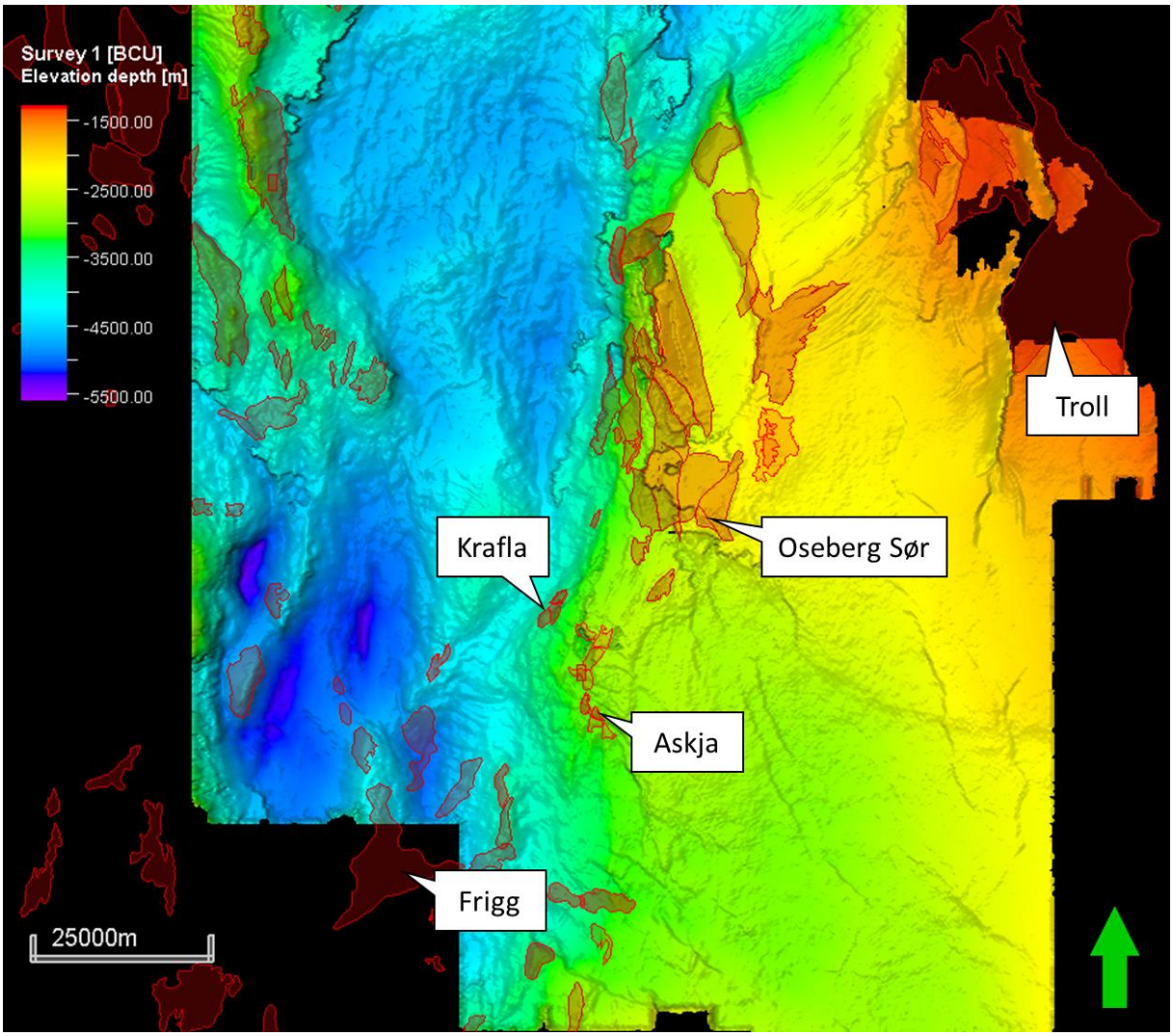

Figure 1.1: Rough interpretation of the Base Cretaceous Unconformity (BCU) in the northern North Sea. Fields and discoveries in the surrounding area are represented by a transparent red color superimposed on the BCU.

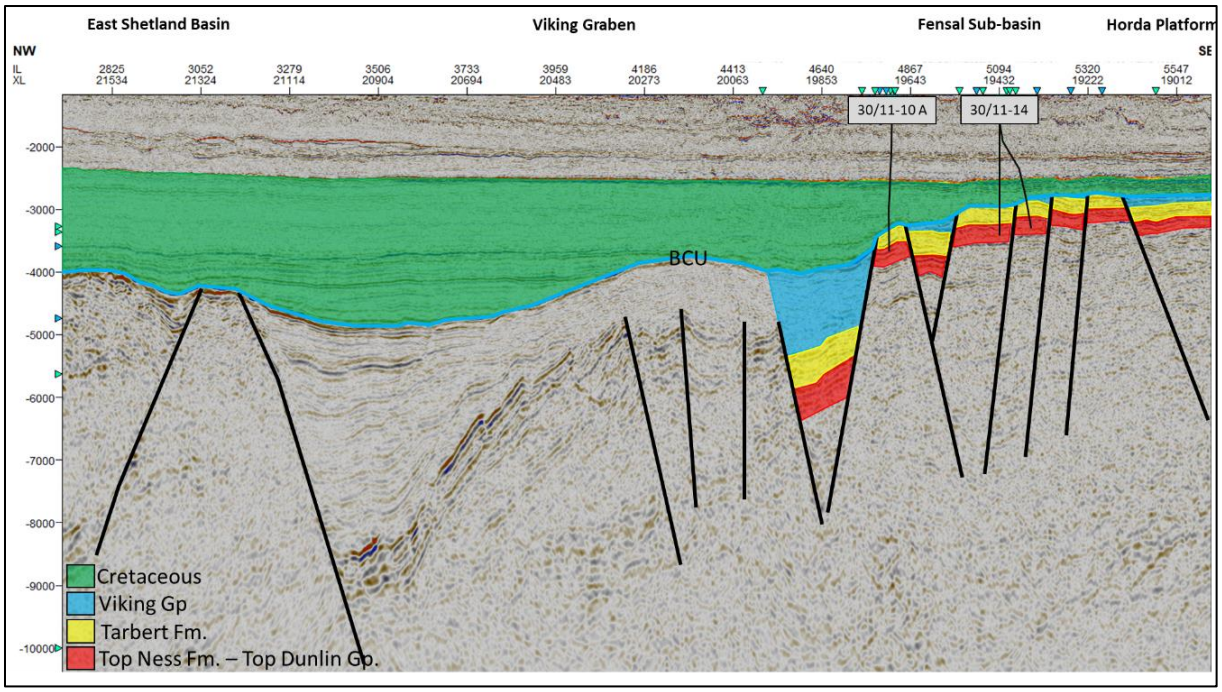

Figure 1.2: NW-SE cross-section of the study area and the Viking Graben showing the Krafla Main horst next to the Viking Graben to the west. The area east of the Krafla area consists of westwards dipping normal faults with the easternmost fault dipping towards the east. Formations in the Viking Graben and East Shetland Basin are not interpreted.

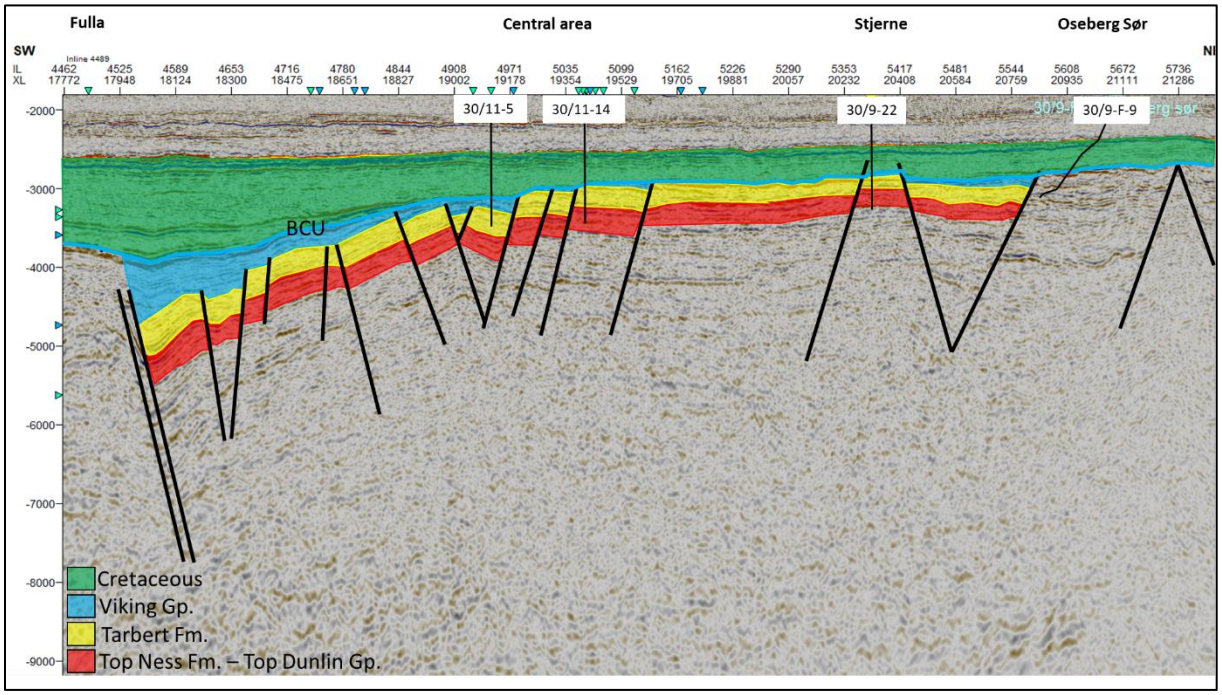

Figure 1.3: SW-NE cross-section of the study area showing a shallowing towards Stjerne and Oseberg Sør. The reservoir blocks are northward dipping normal faults. Formations in Oseberg Sør are not interpreted.

Chapter 2 - Theoretical Background

This chapter provides a brief overview of the definitions and terminology used in this study. The topics described are relevant in the discussion of hydrocarbon migration, geological constraints, and fault reactivation.

2.1 Hydrocarbon generation, migration, and accumulation

Hydrocarbons are generated from organically rich fine-grained source rocks and accumulated and trapped in reservoir rocks with relatively higher permeability and porosity. A typical petroleum system consists of a mature source rock, a porous and permeable reservoir rock, an impermeable cap rock, and a migration pathway.

2.1.1 Hydrocarbon generation

Several factors need to take place to generate hydrocarbon. Hydrocarbons occur when sedimentary rocks with enough organic matter are buried and heated. The organic-rich Draupne Formation is the primary source rock in the northern North Sea, earlier known as the Kimmeridge clay Formation. The Draupne Formation is rated as an excellent oil source rock, generating gas at high maturity levels. Gas can form from Heather Formation mudstones and Brent Formation coals, and vitrinite rich mudstones. However, the volumes of generated hydrocarbons are small compared to the Draupne Formation and are usually ignored (Goff, 1983). According to Goff (1983), the Draupne Formation is at oil floor maturity below 4 500 m, where oil peak generation began 70-80 and 55-65 Ma ago. The Formation went through peak generation 40 Ma ago and cracking of oil into gas began. Peak dry gas generation from Brent coals occurred below 5 000 m and began 40 Ma ago (Goff, 1983). Calculations from Moretti and Deacon (1995) suggest that the present-day maturity of the northern North Sea source rocks enters the gas window at ~4 000 m depth and the oil window at ~3 100 m depth.

2.1.2 Hydrocarbon migration

The movement of hydrocarbons from the source rock to a reservoir is called migration. This migration can be described as a two-part process (Barnard & Bastow, 1991).

2.1.3 Primary migration

The first part is an initial primary process of mobilization and migration of oil within the fine-grained source rock to reach the point where it can move freely in a more porous and permeable carrier bed (Figure 2.1). Hydrocarbons usually start to be liberated in the source rock at a depth of about 2.28 to 2.74 km in The North Sea Basin (Chapman, 1972; Bernard & Bastow, 1991). The initial porosity of the source rock decrease when buried. Initial low permeabilities would decrease to extremely low permeabilities. Pressure buildup occurs due to increased burial and liberation of hydrocarbons (Bernard & Bastow, 1991). Conversion of kerogen to oil and/or gas results in an increase in volume. A consequence of this volume change is overpressure. When this overpressure reaches a critical value, microcracks start to appear in the source rock. These microfractures served as a further migration pathway for the hydrocarbons (Zhiqiang, 2013).

2.1.4 Secondary migration

The second part of hydrocarbon migration is migration within the carrier bed. The main driving force of secondary migration is buoyancy, with hydrocarbons rising upwards to the upper part of the carrier bed, with capillary pressure being the main resistant force (Schowalter, 1979). The source rock escape point can be any point where hydrocarbons can begin to migrate as continuous-phase fluid through water-saturated porosity. The escape point could be anywhere the source rock is adjacent to a reservoir rock, an open fault, or an open fracture. Secondary migration is the movement of hydrocarbons as a single continuous-phase fluid through water-saturated rocks, faults, or fractures and the fluid concentration in trapped accumulations of oil and gas (Schowalter, 1979). The juxtaposition between a carrier bed and an impermeably bed with a high capillary entry pressure favors hydrocarbon accumulation, while juxtaposing a carrier bed and a permeable bed could result in hydrocarbon migration if the fault is open and the trap is filled to spill (Figure 2.1). Sealing faults can act as a barrier to fluid flow and prevent migration into possible hydrocarbon traps. Migration in Jurassic reservoirs is affected by the fault orientations, with migration direction aligned with the orientations of major faults (Johnsen et al., 1995).

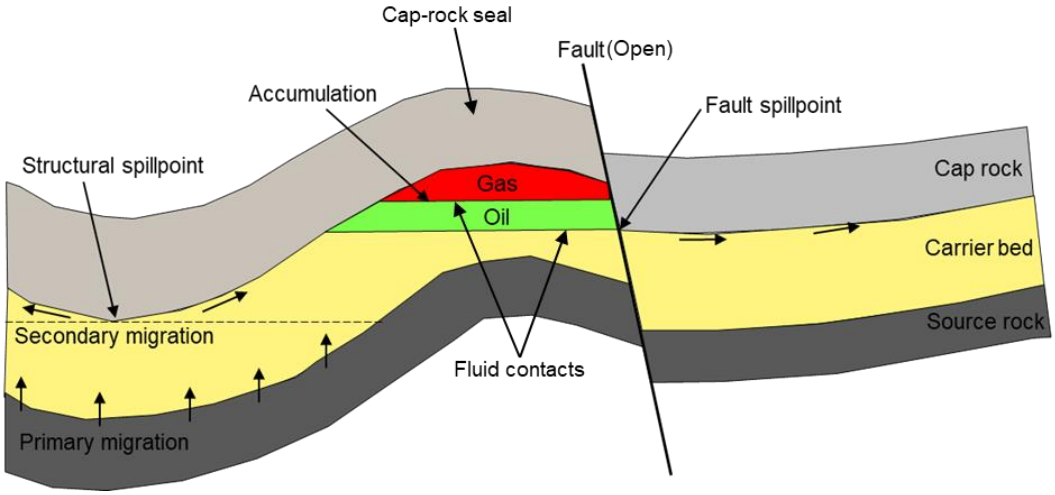

Figure 2.1: Illustration showing primary and secondary hydrocarbon migration and accumulation controlled by a structural trap, fault juxtaposition and spill points (Modified from Sollie, 2015).

2.1.5 Fault migration

Hydrocarbons can migrate both along and across a fault plane. Across fault migration is when the hydrocarbons migrate across the fault plane from one reservoir to another. This is the case when the fault does not have any sealing properties, rather a conduit for the fluids. Along fault migration is when the hydrocarbons migrate along the fault plane rather than across. The fluids migrate from a downfaulted reservoir up along the fault plane into an upfaulted reservoir. This migration occurs when the fault plane acts as a conduit to fluid flow (Figure 2.2).

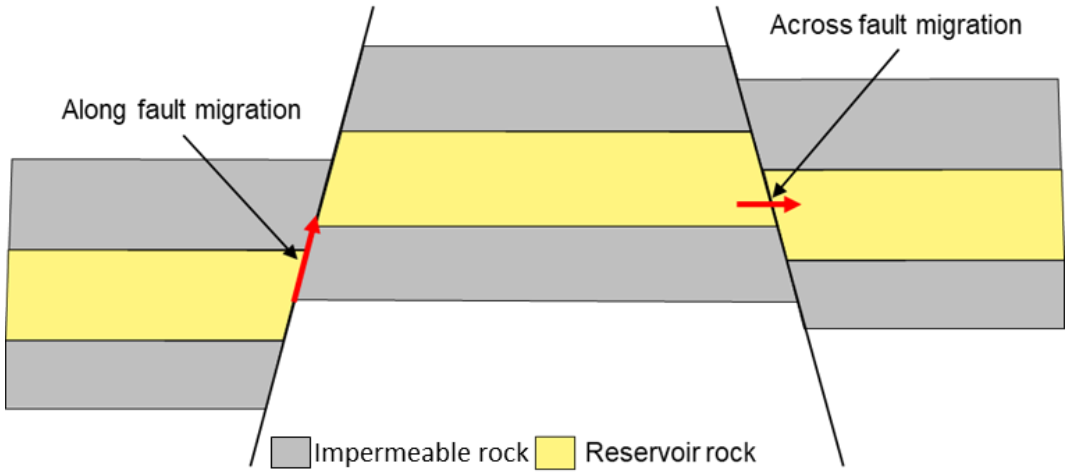

Figure 2.2: Illustration showing along and across fault migration.

2.1.6 Hydrocarbon accumulation

When the hydrocarbon reaches the trap (structural or stratigraphic), the capillary entry pressure of the cap-rock prevents the hydrocarbons from migrating further upwards. The hydrocarbons will then start to accumulate. The caprock may not be 100% effective in preventing the upward migration of the hydrocarbons. However, the hydrocarbons will still accumulate if the leakage is less than the supply rate to the trap. Cap rocks are usually not totally impermeable with respect to water but may be impermeable to oil and gas due to capillary resistance in the small pores (Bjørlykke, 2010).

2.1.7 Spill point

Accumulation of hydrocarbon can occur until a certain point where the hydrocarbons can leak out of the structure. This point is called the spill point (Bjørlykke, 2010). A trap can be controlled by a structural and/or a fault spill point (Figure 2.1). The fault spill point is where two reservoir beds are juxtaposed, letting the hydrocarbons through if the fault is open. If the fault is sealing, then the hydrocarbons will continue to accumulate until the structural or the next fault spill point if the source is sufficient. A structural spill point refers to the shallowest point of the top reservoir along the hinge of a syncline.

2.1.8 Filled and underfilled structures

A filled structure is when the trap is filled with hydrocarbons down to the spill point (filled to spill). This can either be down to the fault spill point (juxtaposition point) or at the structural spill point (the deepest part of the anticline). A structure is referred to as being underfilled when the hydrocarbon accumulation does not reach the depth of the spill point. The hydrocarbon-water contact will then be located shallower than the spill point. This can be the case if the seal is leaking faster than the supply rate to the trap, fault intersections, or limited supply of hydrocarbon to the trap. When the hydrocarbon accumulation is situated deeper than the spill point, then the structure is referred to as being overfilled. This can happen due to a sealing mechanism like shale smear along the fault plain or cementation preventing the hydrocarbons from migrating at the fault spill point.

2.1.9 Fill spill models

The fill-spill model is a simple model that implies that if the hydrocarbon supply reaches the spill point of a trap, then the trap is filled, and the hydrocarbons will migrate up-dip and accumulate in shallower traps before spilling further. A fill-spill model puts multiple traps along a migration pathway into one system and incorporates different phases present at different stages in the petroleum generation. Figure 2.3 shows a general fill-spill model along different fault blocks. The fill-spill model explains why some plausible good fields are gas fields rather than oil fields, while others contain little to no hydrocarbons. It also explains why gas fields may occur in a down-dip position and produce little or no oil while structures in an up-dip position produce oil with little or no gas, and others in a still further up-dip position are water-bearing (Gussow, 1953). Oil and gas will create two layers above the water due to buoyancy and different densities. Once the oil-water contact reaches the structural spill point, the trap will be filled and any additional hydrocarbon to the trap will cause oil to spill up-dip from the trap (Figure 2.4). Once the gas-oil contact has reached the depth of the spill point, the oil-water contact will go over to a gas-water contact as the last of the oil will migrate out of the trap. This represents the endpoint and the final stage of the trap (Figure 2.5).

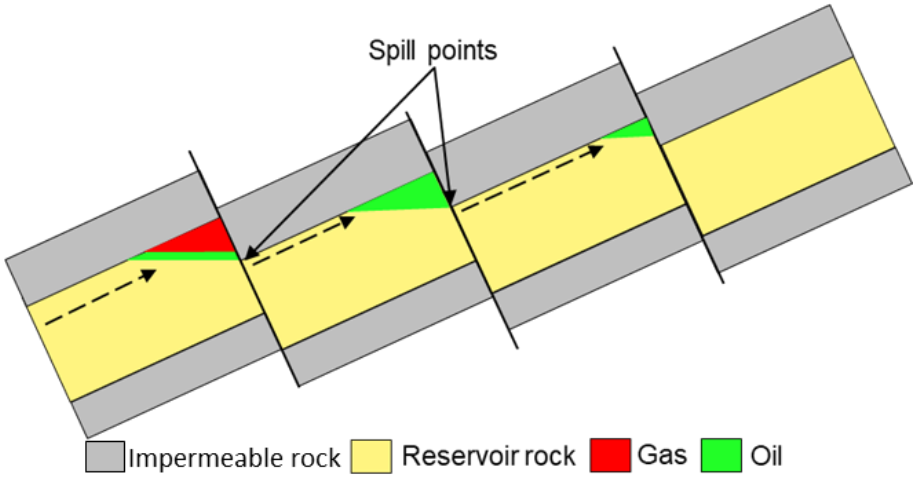

Figure 2.3: Illustration showing an example of the fill-spill model with rotated fault blocks.

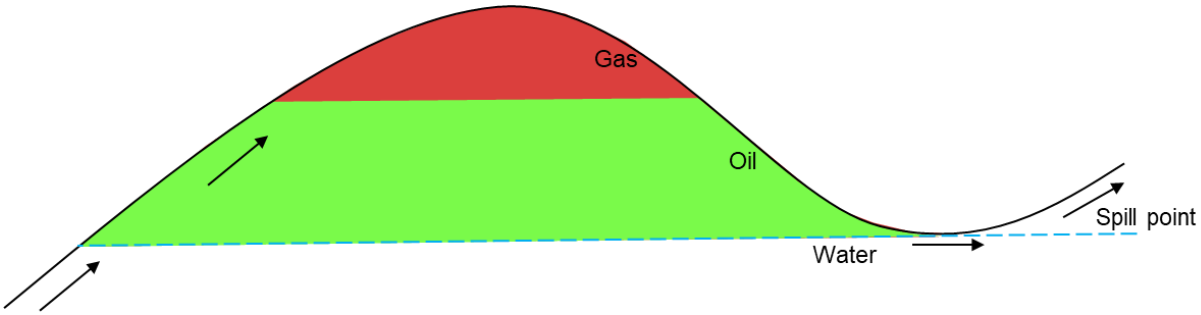

Figure 2.4: Illustration showing the stage of selective entrapment. Gas continues to be trapped while oil is being spilled up-dip due to additional hydrocarbon to the trap. (Modified from Gussow, 1953).

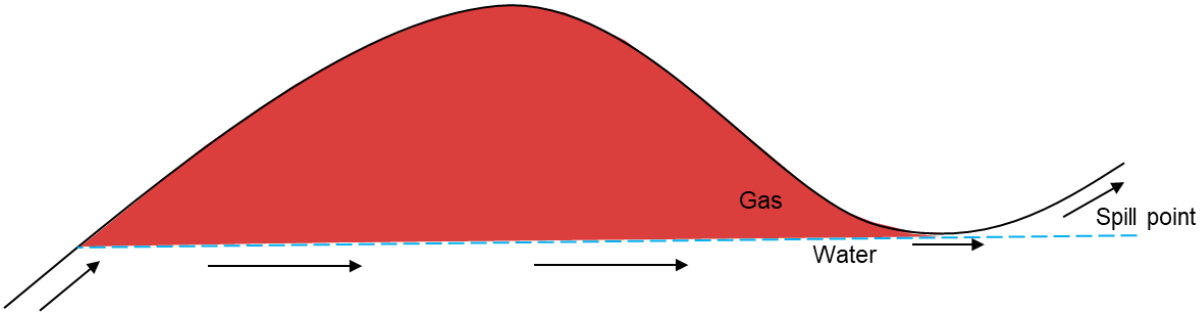

Figure 2.5: Illustration showing the end state of the trap where the trap is filled with gas down to the spill point. Gas will migrate up-dip if additional gas enters the trap. Oil will bypass the trap and continue to spill up-dip. (Modified from Gussow, 1953).

2.2 Pore Pressure

Pore pressure, also referred to as formation pressure, is the fluid pressure within the pore space of porous rocks. Pore pressures tend to vary both laterally and vertically. Due to this, pore pressures are compared to hydrostatic pressures at the same depth. As a formation is increasingly buried, the water pressure in the formation will increase. This increase in pressure is close to linear and is known as the hydrostatic gradient. The hydrostatic pressure gradient is the pressure that is expected by a continuous column of static fluid. This pressure will vary depending on the density of the pore fluid (Osborne & Swarbrick, 1997).

Normally pressured formations are plotted along the hydrostatic gradient, implying that the formation pressure is in equilibrium with the hydrostatic pressure. Buhrig (1989) has described different pressure systems: open, restricted, and closed. An open system consists of hydro pressured reservoirs in pressure communication with the regional hydrostatic aquifer system. A restricted system consists of moderately pressured reservoirs, and an overpressure stabilization characterizes a closed system (Buhrig, 1989).

When the pore fluid pressure is higher than the hydrostatic gradient at a specific depth, then it is referred to as being overpressured. Overpressured formations have often restricted or no connection with the overburden and are either restricted or in a closed system (Buhrig, 1989). Different processes can cause overpressure. One of the causes that has been proposed is overpressure due to an increase in compressive stress (i.e., reduction in the pore volume) caused by disequilibrium compaction and tectonic compression. Other processes are fluid volume change caused by temperature increase, diagenesis, hydrocarbon generation, cracking to gas, and fluid movement and processes related to density differences between fluids and gases caused by hydraulic head, osmosis, and buoyancy (Osborne & Swarbrick, 1997). When the pore pressure is significantly lower than the hydrostatic pressure, it is referred to as underpressured. Underpressure in sedimentary basins is commonly explained by erosional unloading (Neuzil & Pollock, 1983).

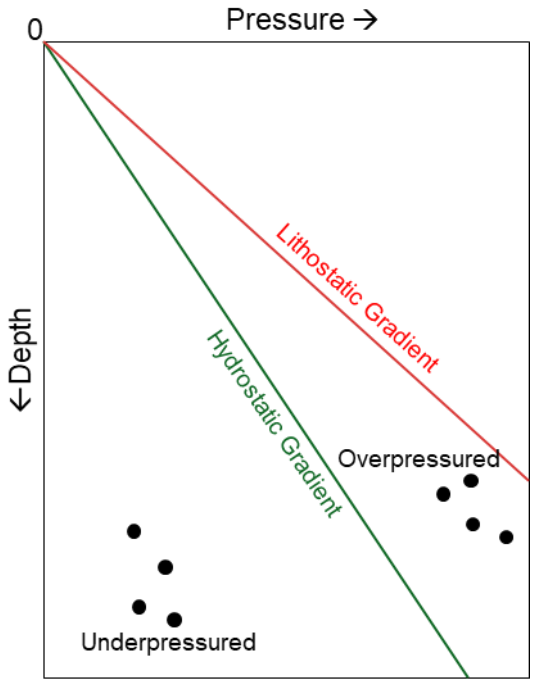

Figure 2.6: Pressure/depth plot with examples of underpressured and overpressured fluids compared to the hydrostatic and lithostatic gradients.

2.3 Cap-rock and fault-related seals

Traps in the Krafla-Askja area are rotated fault blocks created by rifting during the Late Jurassic and a horst delineated by normal faults. The rifting resulted in numerous individual traps separated by normal faults.

Cap-rock seals can be divided into two types: those that fail by capillary leakage (membrane seals) and those where the capillary entry pressures are so high that seal failure preferentially occurs by fracturing and/or wedging open of faults (hydraulic seals) (Watts, 1987). The main control on failure of membrane seals is the capillary entry pressure of the seal rock (the pressure required for hydrocarbons to enter the largest interconnected pore throat of the seal). It is considered a hydraulic seal when the entry pressure must exceed the strength of the rock to breach the seal (Watts, 1987; Yielding et al., 1997).

Fault-related seals are effectively analogous to membrane cap rocks which have been tilted to the angle of the fault plane. Fault sealing can be divided into two categories: juxtaposition faults where the hydrocarbons are trapped laterally against a juxtaposed sealing unit, and faults where the fault plane itself is sealing (Watts, 1987). Fault seals can arise from a reservoir rock being juxtaposed to a non-reservoir rock or the development of fault rock with high entry pressure (Yielding et al., 1997). Yielding et al. (2010) separates the sealing behavior of a fault in siliciclastic sequences into three fundamental conditions:

- The juxtaposition of the reservoir against sealing lithologies across the fault.
- Fault-zone products are created by deformation during the fault displacement and subsequent evolution.
- The current stress state of the fault and its proximity to failure (slip).

2.3.1 Juxtaposition

Juxtaposition seal is when reservoir sands are juxtaposed against a low permeability unit with a high entry pressure (Figure 2.7). Normal faulting of sand-shale sequences in an extensional setting often results in permeable units juxtaposed to impermeable units. Juxtaposition seals can be recognized explicitly by mapping the juxtaposition units across the fault plane (Yielding et al., 1997).

2.3.2 Membrane seal

The fault zone itself can provide the necessary conditions for a side-seal in reservoir-reservoir juxtaposition areas.

Self-juxtaposed reservoirs are reservoirs that are partially juxtaposed to themselves across the fault. Sand-sand juxtapositions are commonly ideal for migration, but brittle deformation with faulting can lead to membrane seals. Mechanical shearing with grain reorganization and grain compaction could alter the capillary properties of the fault rock and prevent further migration until the net buoyancy pressure exceeds the entry pressure (Watts, 1987; Bjørlykke, 1999; Færseth et al., 2007). Sand-sand juxtaposition between two permeable sand units is regarded as high-risk traps (Færset et al., 2007).

Cataclasis is the brittle deformation of sand grains in the fault zone to produce a fault gouge of finer-grained material, giving the fault a high capillary entry pressure (Fristad, 1997; Yielding et al., 1997).

Cementation along an originally permeable fault plane may partially or completely remove porosity, ultimately creating a hydraulic seal (Yielding et al., 1997). According to Blatt (1979), quartz cementation is the most important process resulting in porosity reduction in sandstone reservoirs. Quartz cementation becomes significant at depths greater than ~3 000 m and temperatures higher than 75-92˚C (Walderhaug, 1990; Bjørlykke et al., 1992; Giles et al., 1992).

Where a shale layer is offset by a fault throw greater than the vertical thickness of the layer, then shale smear may occur along the reservoir-reservoir fault surface between the cutoffs of the shale layer (Lindsay et al., 1993). Shale smear is the entrainment of clay or shale into the fault plane, thereby giving the fault itself a high capillary entry pressure (Fristad, 1997; Yielding et al., 1997). Cataclasis seals can hold an oil column of tens of meters, while a shale smear seal can hold a column of hundreds of meters (Knipe, 1992).

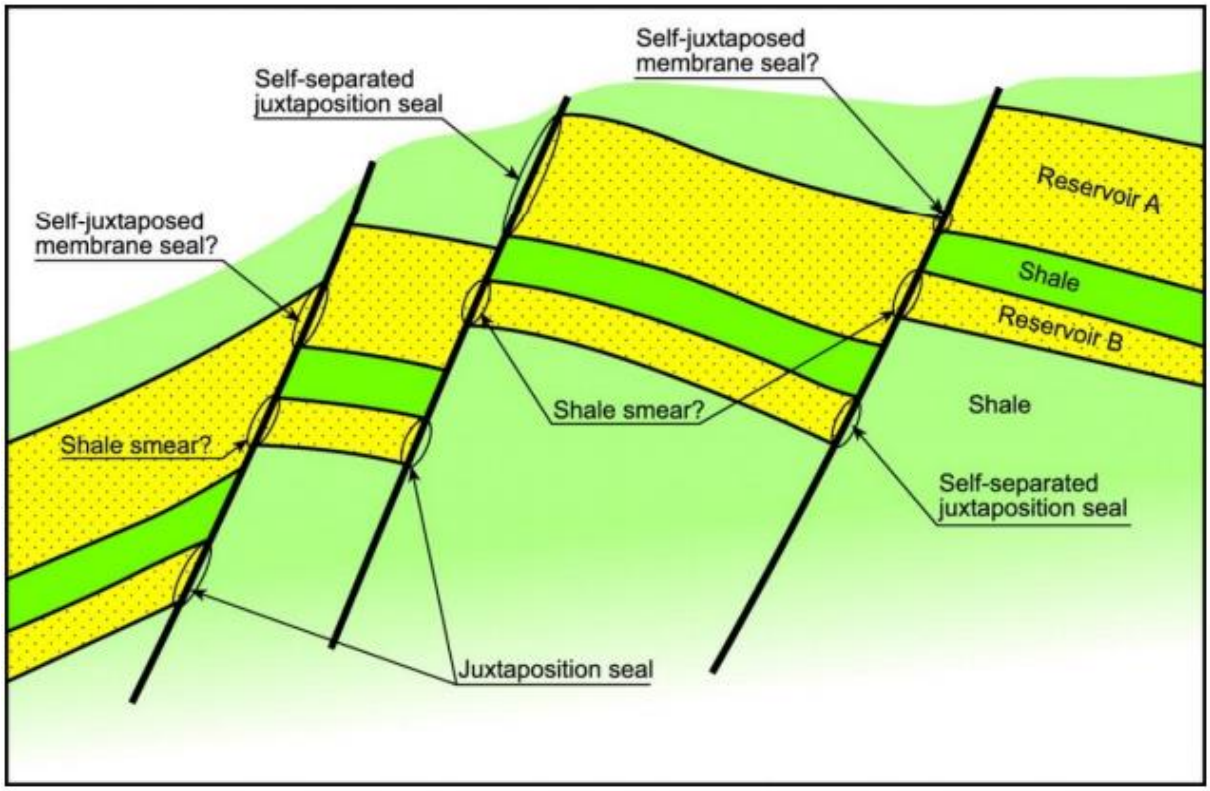

Figure 2.7: Figure by Færseth (2006) showing a schematic illustration of potential hydrocarbon traps resulting from a sand-shale sequence in an extensional setting.

Fault seal algorithms are a simple method to predict the properties of the fault zone. These algorithms fall into one of two categories: smear factors which describe aspects of smearing clay or shale beds, and gouge ratio, which describes the composition of the fault rock (Yielding et al., 1997; 2010).

The gouge methods make a simple assumption that the wall rocks are, on average, uniformly mixed into the fault zone. The key component for sealing potential is the clay content since small grain sizes lead to small pore-throats and high capillary threshold pressure. The Shale Gouge Ratio (SGR) algorithm takes the average clay content of those beds that have been faulted past any point and treats this as an estimate of upscaled fault-zone composition. When the SGR value is high (above 40-50%), the fault rock is dominated by clay smears. If the Brent Group juxtapositions have less than 15-20% SGR, then the shale smears are discontinuous, and the dominant fault-zone materials (disaggregation zones and cataclasites) are generally unable to provide a recognizable seal (Yielding, 2002; Yielding et al., 2010).

Fristad et al. (1997) did a study about quantitative fault seal prediction in the Oseberg Sør area. They concluded that clay smearing and sealing by juxtaposition are the main contributors to static seals in the western part of Block 30/9 where the Brent Group is the main reservoir. They

observed that SGR values below 15% gives no seal. Values between 15% and 18% will give a slight seal, while values above 18% gives a considerable seal. The lowest SGR values were generally observed in the Tarbert Formation.

2.4 Fault reactivation

Leakage because of fault reactivation could lead to hydrocarbon leakage (Wiprut and Zoback, 2000; 2002). Favorably oriented faults will slip before the pore pressures can reach levels resulting in cap rock failure. They suggest that fault reactivation and hydrocarbon leakage in the northern North Sea appear to be caused by three factors:

- Locally elevated pore pressure due to buoyant hydrocarbons abutting faults. As the height of the hydrocarbon column increases, the pore pressure at a certain point becomes sufficient to induce the fault to slip, increasing the fault's permeability and allowing leakage from the reservoir.
- Fault orientations that are nearly optimally oriented for frictional slip in the present-day stress field. Fault networks formes at different geological times and settings where critically stress faults in the current stress regime are permeable, while faults not critically stressed are not permeable.
- A recent perturbation of the compressional stress associated with postglacial rebound.

2.5 Stress regimes

Knowledge about the stress state of the subsurface is highly relevant for hydrocarbon exploration, as changes in stress can influence the integrity of hydrocarbon traps (Wiprut & Zoback, 2002; Gartrell et al., 2003; Grollimund & Zoback, 2003; Bolås et al., 2005).

As hydrocarbon migration in the northern North Sea began in the Early Cenozoic and increased in the Pliocene (Goff, 1983), stress changes before this time are not relevant for hydrocarbon leakage. Bolås et al. (2005) suggest the following events to have caused stress anisotropy in recent geological time:

- Thick, westward prograding sedimentary wedges during Pliocene-Pleistocene, causing increased vertical and horizontal stress in the underlying sediments.
- Glacial advance and withdrawal during the Pleistocene caused crustal flexing and increased stress anisotropy.

- Abrupt vertical stress changes at the shelf edge caused by loading and unloading of glaciers.

Fejerskov and Lindholm (2000) calculated the maximum horizontal stress direction in the northern North Sea to be WNW-ESE with a compressional stress regime. Brudy and Kjørholt (2001) observed that the orientation of the maximum horizontal stress in the Oseberg/Troll area has a general E-W orientation. The Oseberg/Troll area observations made by Brudy and Kjørholt (2000) can be seen in Figure 2.8.

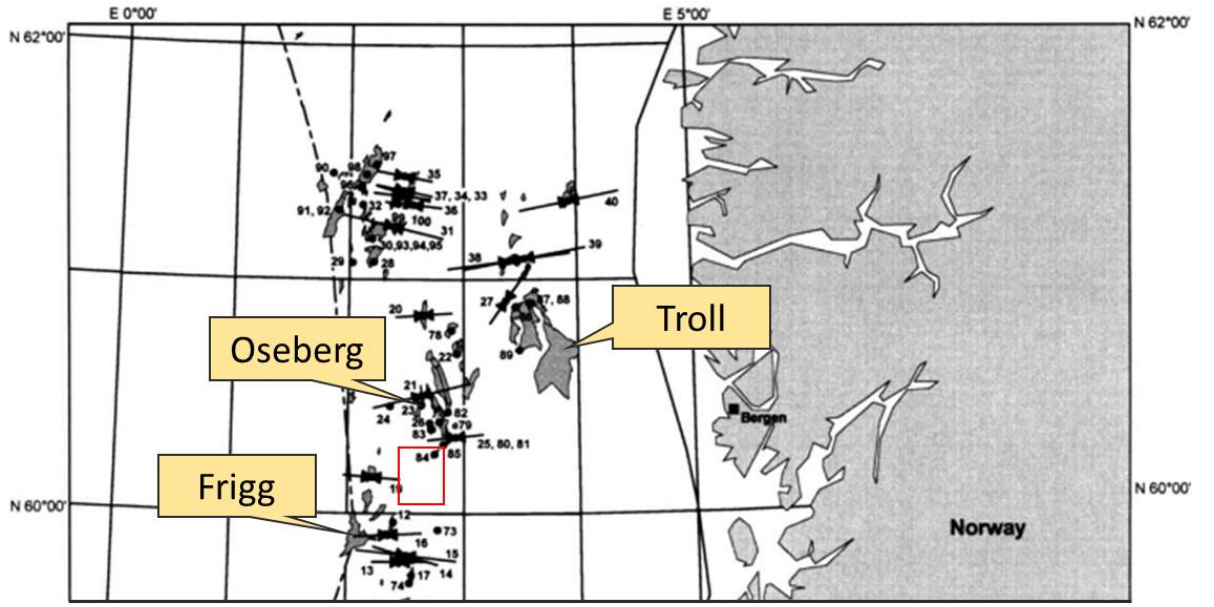

Figure 2.8: Map over the Oseberg/Frigg area showing the maximum horizontal stress directions observed by Brudy and Kjørholt (2000). The Krafla-Askja area is highlighted with a red square. (Modified from Brudy and Kjørholt, 2000).

2.6 Allan diagrams/2D fault plane maps

Allan (1989) proposed a model for hydrocarbon migration and entrapment within faulted structures. The model is based on a few assumptions: (1) A fault itself has no sealing properties. (2) A fault is not an open conduit. (3) The trapping and migration relationships at a fault depend upon the fault juxtaposed stratigraphy. These type of diagrams are used in this study to map juxtapositions across the faults of interest.

Chapter 3 - Geological setting

The following chapter gives a brief overview of the geological evolution of the northern North Sea and the stratigraphy of the Middle and Upper Jurassic deposits in the Oseberg Sør area.

The North Sea is an example of an intracratonic basin bounded by mainland Norway and the Shetland Platform to the west (Faleide et al., 2010). The basins consist of three rift arms: the Viking Graben, the Central Graben, and the Moray Firth Basin (Figure 3.1). These three rift arms represent a failed arm of the Artic-North Atlantic rift system (Whipp et al., 2014; Bartholomew et al., 1993).

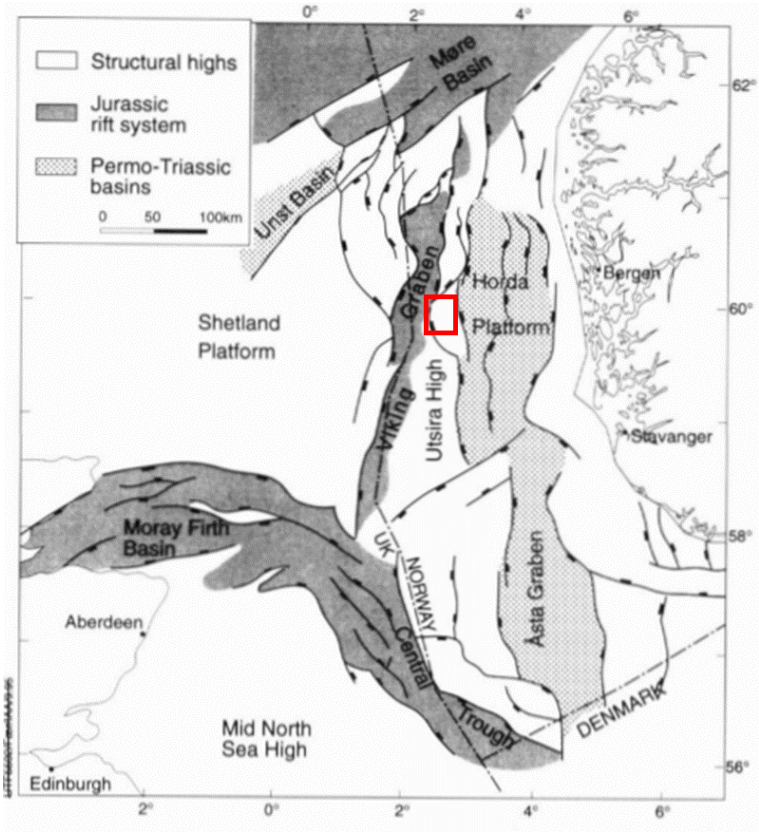

Figure 3.1: Structural elements of the North Sea with the study area represented by the red square. (Modified from Færseth, 1996).

The northern North Sea province is dominated by the Viking Graben and is flanked by the East Shetland Basin and the Tampen Spur to the west, and the Horda Platform to the east. The North Sea has undergone periods of stretching/thinning and subsidence where rifting started at the transition from the Permian to the Triassic and intensified during Middle Jurassic to Early Cretaceous times and subsequently gradually diminished during the Cretaceous (Ziegler, 1992; Faleide et al., 2010).

The northern North Sea underwent two rift phases, with the first rift phase occurring in the Permian-Early Triassic and the second phase in the Middle Jurassic-Early Cretaceous. Rift-related normal faults in the northern North Sea strike N-S, NE-SW and NW-SE, and relate to both extension phases. Faults active during the early rifting phase were reactivated during the Jurassic rifting (Færset & Ravnås, 1998).

3.1 Pre-rift history of the North Sea

The structural formation of the North Sea can be traced back to the Caledonian orogeny. Compressional tectonics during the Caledonian and Variscan orogenies led to the formation of a heterogeneous crystalline basement (Whipp et al., 2014). The Caledonian crust thinned during post-collisional Devonian extension and erosion (Fossen, 2010). The easternmost part of the North Sea is underlain by Precambrian basement forming parts of the Fennoscandian shield (Ziegler, 1992). Pre-existing crustal discontinuities often play an important role in the localization of rift systems, as well as in the geometry of their fault patterns (Færseth, 1996). NE-SW and ENE-WSW-oriented structural lineaments associated with the Caledonian and Variscan orogenic cycles were reactivated as normal faults during Devonian and Carboniferous extension (Whipp et al., 2014). The Devonian post-orogenic collapse of the Caledonian fold belt and a sinistral translation between Greenland and Europe resulted in rapid subsidence controlled by northeasterly striking fault systems crossing the northern North Sea (Ziegler, 1992).

During Late Carboniferous–Early Permian, northwest Europe was transected by a complex conjugate wrench fault system that developed in response to a modification in the convergence direction of Gondwana and North America-Europe (Laurussia). The entire North Sea area was uplifted above the erosional base level, resulting in deep truncation of Devonian and Carboniferous sediments (Ziegler, 1992).

Towards the end of the Early Permian, wrench fault and volcanic activity declined in northwest Europe, and the Northern and Southern Permian basins began to subside in response to thermal relaxation of the lithosphere (Ziegler, 1992).

3.2 Rifting and deposition in the Mesozoic era

Throughout the Mesozoic era, the Viking Graben along with surrounding terraces and platform areas in the northern North Sea underwent two major episodes of lithospheric stretching, separated by a period of tectonic quiescence (Nøttvedt et al., 1995; Færseth, 1996).

Rifting in the Arctic-North Atlantic accelerated at the transition from the Permian to the Triassic period. The Mesozoic North Sea rift system consist of the Viking, Central and Moray Firth-Witch Ground grabens and the Horda-Egersund half graben (Ziegler, 1992). During the earliest Triassic, the Norwegian-Greenland Sea rift propagated into the North Sea area where the Viking and Central Grabens, the Horda-Egersund half-graben and the Moray Firth-Witch Ground graben system started to subside (Ziegler, 1992).

The first major rift phase affecting the northern North Sea rift started in the late Permian and continued into the Early Triassic, followed by post-rift thermal subsidence (Ziegler, 1992; Færseth, 1996; Phillips et al., 2019). The Permian–Early Triassic rift phase is generally assumed to have occurred during E-W extension triggered by the break-up of the supercontinent Pangea affecting the entire northern North Sea basin, with the rift axis located beneath the Horda Platform. The E-W extension resulted in an N-S-oriented, 130-150 km wide basin, consisting of tilted half-graben bound by large displacement of 3-5 km (Færset, 1996; Whipp et al., 2014). The large faults that controlled the extension, subsidence, basin geometry, and sedimentation patterns are assumed to have been established during the Permo-Triassic stretching period and then reactivated during the Jurassic stretching period. Both the stretching periods are believed to have the same magnitude of importance on the structural evolution of the North Sea (Færseth, 1996).

The transition from the Triassic to the Jurassic period approximately coincides with a change from continental to shallow marine depositional environments. The climate also gradually became more humid in the Jurassic as northwest Europe was pushed out of the arid belt at about 30˚ N (Faleide et al., 2010). Following the pre-Jurassic rift event, a fluvial-deltaic-to-shallow marine succession, consisting of the Statfjord, Dunlin and Brent Groups, was deposited during Early-Jurassic to early Middle Jurassic (Helland-Hansen et al., 1992; Steel, 1993; Whipp et al., 2014). The Dunlin Group succeeds the Statfjord Formation and is a dark marine shale but is usually without enough organic content to become a significant source rock (Faleide et al., 2010).

During the late Aalenian and Bojacian in the Middle Jurassic, a broad arch was uplifted in the Central Graben. During the Bojacian and Bathonian, a large volcanic center developed at the triple junction between the Viking, Central, and Moray Firth-Witch Ground grabens. Over the crest of this dome, Early Jurassic, Triassic, and even Permian sediments were deeply truncated. Erosion products were deposited in adjacent continuously subsiding basins in major deltaic complexes, such as the Brent Sand Group in the Viking Graben (Ziegler, 1992).

The Middle-to-Late Jurassic extension of the northern North Sea resulted in the collapse of the North Sea dome. NW-SE extension during the rifting phase caused reactivation of older faults and formed new Jurassic faults throughout the basin. The Jurassic faults have a larger spread in orientation than those resulting from Permo-Triassic extension (Færseth, 1996). The Middle-to-Late Jurassic extension can be divided into two main stages, Late Bojacian-Middle Callovian stage (168-162 Ma) and Kimmeridgian to Tithonian stage (156-146 Ma) (Whipp et al., 2014). The subsidence was greater than the sediment supply resulting in a gradually drowning of the prograding parts of the Brent delta. The basin deepening led to the deposition of the marine Viking Group, whose transgressive-regressive stratigraphy may reflect pulsed rifting. The organic-rich Draupne shales in the Viking Group act as an important source rock in the North Sea. The Viking Group is capped by the Base-Cretaceous Unconformity (BCU) (Faleide et al., 2010; Whipp et al., 2014).

During the initial Bathonian-latest Callovian stage of rifting, a series of faulted terraces developed between the Viking Graben and the Horda Platform (Holgate et al., 2013). Rotation of the normal fault blocks and their overlaying sediments exposed parts of the blocks resulting in erosion of Lower-Middle Jurassic and Locally even Upper Triassic strata (Holgate et al., 2013; Faleide et al., 2010). A late-Kimmeridgian rifting pulse lasting about 10 Ma affected the Viking Graben and was accompanied by a relative drop in sea level. Accelerated crustal stretching took place in the Viking Graben resulting in rapid subsidence of large rotational fault blocks. The rate of crustal extension gradually diminished after the rifting pulse, with only master faults delineating the Viking and Central Grabens being active throughout the Cretaceous (Ziegler, 1992).

At the transition to the Cretaceous period, rifting activity peaked in the entire Artic-North Atlantic domain, and the North Sea basin went into a period of passive, thermal subsidence (Ziegler, 1992; Whipp et al., 2014). The fault activity diminished during the Cretaceous, and the subsidence was due primarily to crustal cooling (Faleide et al., 2010).

3.2.1 The stratigraphy of the Brent and Viking Groups

The Brent Group was deposited in Middle-Jurassic times during the Aalenian, Bajocian and Bathonian and includes the Broom, Rannoch, Etive, Ness and the Tarbert Formations (Figure 3.2 & 3.3). The Oseberg Formation has been defined as the Broom Formation equivalent on the Norwegian side of the North Sea. The group is a succession of sandstones, siltstones, shales and coals up to 600 m in thickness (Helland-Hansen et al., 1992). The delta prograded northward through the Viking Graben due to a thermal uplift and associated volcanism in the south. The sediments were sourced from the uplifted area in the south (Løseth et al., 2009; Faleide et al., 2010). The Broom and Oseberg Formations represent early Aalenian lateral infill of the basin, whereas the rest of the formations comprise a major regressive (Rannoch, Etive and Ness Formations) to transgressive (Ness and Tarbert Formations) siliciclastic wedge deposited in the Bojacian (Helland-Hansen et al., 1992). A regressive maximum occurred in the latter stages of Early Bojacian, followed by transgressive backstepping and delta retreat during Late Bojacian–Early Bathonian. By the Callovian, the deltaic system had retreated into the southern part of the Viking Graben south of the study area (Løseth et al., 2009).

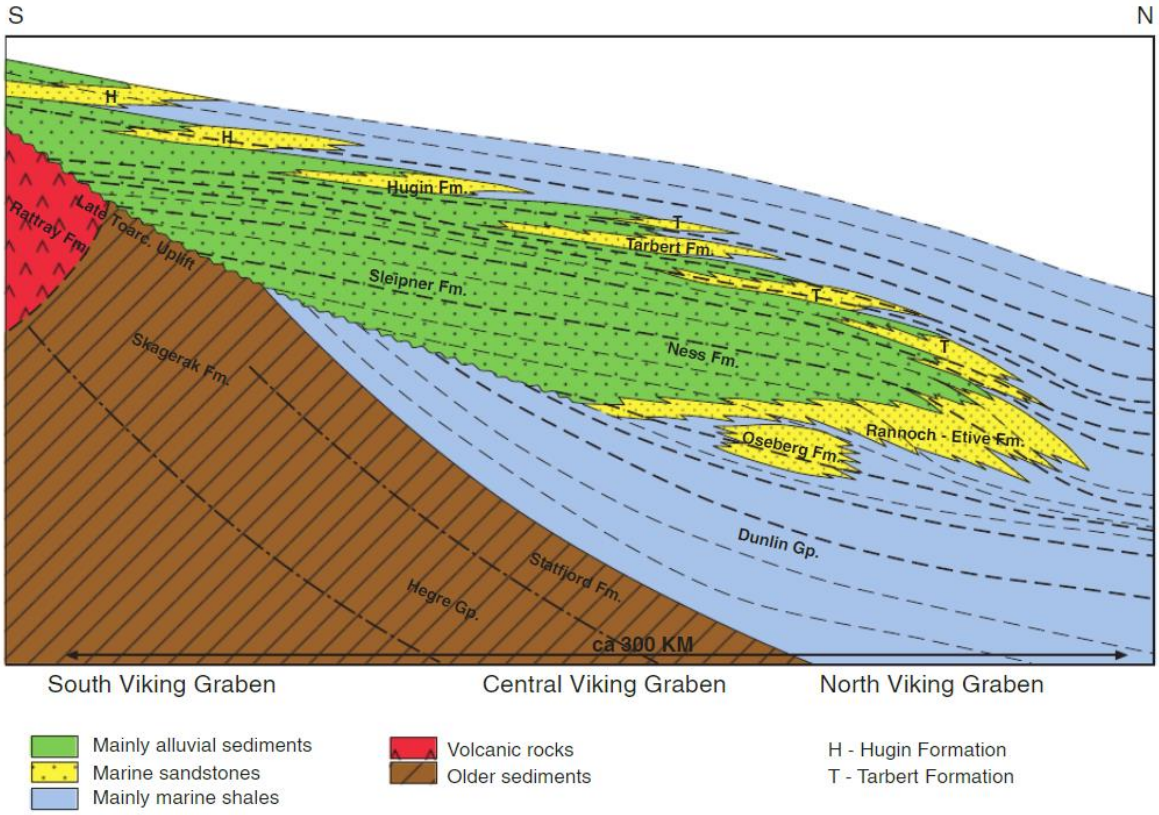

Figure 3.2: Schematic stratigraphic section of the Brent- and Vestland Groups (Løseth et al., 2009 modified from Helland-Hansen et al., 1992).

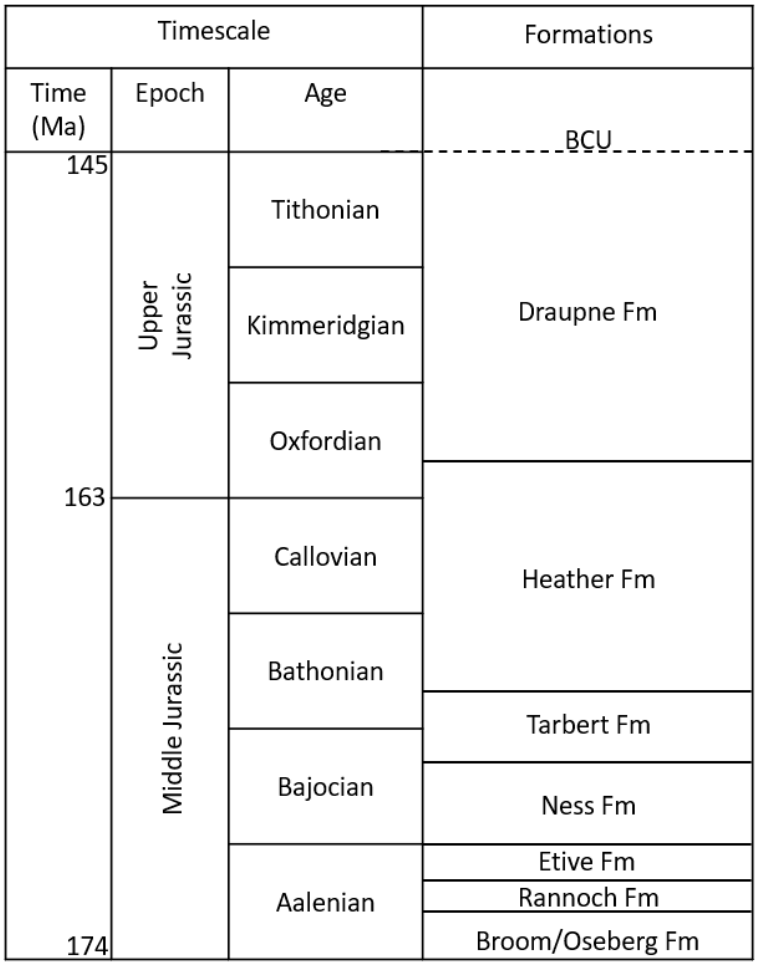

Figure 3.3: Approximate time of deposition for the formations in the Brent and Viking Groups.

There was a significant basinward shift of sedimentation in the Aalenian, where the younger sand lobes (Oseberg Formation) were deposited beyond the Horda Platform. These sand lobes are basin margin-attached with steeply inclined progradational surfaces indicating a fast outbuilding of coarse-grained sediments into shallower water. The shallow marine and alluvial deposits overlayed the Toarcian marine and shales and sands, suggesting a relative fall of sea level (Helland-Hansen et al., 1992). The data from Helland-Hansen et al. (1992) suggest that the study area was not majorly affected by the Oseberg Formation. The Oseberg Formation was not encountered by any of the wells used in this study.

The remaining formations define the Bajoician-Bathonian Brent deltaic complex, where the Rannoch, Etive and Ness Formations represent the regressive part of the delta (Løseth et al., 2009). The Rannoch and Etive Formations form a variably thick, storm-wave-dominated, delta-front or barrier/shoreface coarsening-up sequence (Hellen-Hansen et al., 1992).

The Ness Formation comprises a variably thick and heterolithic interval of delta-plain deposits. The mixed sandstone, mudrock and coal sequences reflect fluvial channel/mouth-bar, overbank,

interdistibutary bay and lagoon subenviroments of the delta-plain (Helland-Hansen et al., 1992). Due to the variation in lithology, the Ness Formation can have multiple different pressure compartments and accumulation of hydrocarbons within the different channel sands. Where the coals are found suggests a non-marine (continental) environment. Figure 3.4 shows how the Ness Formation generally looks like in the area. Fristad et al. (1997) have divided Ness into four segments (Lower Ness sand, Lower Ness, Middle Ness and Upper Ness). Lower Ness sand is fluvial channel deposits, and Lower Ness is upper delta plain. Middle Ness is Upper delta plain with abandoned lobe, lacustrine and swamp deposits with poor reservoir quality, while Upper Ness is upper to lower delta plain deposits.

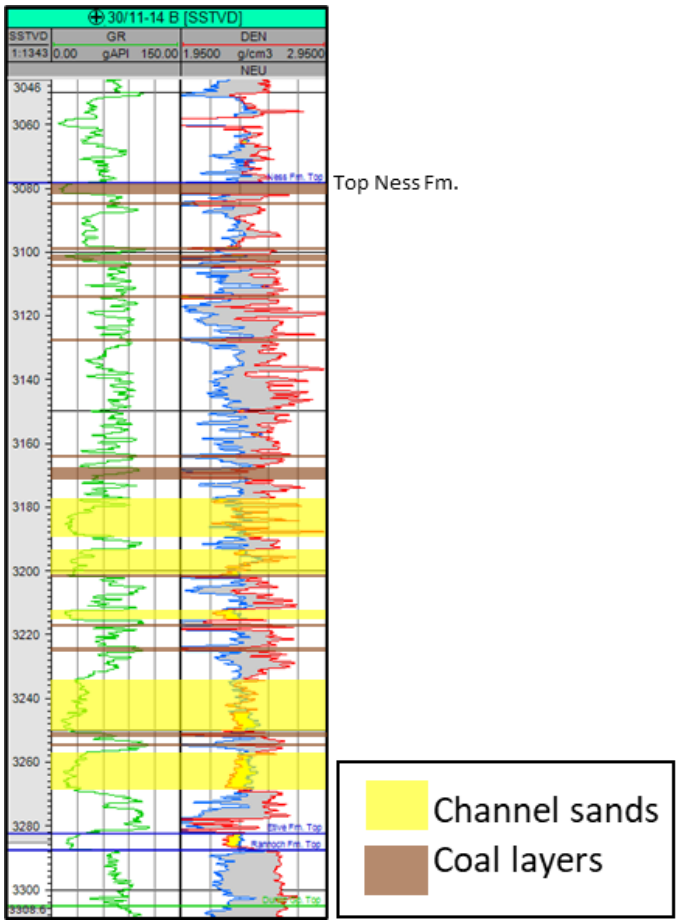

Figure 3.4: An example from well 30/11-14 B showing typical well log signatures of the Ness Formation. Channel sandstones and coals are color-shaded across the gamma ray and density/neutron logs.

A regressive maximum was reached at the end of Early-Bojacian. The Tarbert Formation is the last formation of the Brent Group and represents the transgressive part of the delta together with the upper parts of the Ness Formation. The delta retreated to the study area and deposited the Tarbert Formation (Figure 3.5). The formation is absent in the wells south of the study area. The sands in the Tarbert Formation are the most important reservoirs in the study area. Studies

of the Tarbert Formation have been done in the Oseberg Sør area e.g. Fristad et al. (1997) and Løseth et al. (2009).

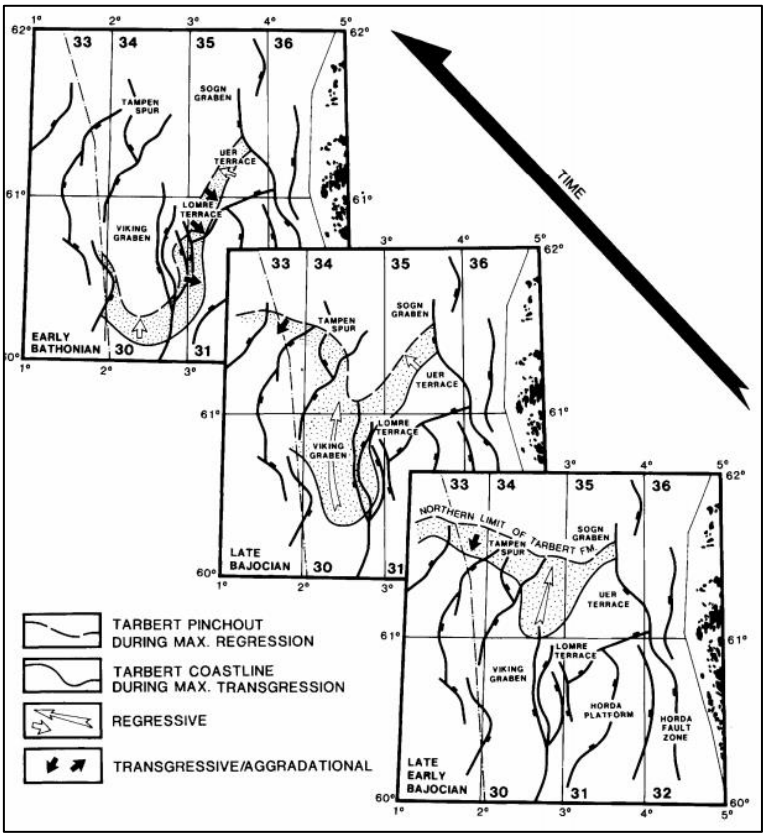

Figure 3.5: Successive stages of Brent Delta retreat (Helland-Hansen et al., 1992).

The Tarbert Formation is divided into two regressive-transgressive wedges that have been thought to be the main part of a long-term transgressive system tract. The formation comprises stacked, smaller regressive units of wave-dominated shoreface deposits, commonly resting on wave-generated refinement surfaces and capped by coal-bearing continental strata and/or lagoon deposits. These progradational units are stacked as a series of generally back-stepping wedges deposited during the overall southwards retreat of the Brent Delta system (Løseth et al., 2009).

Løseth et al. (2009) have studied the sedimentology and sequence stratigraphy of the Tarbert Formation in the Oseberg Sør area. They have divided the Tarbert Formation into two wedges, one regressive (wedge 1) and one transgressive (wedge 2), and five main facies associations (FA1-FA5). Fristad et al. (1997) have divided the formation into an Upper, Middle, and Lower part which is the classification used in this study. Lower Tarbert (FA1) overlays coastal plain deposits and represents lower shoreface to foreshore deposits. Middle Tarbert 1 (FA2) is interpreted to be swamp and embayment deposits. Middle Tarbert 2 (FA3 and FA4) are tide-

influenced channels and central to outer estuary deposits. Upper Tarbert (FA5) is wave-dominated shoreface environments and makes up wedge 2. A transgression occurred during the deposition of Upper Tarbert where the depositional environment went from middle shoreface to offshore transition/lower shoreface (Fristad et al., 1997; Løseth et al., 2009). A simplified example of the stratigraphy of the Tarbert Formation in the study area is shown in Figure 3.6 showing that the sands within the formation are not in communication.

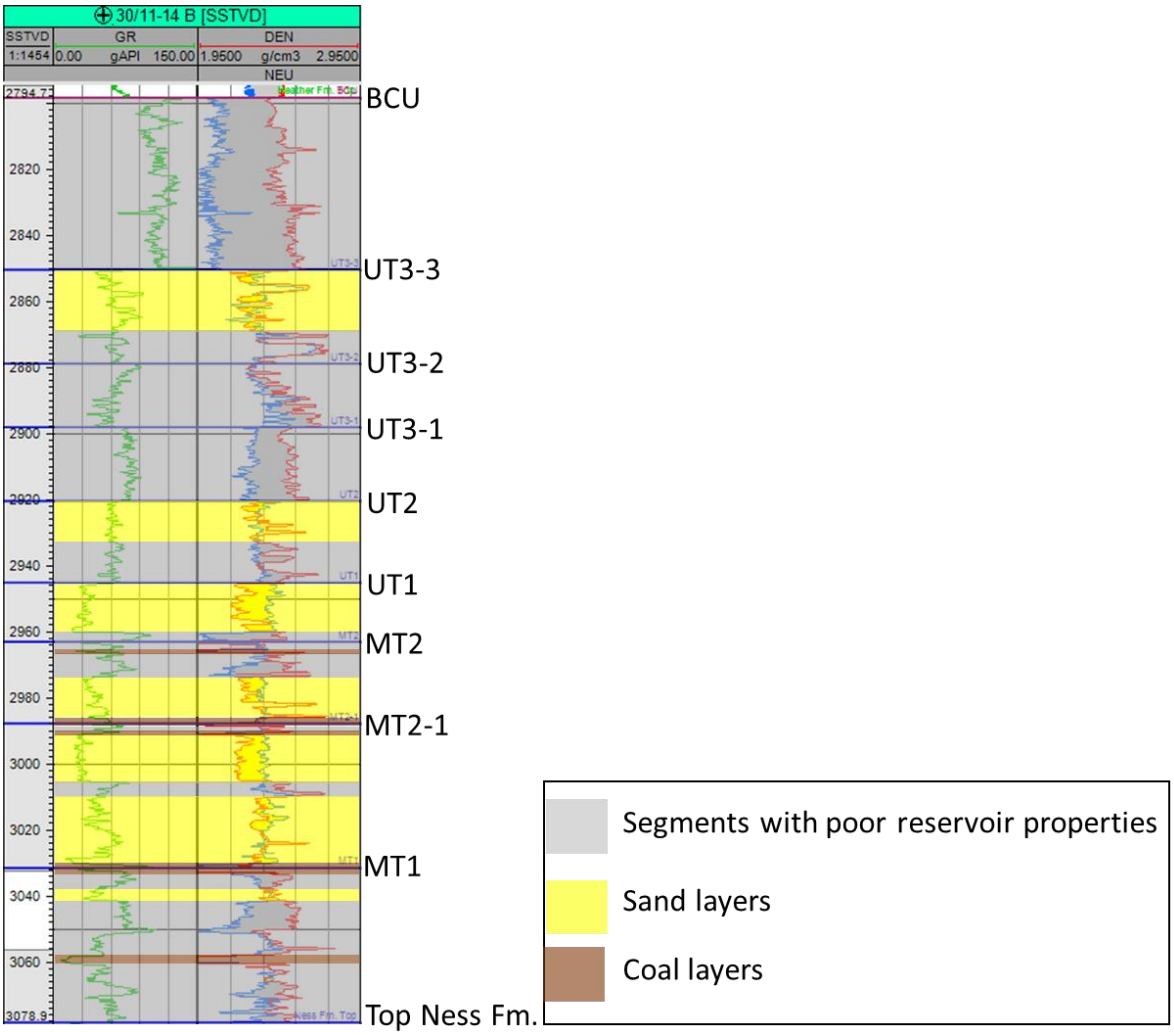

Figure 3.6: An example of the Tarbert Formation from well 30/11-14 B showing a simplified interpretation with alternating sand and siltstone/shale layers.

The transgression flooded the Brent delta and deposited the Heather Formation. Fristad et al. (1997) have classified the Heather Formation into three segments. The deepest segment is lower shoreface to offshore transition zone. The second segment is lower to upper shoreface and the third is offshore deposits. The Draupne Formation was deposited after the Heather Formation and consist of one sandy and one shaly segment. The sand is turbidite fans, while the uppermost

segment is offshore shales, also known as the Kimmeridge clay Formation, and is the primary source rock in the North Sea (Fristad et al., 1997; Faleide et al., 2010).

3.3 Post-rifting

The third and final post-rift stage is the mature post-rift stage. The stage took place from Coniacian (Upper Cretaceous) to early Paleocene (Paleogene). In this stage the basin transformed into a wide "saucer-shaped" basin where the syn-rift features vanished due to the overlying sediments (Faleide et al., 2010). During the early stages of Paleogene (55 Ma), Mesozoic rifting between Norway and Greenland led to volcanism and the opening of the Norwegian Sea at the Paleocene-Eocene transition (Eldholm et al., 1989; Skogseid, 1994). This continental break-up was associated with uplift of the rifted margins on both sides of the spreading Atlantic, leading to enhanced sediment supply from the elevated areas to the newly formed basins (Doré et al., 1999; Faleide et al., 2010). As a result of thermal subsidence, the subsidence had the most impact over the rift structures in the Viking Graben during the Paleogene and Neogene. While the Shetland Platform was elevated due to a volcanic center underneath Greenland and Iceland. A factor that caused the North Sea Basin to be filled up with mud and sand from the elevated mainland in the west dominated and characterized by large delta systems. Tectonic subsidence accelerated in Paleocene throughout the basin, with uplifted areas to the east and west. Subsidence rates outpaced sedimentation rates along the basin axis and a water depth of 600 m are indicated (Faleide et al., 2010). The Cenozoic sedimentation was relatively rapid, and the clayey sediments had little time to compact sufficiently to reduce the water content. Therefore, some beds display plastic folding and diapir structures due to the under-compacted clays, especially in the Eocene. Polygonal faults are also common in these mudstones. They form a network which are from several hundred meters to 1 km across (Faleide et al., 2010). At the Eocene-Oligocene transition, southern Norway became uplifted. This uplift, in combination with prograding units from both the east and west, gave rise to a shallow threshold in the northern North Sea, separating deeper waters to the south and north (Faleide et al., 2010). The Quaternary marks a cold period characterized by alternating intervals of ice ages and interstadials, with prograding and erosive ice sheets during glacial stages along with isostatic rebound of the mainland during interstadials. As a result of prograding ice sheets, it led to rapid and large glacial erosion onshore as well as rapid deposition offshore, causing large accumulations of sediments (about 1 km thick) on the seafloor over a short period of time (Ottesen et al., 2018).

Chapter 4 - Data and Methodology

The following chapter gives an overview of the data and methodology used in this thesis. 2D fault plane maps were generated based on fault models, pillar grids, and petrophysical modeling, made from seismic interpretation and well data. The software used in this thesis are Petrel, Excel, and PowerPoint.

4.1 Seismic data

The seismic dataset consists of seismic cubes and well data provided by CCG and Equinor ASA. The seismic cubes provided are CGG18M01 and NVG Final_Ki-PreSDM_Z_Fullstack_5.3.1_8 bit (Figure 4.1 and Table 4.1).

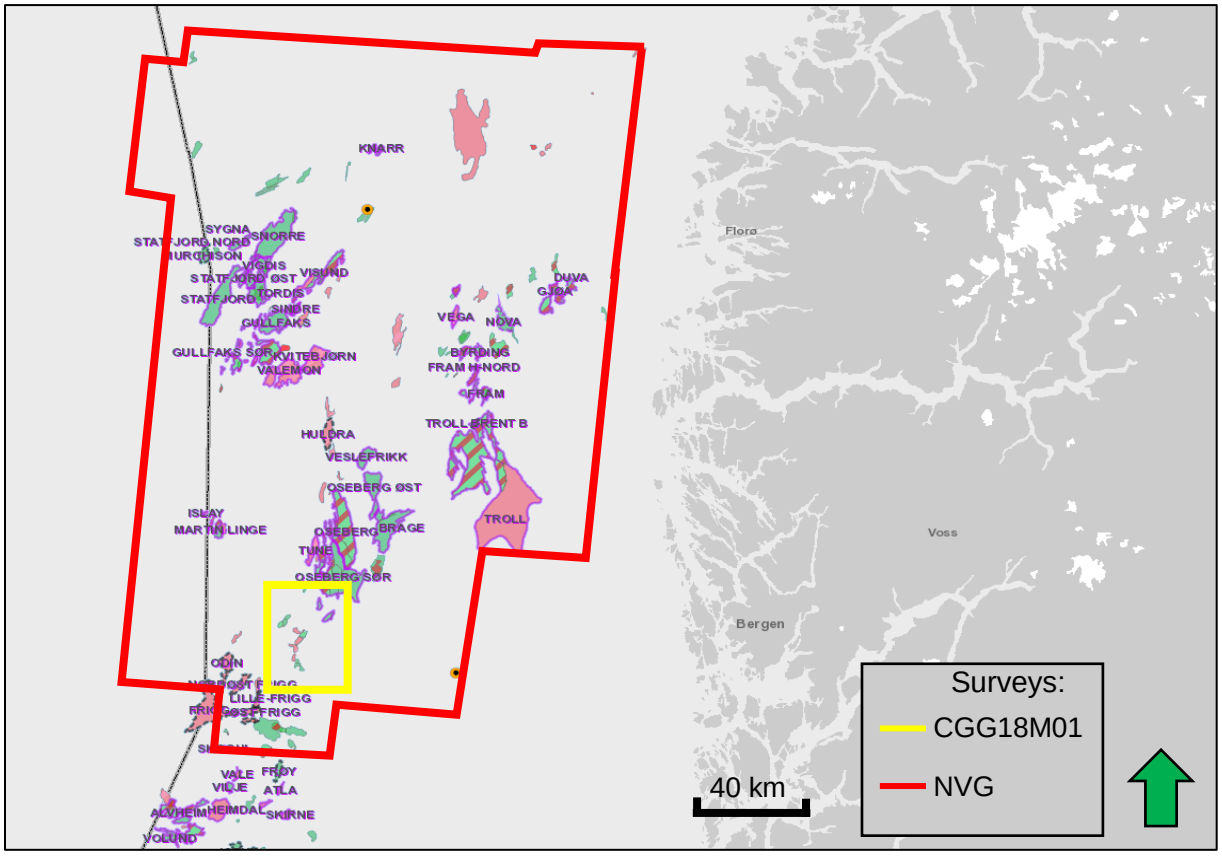

Fig 4.1: Map of the area covered by the two seismic surveys. (Modified from NPD fact-maps, 2021).

Table 4.1**:** Information on the 3D-seismic cubes.

Seismic survey	Inline rotation from North [deg]	Line orientation	Domain	Line spacing [m]
NVG	0.01	N-S E-W	Depth	18.75 12.5
CGG	0.01	N-S E-W	Time	18.75 12.5

The 2D seismic datasets are zero-phased (wavelets are symmetrical about zero). Acoustic impedance is given as $AI = \rho \cdot v$ where ρ=desity and v=velocity. Wavelets have a sinusoidal shape and represent compression and expansion. Peaks represent an increase in acoustic impedance shown as red reflectors in the seismic, and throughs represent a decrease in acoustic impedance with blue reflectors. The BCU was picked on a through (Figure 4.2). Gas-filled sands have a low acoustic impedance, while waterfilled sandstones have a higher acoustic impedance, resulting in the reflectors varying in the area.

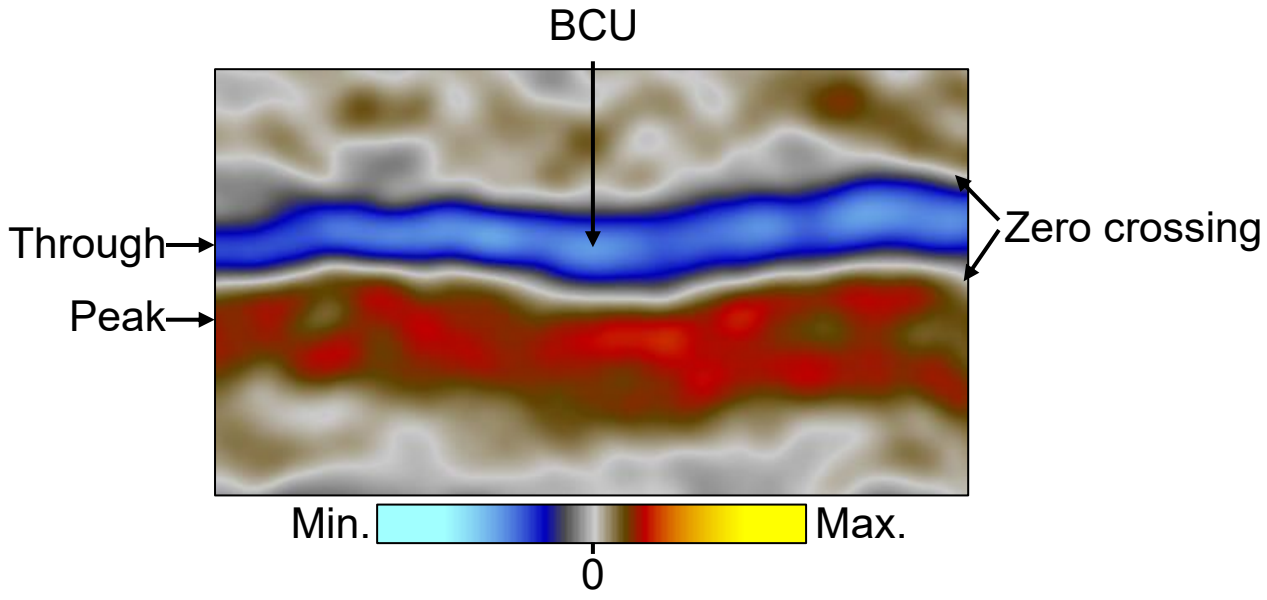

Figure 4.2: Illustration of the polarity of the seismic surveys, with red representing an increase in acoustic impedance and blue representing a decrease in acoustic impedance.

4.2 Well data

Equinor ASA provided 56 wells from the Krafla-Askja area and Oseberg Sør, with 17 wells being used in this thesis. A list of the wells used in this study is presented in table 4.2. Wells used for guidance when interpreting is also included. The locations of the wells inside the CGG cube are presented in Figure 4.2.

Table 4.2: List of the wells used in this study.

Well	Structure
30/11-5	Steinbit
30/11-8 A	Krafla West
30/11-8 S	Krafla Main
30/11-9 A	Askja E
30/11-9 ST2	Askja
30/11-10	Krafla North
30/11-10 A	Krafla Main
30/11-11 A	Viti
30/11-11 S	Madam Felle
30/11-12 S	Askja SE
30/11-13	Beerenberg
30/11-14	Slemmestad
30/11-14 B	Haraldsplass

Other wells used for seismic interpretation
30/9-16
30/9-22
30/11-6 S
30/11-12 A

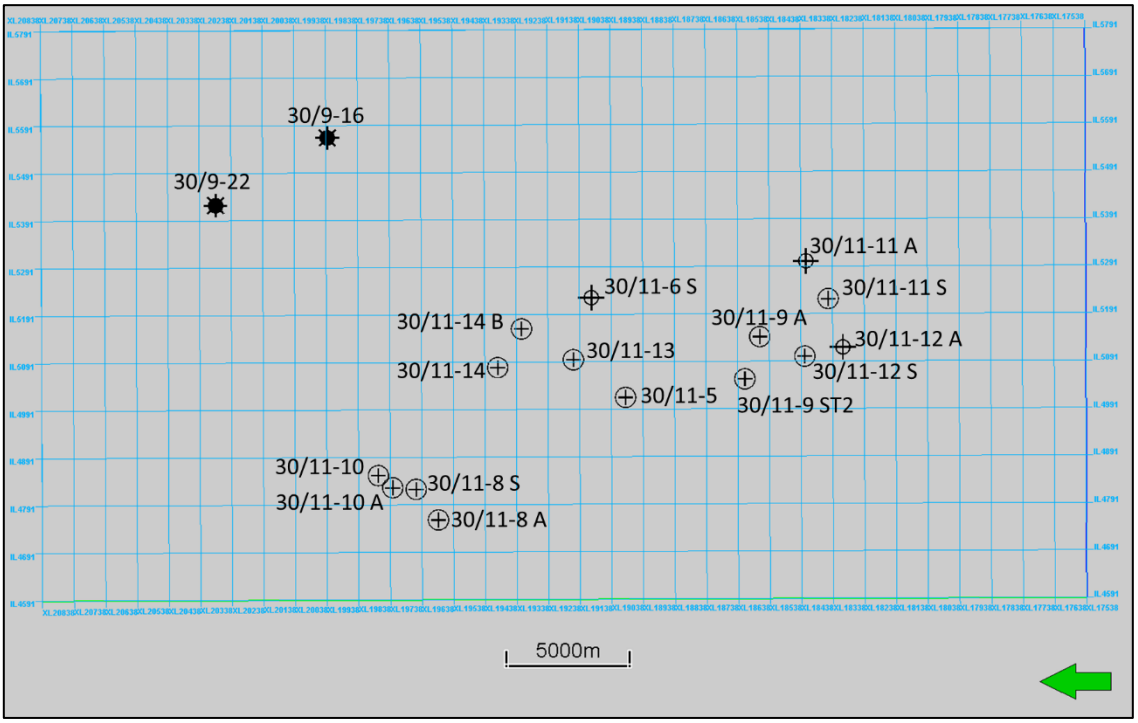

Figure 4.2: Well data used in this thesis within the CGG18M01 seismic cube.

4.3 Pressure data

Pressure data was acquired from MDT (Modular Formation Dynamic Tester) measurements from available well reports from the Norwegian Petroleum Directorate database and the Diskos database. Formation pressures from the MDT measurements were plotted using Excel, and pressure data not in SSTVD were converted. The hydrostatic pressure is the pressure applied by a fluid at equilibrium at a given point within the fluid due to the force of gravity given an open pore system. Hydrostatic pressures were calculated by using the following equation:

$$\text{P[bar]}= \frac{r \cdot g \cdot z}{10^5}$$

P=pressure, r=seawater density (1 027.3kg/m^3), g=gravitational constant (9.81m/s^2) and z=depth in SSTVD.

Overpressure was calculated based on pressure data. Overpressures were calculated using the following equation:

$$Overpressure[bar] = P - \left(\frac{r \cdot g \cdot z}{10^5}\right)$$

P=pressure, r=seawater density (1 027.3kg/m^3), g=gravitational constant (9.81m/s^2) and z=depth in SSTVD.

4.4 Fluid contacts

Fluid contacts were found using fluid gradients. The contacts were picked at the depth where the gas and oil gradients crossed the water gradients. Oil-down-to (ODT) and water-up-to (WUT) were used where contacts were not possible to be estimated. ODT and WUT gives the closest estimation of the hydrocarbon-water contacts in the wells when a fluid contact can not be found. Fluid contacts for Steinbit, Stjerne and Oseberg K was gathered from NPD.

4.5 Methodology

4.5.1 Seismic interpretation

The seismic interpretation was performed using the Petrel E&P Software Platform version 2019.3.

A detailed regional interpretation was conducted for Base Cretaceous Unconformity (BCU), top Brent Group, and top Ness Formation. The remaining interpreted horizons were conducted in the areas of interest.

The interpretation was carried out using a combination of manual interpretation and seeded 3D autotracking. The Manual interpretation tool was mainly used due to chaotic reflections and low reflection coefficient within the Brent Group. Seeded 3D autotracking was used where the reflections were clear and continuous. Random composition lines perpendicular to the faults were used for fault interpretation and interpretation across the faults of interest. Horizons were interpreted in increments of 1-64 lines depending on the structural complexity.

Gamma ray logs, resistivity, density, neutron, and porosity were used together with well reports to determine which segments of the stratigraphy that have good and poor reservoir properties (Figure 4.3). The API cut off was chosen at 60, with values less than 60 meaning sandstones and values above 60 being shales.

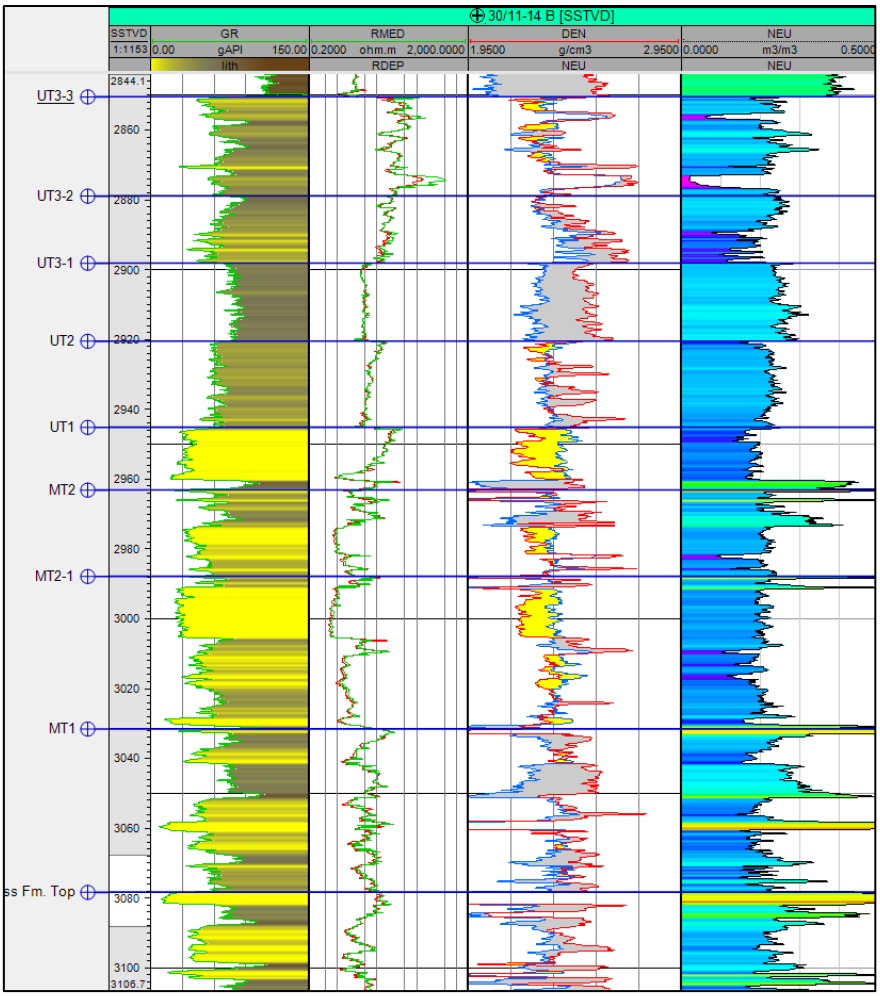

Figure 4.3: Figure showing different well logs used to determine the zones which have god reservoir properties.

4.5.2 Fault analysis

The interpreted faults were converted into faults in a fault model in the depth domain. The faults were then cut/extended to cover the area between the BCU and top Dunlin Group, before a pillar grid was created using the fault model. Ten Horizons (11 when working in the Krafla area) were inputted together with the corresponding well tops.

For fault seal analysis, identifying reservoir juxtaposition areas across the fault surface is important. Therefore, 2D fault juxtaposition plots were created from the faults in the model to identify the reservoir juxtapositions. The operation creates 2D fault plane maps for each of the faults that occur within the grid. This feature shows which zones are juxtaposed across the fault, giving a clear and vital view of where the sands are juxtaposed across the fault and if the juxtaposed areas could be sealing or work as a migration route.

After the reservoir juxtapositions were mapped, the pressure on both side of the sand-sand contacts were assessed to find the across fault pressure difference.

Vshale logs are used from well data to calculate the Shale gouge ratio (SGR) along the faults. The logs have a Vshale value going from 0% being sandstone and 100% being shale. The 100% value is likely to be computed from shales in the Heather Formation and 0% from sands in the Tarbert Formation (Figure 4.4). An API cutoff of around 45 looks to be set to 0% shale for the Vshale logs.

The Vshale log varies within the zones. The zones in the model were thus divided into multiple layers until the average zinc had a value between 1.5 and 2.5, creating the layering seen on the right-hand side in Figure 4.4. Well log upscaling was used to assign the Vshale values to the cells penetrated by the wells in the 3D grid.

A petrophysical model was made using the Vshale logs. The method used for the zones is "Moving average." This method finds an average of input data and weights according to the distance from the wells. The algorithm creates values for all cells and will not generate values larger or smaller than the min/max values of the input data. The major/minor ratio and the vertical range were set to 1. The moving average algorithm is given as:

$$p(x, y, z) = \frac{1}{W} \sum (w_i \cdot q_i)$$

Where (x,y,z) is the location of the cell center, q_i is the upscaled cell values included in the summation, w_i is the weighted values, and W is the sum of the weights, which forces the effective sum of the weights to be one. The point weighting used is "inverse distance squared" given as $1/(d_i \cdot d_i)$. This method weights far points less than the points closer to the grid node and is recommended in most cases. The interpolation is set to follow the layers.

The fault clay prediction was then calculated from fault seal analysis. SGR was chosen for the clay mixing model.

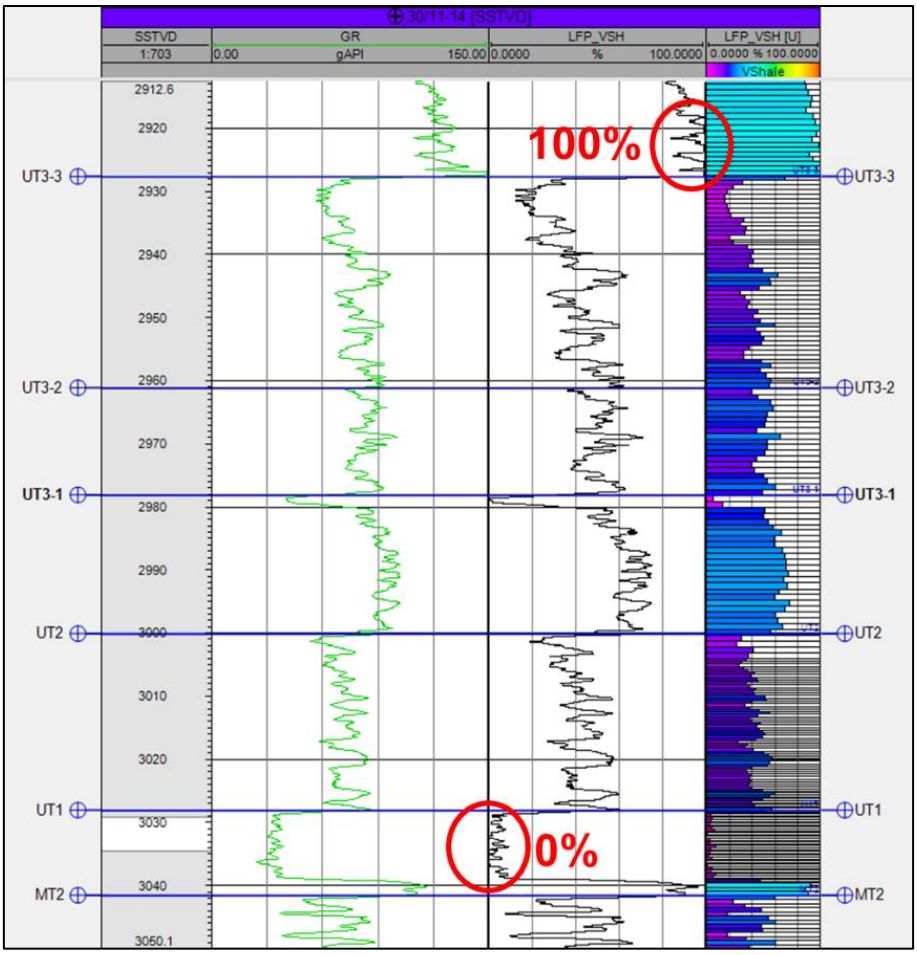

Figure 4.4: Gamma-ray and Vshale logs from well 30/11-14 showing 100% Vshale in the Heather Formation and 0% Vshale in UT1.

Chapter 5 - Results

The following chapter will present the results from the seismic interpretations, modeling, and fault analyses. Firstly, a map view of the seismic interpretations of Base Cretaceous Unconformity and Top Brent are presented to give a broader understanding of the study area, followed by proven fluid contacts and the stratigraphy of the different structures (Subchapter 5.1). Secondly, the study area has been divided into three smaller areas (Askja, Central & Krafla), where pressure data and fault plane diagrams will be presented (Subchapters 5.2-4). Only faults separating wells containing hydrocarbon(s) and a possible open fault will be presented. Fault planes towards Viti (dry structure) and Steinbit (minor oil) are not presented in this chapter. The data collected from the 13 faults are presented in the Appendix.

5.1 Horizons, compartmentalization, and fluid contacts

The Base Cretaceous Unconformity (BCU) is presented in Figure 5.1 The horizon show that the area is at its shallowest in the northeast and is deepening towards the Viking Graben in the west. The locations of where the wells used in this study have been drilled are shown on top of the BCU. The main reservoir in the area is the sandstones in the Middle Jurassic Brent Group. Hydrocarbons have also been found in parts of the Viking Group; however, this thesis will only focus on the hydrocarbons in the Brent Group, mainly the hydrocarbons in the Tarbert Formation.

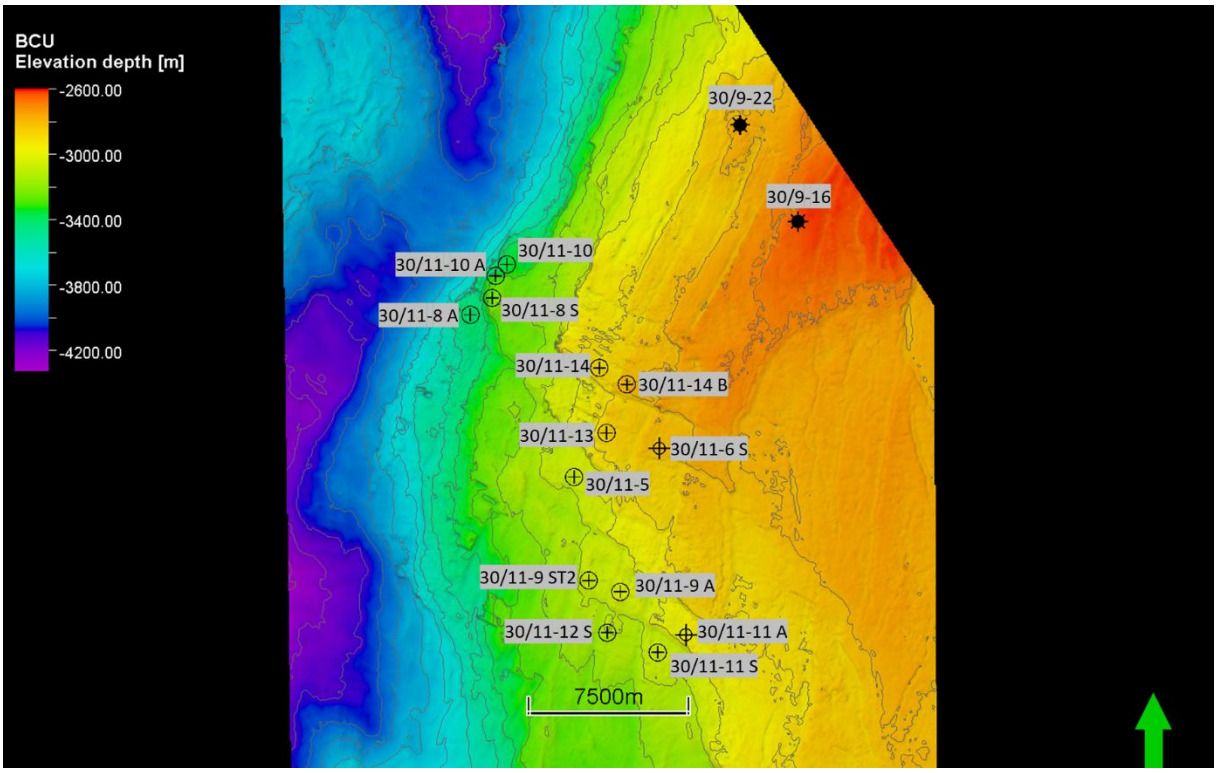

Figure 5.1: Map view of Base Cretaceous Unconformity with the wells used in this thesis.

The top Tarbert Formation (Top Brent Group) is presented in Figure 5.2 with interpreted faults and the 15 structures mentioned in this study. The Tarbert Formation is found at a depth of 2 750 – 4 000 m and has a thickness of 240 to 360 m. The fault pattern in the area is complex, creating multiple individual structures with different fluid contact depths and hydrocarbon columns that reach deeper than the spill points. The majority of faults have a strike orientation of either NNE-SSW parallel to the Viking Graben, or WNW-ESE perpendicular to the Viking Graben (Figure 5.2). The three Krafla structures next to the Viking Graben do not follow the same trend as the rest of the area. The three structures make up a horst structure where Krafla Main (the middle block) is the upthrown block. The faults separating the blocks have a fault strike orientation of E-W and N-S, slightly deviating from the study area's main fault trends. The fault throw between the studied structures varies from 0 m of displacement to 350 m measured at sand-sand juxtapositions along 13 fault planes.

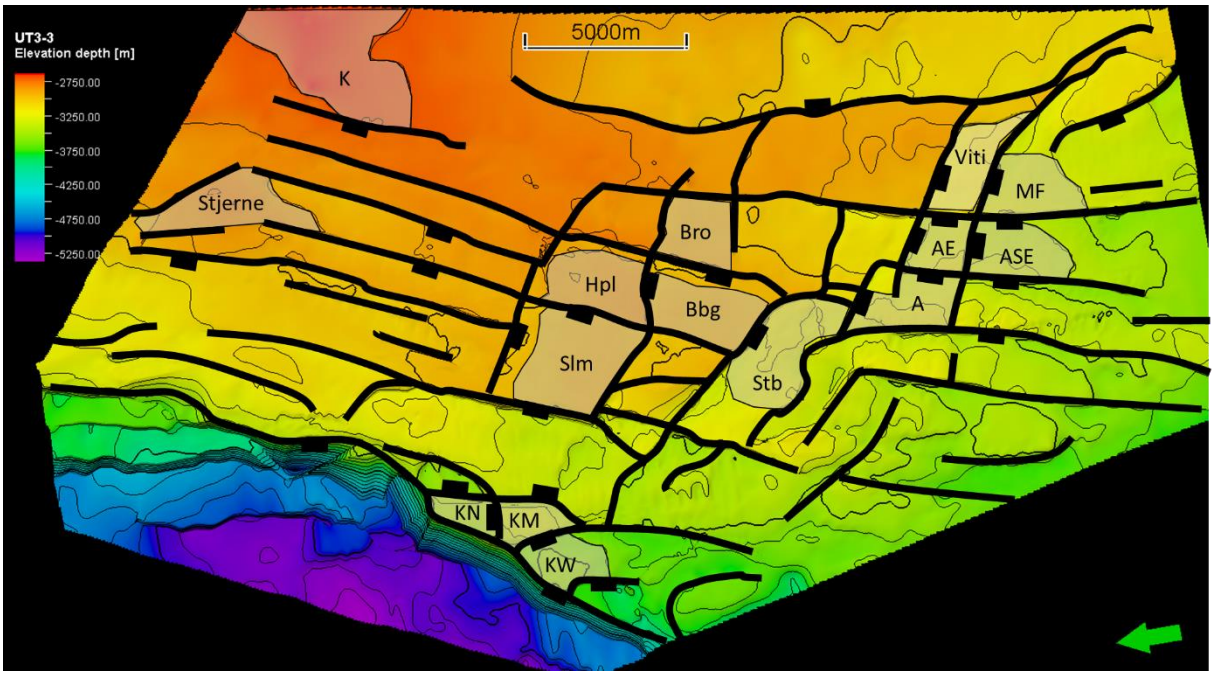

Figure 5.2: Map of Top Brent Group with faults shown with black lines. The structures mentioned in this study are shown with a transparent gray color. KN=Krafla North, KM=Krafla Main, KW= Krafla West, Slm=Slemmestad, Hpl=Haraldsplass, Bbg=Beerenberg, Bro=Brontes, Stb=Steinbit, A=Askja, AE=Askja East, ASE=Askja Southeast, MF=Madam Felle, K=Oseberg K.

5.1.1 Compartmentalization in the Krafla-Askja area

The lithology of the Brent Group and the complex fault pattern in the study area have resulted in compartmentalized structures with multiple fluid contacts and pressure regimes. The Tarbert Formation is divided into an Upper, a Middle, and a Lower part. The transgressive part of the formation is Upper Tarbert and is devived into five zones, UT3-3 (the upper-most zone), UT3-2, UT3-1, UT2, and UT1. Both UT3-2 and UT3-1 are interpreted as poor reservoirs and are shown as one single zone in this study. The regressive part of the formation is Middle and Lower Tarbert. Middle Tarbert is divided into three zones, MT2, MT2-1, and MT1. Lower Tarbert was not interpreted as it is either a thin zone or non-existent in the study area. For the structures where Lower Tarbert does occur, it is interpreted together with MT1 as the two zones are of poor reservoir quality.

The study area is divided into three smaller areas: Askja, Central, and Krafla, based on location and lithological differences in the Tarbert Formation.

The Askja area is located in the southern part of the study area and consists of four hydrocarbon structures, Askja, Askja East, Askja Southeast, and Madam Felle. The zones which are

interpreted to have good reservoir properties are UT3-3, UT2, UT1, and MT2-1, where UT2 and UT1 work as one segment (Figure 5.3).

The Central area consists of Beerenberg, Haraldsplass, and Slemmestad, where the sands with good reservoir properties are the same as those in Askja. However, in the Central area, UT2 and UT1 are interpreted to work as two separate segments. This is due to gas accumulating in UT2 and oil in UT1 Haraldsplass. If this were one compartment, then there would be a gas-oil-contact. This contact would be at a shallower depth than the gas measurements in UT2. Furthermore, the two zones at Slemmestad are interpreted to be two separate compartments. This is due to a formation pressure decrease in the water-bearing UT1 zone.

The lithology in the Krafla area differs from the rest of the study area. The top of the Tarbert Formation has been affected by erosion, which has resulted in hydrocarbon accumulation in the UT3-3 sands in Krafla West only. The UT2 zone does not have good reservoir properties, but the zones from UT1 sown to base MT2-1 do have good reservoir properties (Figure 5.3). The four zones are interpreted to work as one compartment at Krafla West while being compartmentalized in Krafla Main and Krafla North. In Krafla Main, the UT1 zone is interpreted to have two separate compartments as oil is found both shallower and deeper than a water sample. The UT1-1 (lower UT1) compartment is interpreted to be the same compartment as the deeper reservoir sands. Three different oils are found within the three reservoir zones at Krafla North, suggesting three pressure compartments, UT1-2, UT1-1 and MT2, and the deepest being MT2-1 (Figure 5.3).

The Ness Formation is shown as one zone in this study. However, the formation does contain sands with different fluid and pressure compartments, but these were difficult to interpret seismically. Instead, a rough estimation of an upper, middle, and lower compartment were used when necessary.

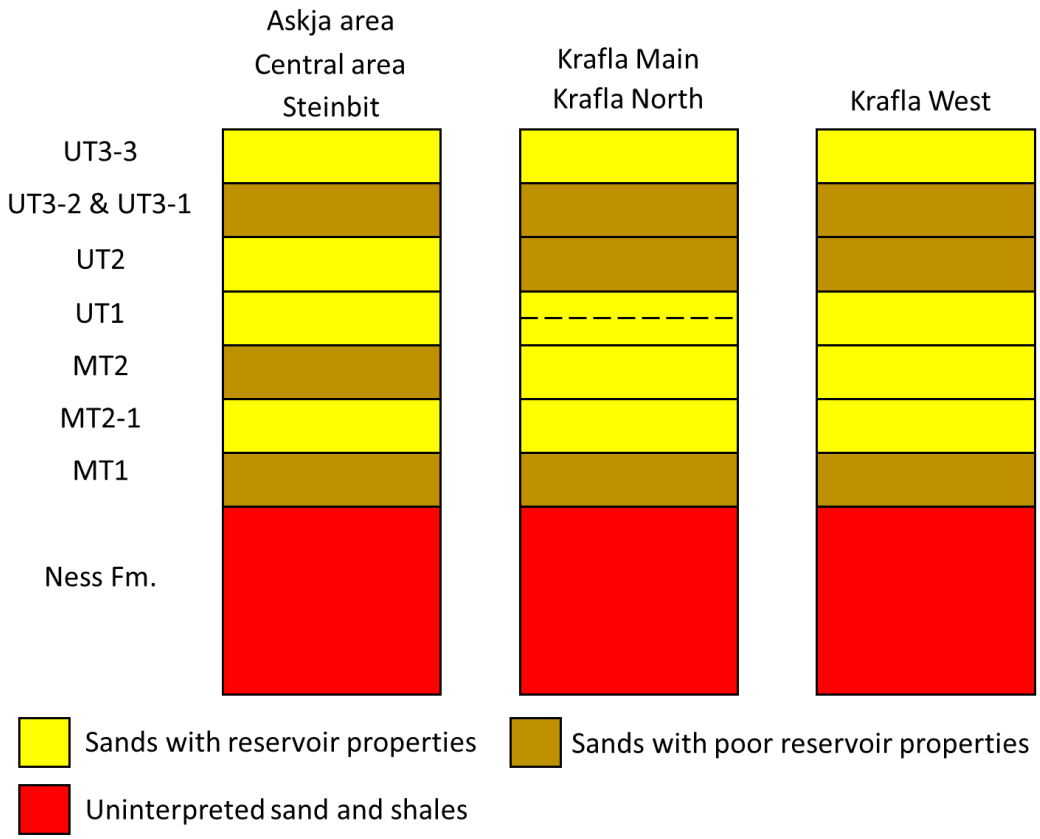

Figure 5.3: Simplified illustration of the Tarbert and Ness Formations in the study area. The yellow color represents the zones with good reservoir properties in the Tarbert Formation. The brown color represents zones with predominantly poor reservoir properties, which acts as a seal to the underlying fluids. The Ness Formation is represented by a red color and consists of rocks with good and poor reservoir properties.

5.1.2 Fluid contacts

Formation pressure data from 11 wells were gathered and used to determine 18 fluid contacts in the Krafla-Askja area. The fluid contacts in Steinbit and the contacts in the Stjerne and K structures north of the main study area are gathered from NPD and converted to SSTVD. A fluid contact was not possible to estimate for all hydrocarbons. For these hydrocarbons, an ODT or a WUT were used. The fluid contacts in the Krafla-Askja area are presented in Figure 5.4 with the contact depths, and Figure 5.5 where the contacts, ODTs, and the WUT are shown on the deepest horizon where the hydrocarbons are accumulating. The depth of the fluid contacts ranges from 2 883 m at Haraldsplass to 3 770 m at Krafla West. The deepest contacts are found in the three Krafla blocks, with Krafla West having the deepest and the Krafla Main horst having the shallowest. The shallowest contacts are observed in the Central area, with Haraldsplass having the shallowest. The fluid contacts are generally shallowing with the bathymetry of the area. The Steinbit structure situated between Askja and Beerenberg does have a deeper contact

than the Askja structure. However, the fluid contact at Askja is found within UT1, while the contact in Steinbit is located within MT2-1. The shallowest contact in Steinbit is found in UT1 with a shallower depth than Askja. None of the hydrocarbons are found to have the same fluid contact depth.

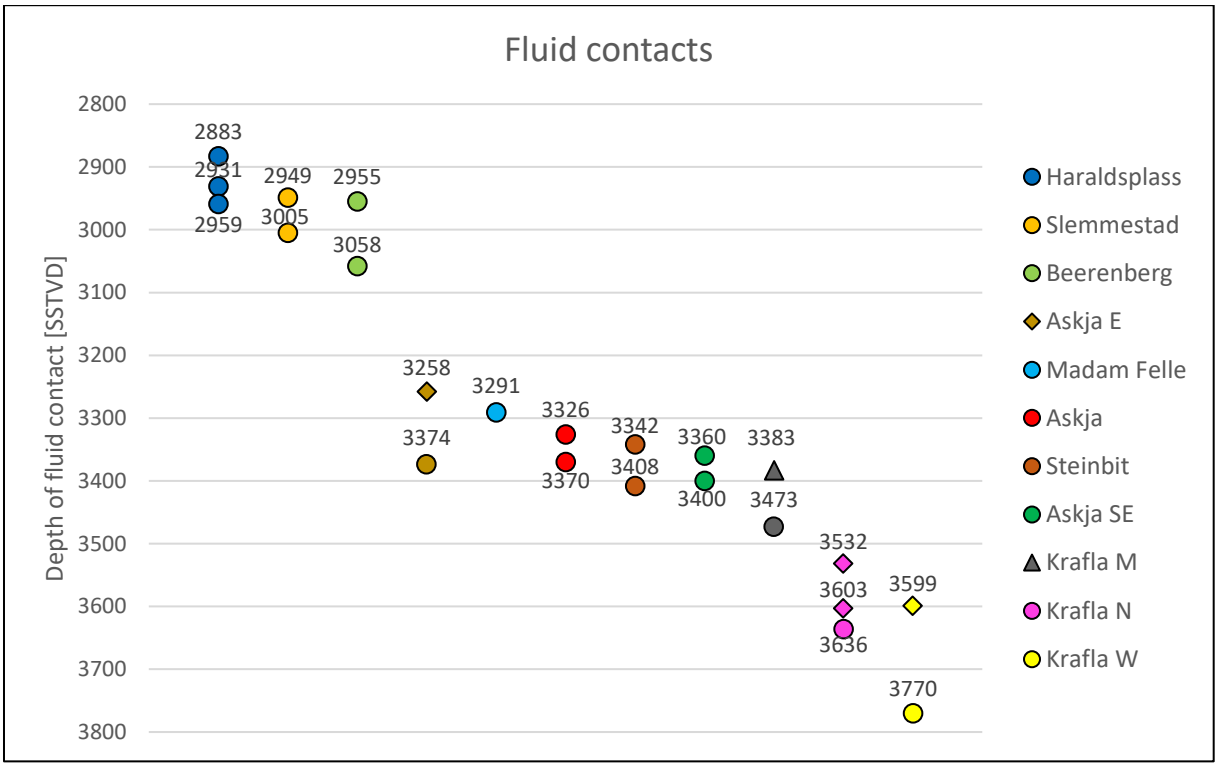

Figure 5.4: Depth of the fluid contacts in the Krafla-Askja area ordered by the shallowest contact in each structure. Circles represent the fluid contacts, diamonds represent ODTs, and the triangle represents WUT.

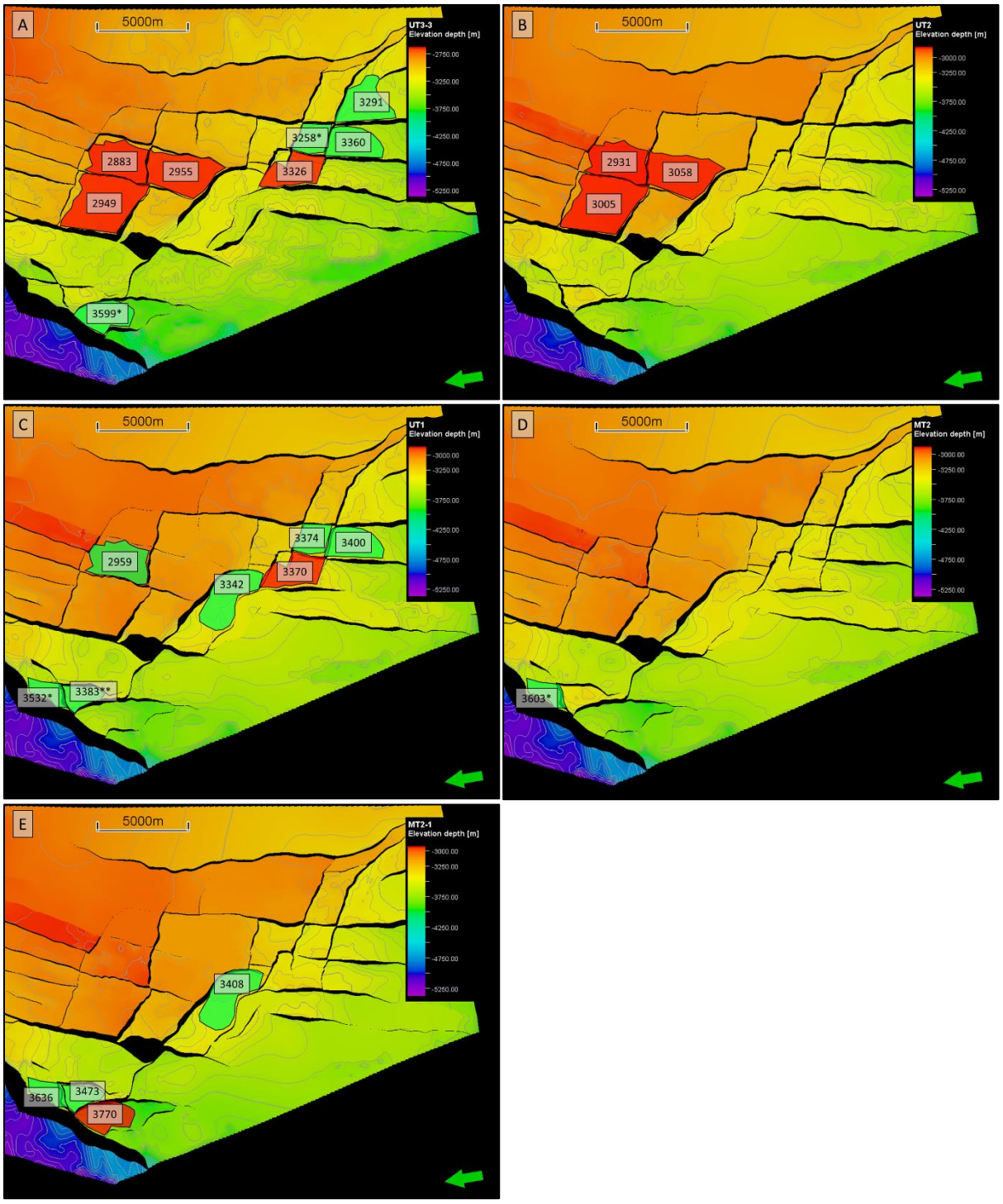

Figure 5.5: Proven fluid contacts in UT3-3 (A), UT2 (B), UT1/UT1-2 (C), and MT2-1 (D). Red=Gas, green =oil, *=ODT, **=WUT.

5.1.3 Pressure data

The Krafla-Askja area consists of a wide range of formation pressures, both across faults and within a structure. Figure 5.6 shows the formation pressures from 13 wells in the area and how the pressures deviate from hydrostatic. The pressures increase with depth, with the Central area having the lowest pressures and the Krafla structures the highest. The amount of overpressure is generally increasing with depth in the area (Figure 5.7). The Central area, Madam Felle, Viti, and most of the Askja structure are moderately overpressured. Askja Southeast and the majority of Askja East have pressures ~20 bars higher than hydrostatic. The Steinbit structure has an overpressure of 38 bars being the highest pressured structure besides the Krafla blocks. The highest overpressures are found within the three Krafla structures. Krafla Main and Krafla North are ~75-94 bars overpressured, while Krafla West have more than doubled the overpressure with 210-234 bars in the Tarbert Formation. Figure 5.8 shows the overpressure in the different pressure compartments. All the studied compartments are moderate to highly overpressured apart from two compartments being normally pressured, these being the water-bearing UT1 and MT2-1 Slemmestad zones.

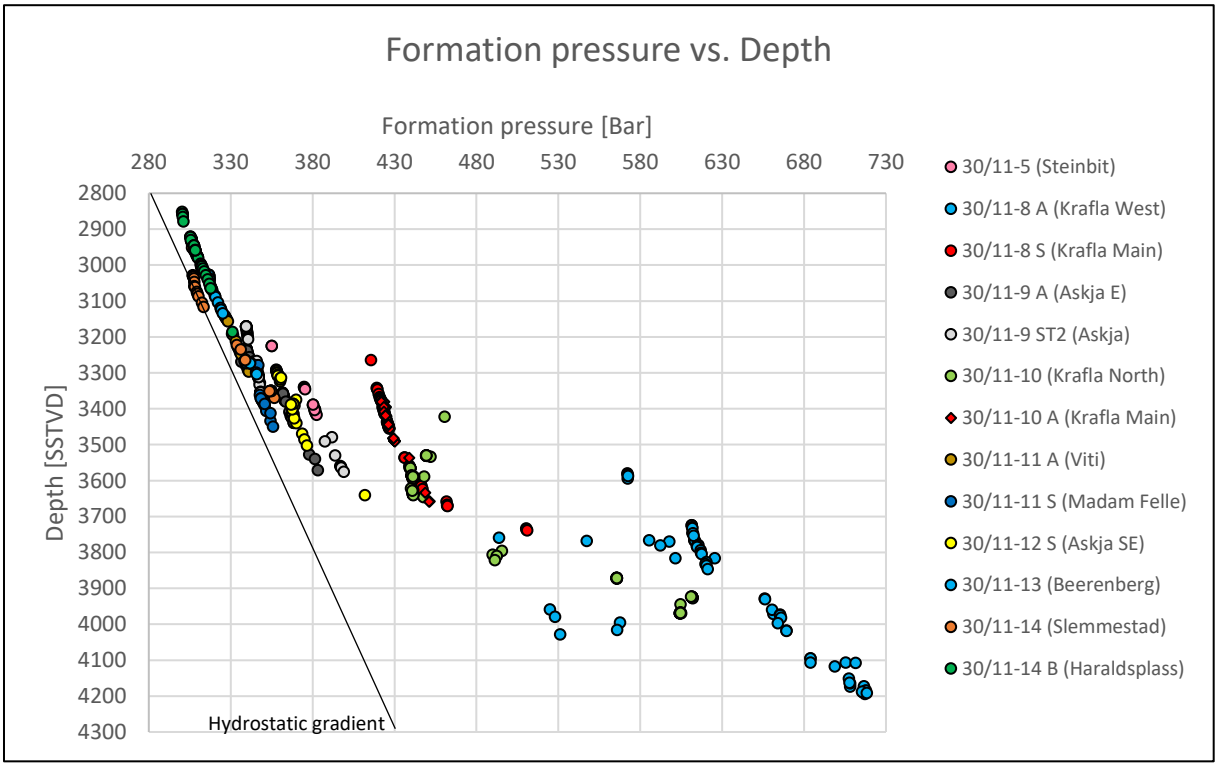

Figure 5.6: Formation pressure vs. depth plot. The hydrostatic gradient is represented with a linear black line.

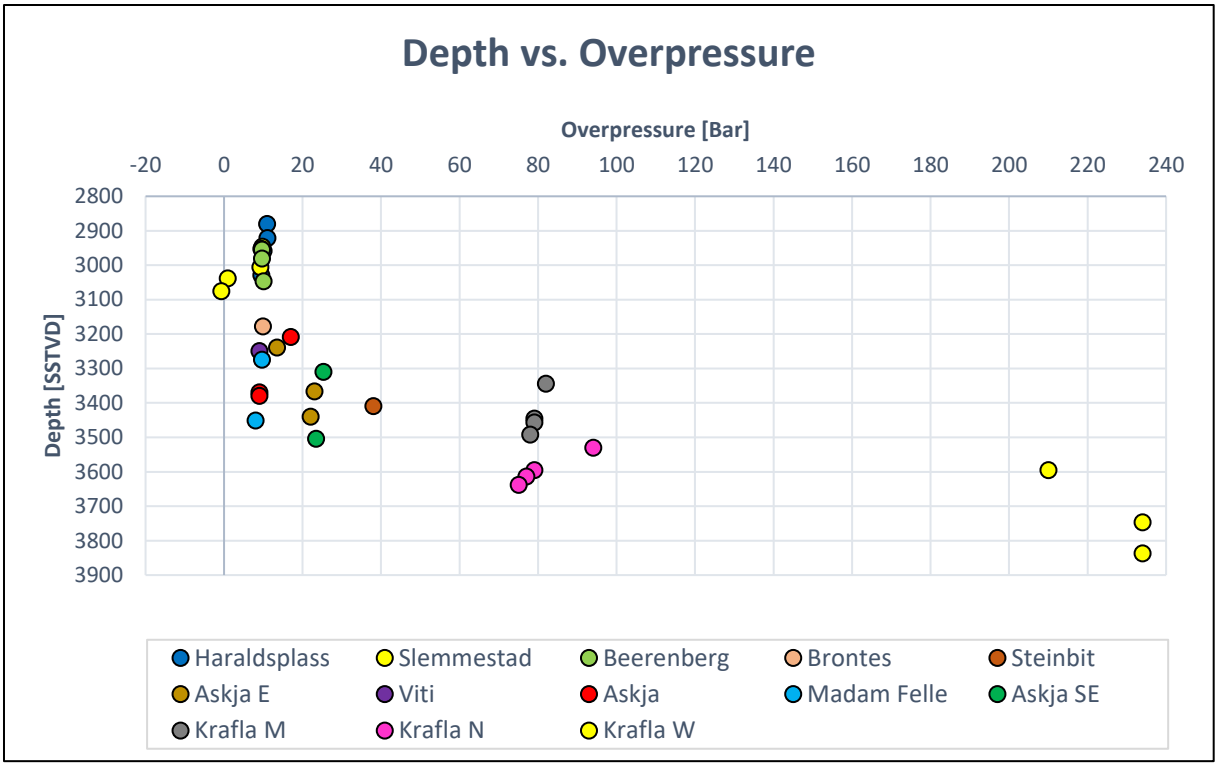

Figure 5.7: Overpressure in the Tarbert Formation vs. depth plot. 0 on the x-axis represent hydrostatic pressures.

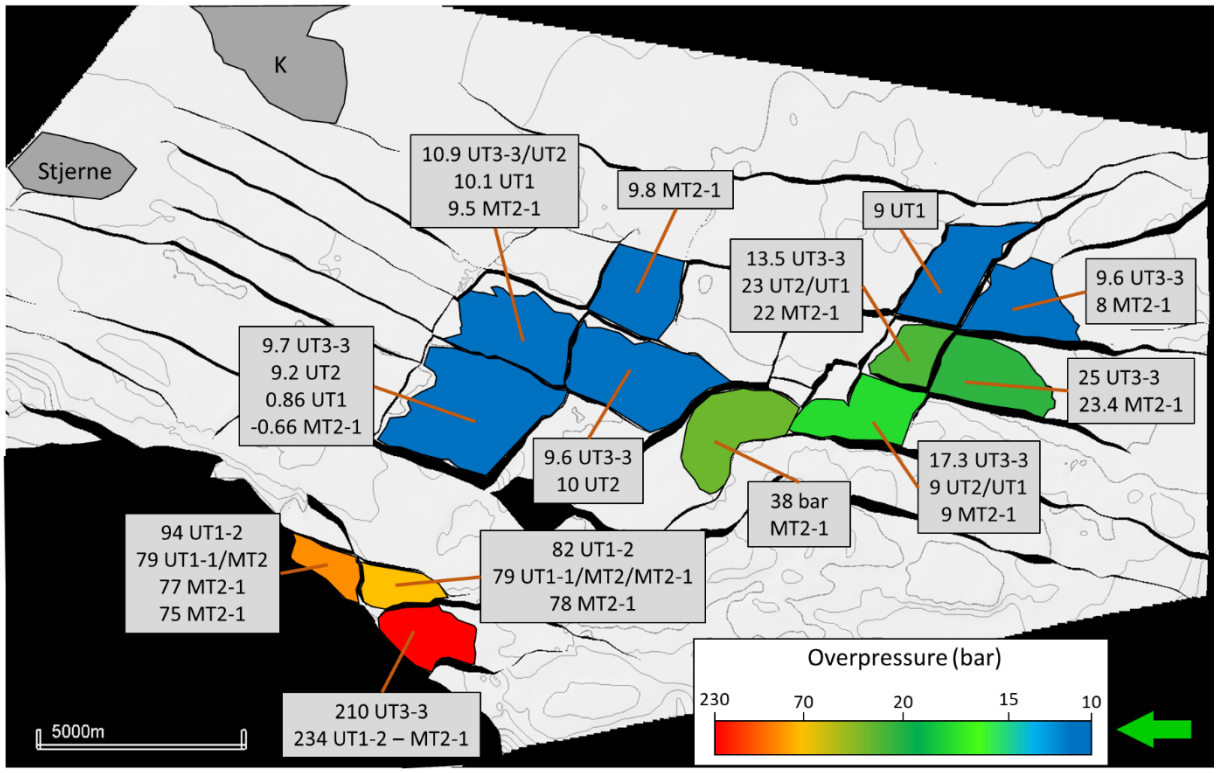

Fig 5.8: Figure illustrating the overpressure in the different pressure compartments. The color is representing the highest observed overpressured compartment within the structure.

5.2 Askja Area

The Askja area is located in the southern part of the study area and consists of four structures with hydrocarbon and six wells (Figure 5.9). The wells are 30/11-9 ST2 (Askja), 30/11-9 A (Askja East), 30/11-12 A, 30/11-12 S (Askja Southeast), 30/11-11 A (Viti) and 30/11-11 S (Madam Felle). Hydrocarbons are proven in two segments within Upper Tarbert, the upper segment is UT3-3 being the top reservoir in the area, and the lower segment consisting of the sands in UT2 and UT1. Madam Felle has hydrocarbon in the upper reservoir, while the three other fault blocks contain hydrocarbons in the upper and lower reservoirs. MT2-1 sands have reservoir properties but are water-bearing in all the structures. None of the fluid contacts have the same depth (Figures 5.4, 5.5 & 5.10). The structures are separated by four faults, two striking NNE-SSW and two striking WNW-ESE. The faults are dipping SSW and WNW, resulting in the western blocks being downthrown in relation to the eastern blocks and the southern blocks being downthrown in relation to the northern blocks. A cross-section going through the structures containing hydrocarbon is presented in Figure 5.10. Three faults separating the structures with hydrocarbon(s) are presented in this subchapter.

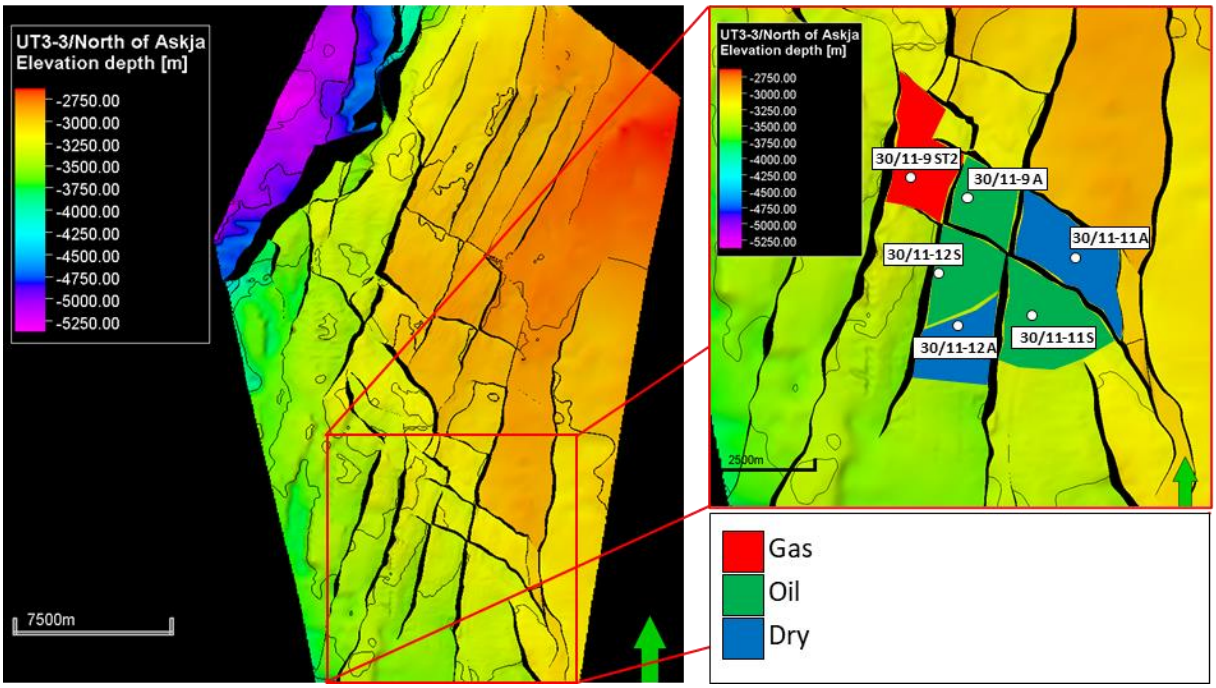

Figure 5.9: Map of Top Brent Group and the location of the Askja area. The wells are shown together with encountered hydrocarbon(s). Red=gas, green=oil, and blue=no hydrocarbons.

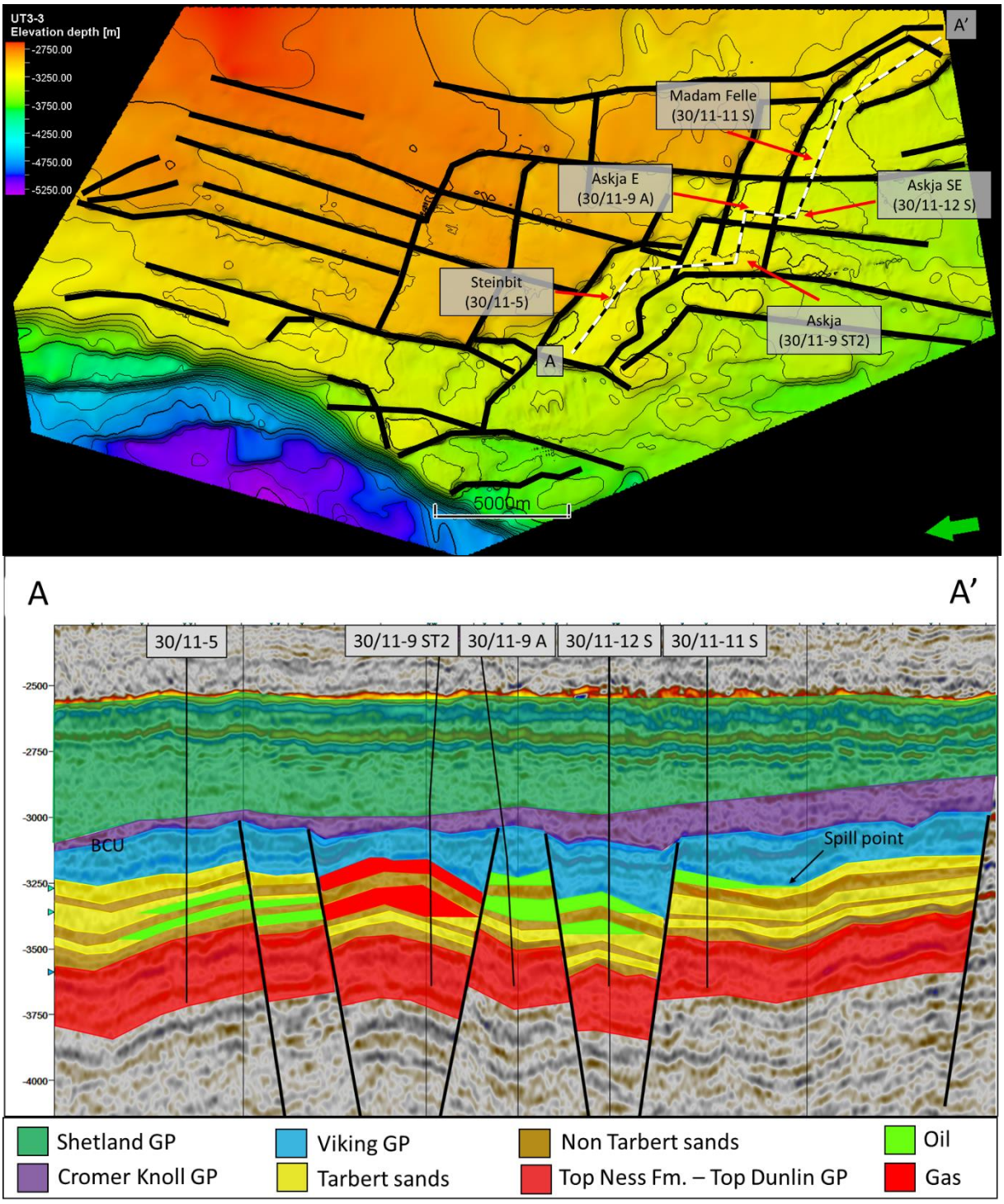

Figure 5.10: Cross-section of Steinbit, Askja, Askja East, Askja Southeast, and Madam Felle. The zones with good reservoir properties in the Tarbert Formation are shown in yellow. Red in the Tarbert Formation is gas, and green in the Trabert Formation represents oil.

Formation pressure from wells 30/11-5, -9A, -9ST2, -11A, -11S, and -12S are presented in Figure 5.11. The scattered pressures indicate multiple pressure regimes. The pressures seem to fall into three different sections. Viti, Madam Felle, the Tarbert Formation in Askja, and UT3-3 Askja East fall into the section with the lowest formation pressures. The second section has

more than 10 bars higher pressures than the lower trend and consists of the rest of the Askja East structure, the Tarbert Formation in Askja Southeast, and UT3-3 Steinbit. The third section has the highest pressures and consists of the rest of Steinbit, the Ness Formation in Askja, and a pressure-point from the Ness Formation in Askja Southeast. These pressures are ~13 bars higher than the pressures in the second section.

None of the hydrocarbons were found to have the same fluid contacts. Two GWCs are observed in Askja (3 326 m for UT3-3 and 3 370 m for UT2 and UT1). Two OWCs are observed in Askja Southeast (3 360 m for UT3-3 and 3 400 m for UT2 and UT1). One contact was observed for UT2 and UT1 for Askja East at 3 374 m depth. An ODT 3 258 m is used for the oil in UT3-3 Askja East. The pressures from the UT3-3 oil have lower pressures than the water gradient for the rest of the structure; an OWC could thus not be estimated. The oil in UT3-3 Madam Felle has a fluid contact at 3 291 m depth and is possibly controlled by spill towards the southeast.

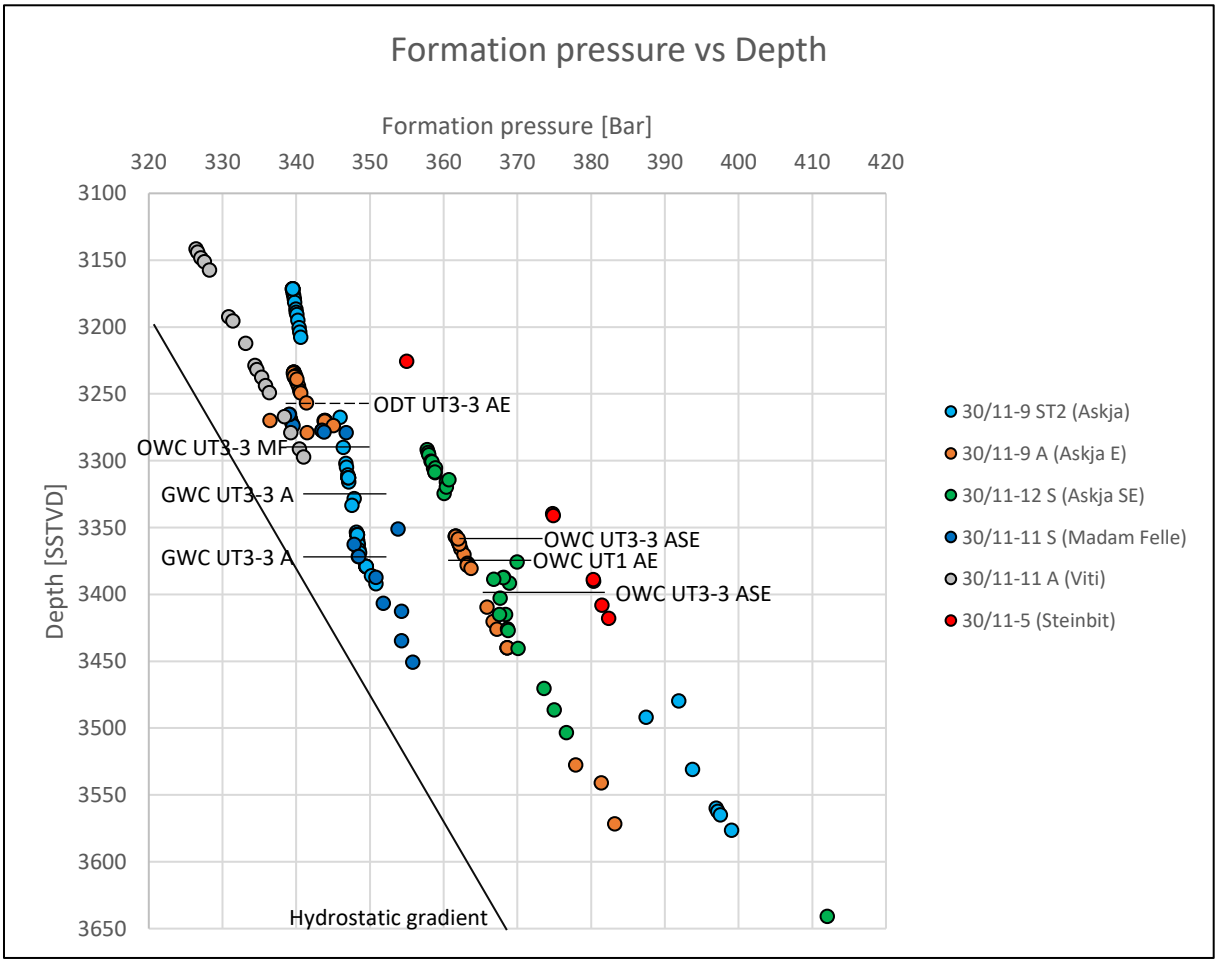

Figure 5.11: Formation pressure from five wells in the Askja area and Steinbit. Fluid contacts are represented with black horizontal lines, and the ODT UT3-3 Askja E is represented with a black dashed line.

5.2.1 Askja

Well 30/11-9 S was drilled in 2013 to prove commercial hydrocarbon in the lower parts of the Heather Formation and the Tarbert, Ness, and Etive Formations (NPD, 2021). The deepest penetrated formation reached by well 30/11-9 ST2 was the Ness Formation. The well proved gas in two pressure compartments within the Tarbert Formation. NPD gives a GDT for the upper compartment and a GWC at 3 369 m for the lower compartment, which is the same as the one used in this study. A GWC at 3 326 m depth for the upper compartment is found using the water gradient from the rest of the well. The Ness Formation was found to have good reservoir properties but was water-bearing with no oil shows.

5.2.2 Askja East

Well 30/11-9 A is a sidetrack of 30/11-9 S and was drilled to prove commercial hydrocarbon in the Tarbert Formation with secondary objectives of proving hydrocarbon in the Ness and Etive Formations (NPD, 2021). The well proved oil in two different pressure compartments. NPD has an OWC at 3 250 m depth (SSTVD) for the upper segment and an OWC at 3 378 m depth (SSTVD). An OWC in UT3-3 was not found in this study. An ODT 3 258 m was used instead. A water sample at 3 270 m was observed but interpreted as a different pressure regime. The difference in OWC in the lower compartment is 4 m, with the contact used in this study being the shallowest.Oil shows are present between the two reservoirs, while the lower part of the Tarbert Formation and the Ness Formation were water-bearing.

5.2.3 Askja Southeast

The Askja Southeast structure was drilled by well 30/11-12 S 2016 to prove hydrocarbons in three sandstone layers within the Tarbert Formation. NPD (2021) has an ODT 3 325 m (SSTVD) for the upper segment. Oil was sampled at 3 389 m depth (SSTVD), with the sandstone also having a water gradient. The deepest formation penetrated by the well was the Ness Formation. The UT3-3 and UT2/UT1 fluid contacts used in this thesis were found by using the water gradient from UT1. No valid pressure points were gathered from the oil in the lower segments. However, an oil sample was found at 3 389 m depth. The OWC was estimated by applying the same oil gradient as for the upper segment for the oil sample and moving it until it crosses the UT1 water gradient. The OWC is estimated to be at 3 400 m depth.

5.2.4 Madam Felle

The hydrocarbons at Madam Felle are detained by a WNW dipping normal fault to the west and a curved SSW to westward dipping normal fault to the north and east. A fault within the Madam Felle structure and the northern/western fault have formed a relay ramp southeast of the accumulating hydrocarbons. Well 30/11-11 S was drilled in 2016 to prove hydrocarbon in the Tarbert and Ness Formations (NPD, 2021). The well proved oil in the UT3-3 compartment, with the rest of the sandstones being water-bearing. No oil shows were recorded in the well apart from UT3-3.

5.2.5 Viti and Steinbit

Well 30/11-11 A was drilled in the Viti structure in 2016. The objective was to test hydrocarbon potential in the Tarbert Formation; however, all the sands were water-bearing with no hydrocarbon shows (NPD, 2021). Well 30/11-5 was drilled in the structure between Askja and Beerenberg. The well, which was drilled in 1996-1997, had the objective to test the presence of hydrocarbon in the Brent Group (NPD, 2021). A total of 19.2 m net oil pay distributed in several thin intervals was encountered in the well. The well was initially classified as a dry well with minor oil, but two OWC's were placed. One in UT1 at 3 342 m, and one in MT2-1 at 3 408 m depth (SSTVD).

A summary of the wells, structures, fluid contacts and pressures in the Askja area is shown in table 5.1.

Table 5.1: Summary of the wells, structures, reservoir units, fluid contacts, pressure points, and overpressure in Steinbit and the Askja area.

Well	Structure	Reservoir unit (SSTVD)	GWC/OWC/ ODT*	Pressure point (SSTVD)	Fluid	P.P. (Bar)	O.P. (Bar)
30/11-5	Steinbit	MT2-1		3 408.08	Water	381.453	37.99
30/11-9 A	Askja E	UT3-3	3 258*	3 238.92	Oil	339.899	13.48
		UT2&UT1	3 374	3 366.13	Oil	362.3	23.06
		MT2-1		3 440.07	Water	368.581	21.89
30/11-9 ST2	Askja	UT3-3	3 326	3 207.73	Gas	340.587	17.31
		UT2&UT1	3 370	3 369	Gas	348.565	9.04
		MT2-1		3 379.26	Water	349.508	8.95
30/11-11 A	Viti	UT1		3249.15	Water	336.312	8.87
30/11-11 S	Madam Felle	UT3-3	3 291	3 273.82	Oil	339.533	9.60
		MT2-1		3 450.78	Water	355.798	8.03
30/11-12 S	Askja SE	UT3-3	3 360	3 308.96	Oil	358.812	25.34
		UT2&UT1	3 400	N/A	Oil	N/A	N/A
		MT2-1		3503.52	Water	376.63	23.44

5.2.6 Askja–Askja East

The fault separating Askja and Askja East is an NNE-SSW striking normal fault with a dip towards WNW. Askja is the downthrown block and is situated west of Askja East (Figure 5.10 and 5.14). The throw along the fault plane ranges from 0 – 160 m. A minor ESE-WNW-oriented fault was found within Askja down throwing the southeastern side of the block. Wells have been drilled in both the upthrown block (30/11-9 A) and the downthrown block (30/11-9 ST2). The two fault blocks are compartmentalized, containing hydrocarbon in two segments within the upper Tarbert Formation (UT3-3 and UT2/UT1). Pressure data from wells -9A and -9ST2 indicate different pressure regimes for both wells (Figure 5.12). The Tarbert Formation seems to have one pressure regime in well -9ST2, while the Ness Formation has ~30 bars higher pressures. Well -9A shows that the UT3-3 gas has lower pressures than the rest of the well. The two fault blocks do not share any formation pressures or fluid contacts.

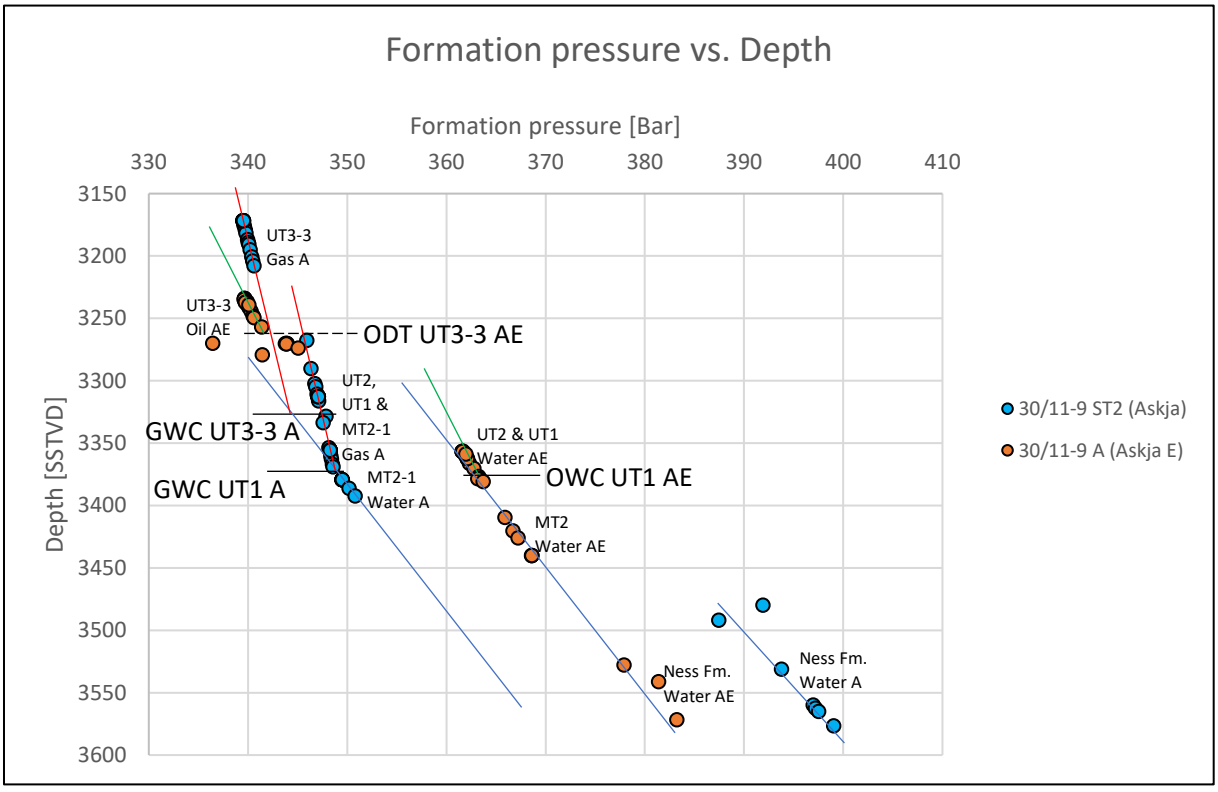

Figure 5.12: Formation pressure vs. depth. Pressure data from wells -9A (orange) and -9ST2 (blue) are plotted with fluid gradients (red=gas, green=oil, blue=water) and fluid contacts.

A 2D fault plane diagram was created to map sands-sand juxtapositions along the fault plane. These juxtaposed areas work as the fault spill points when the fault is open. The fault itself should be sealing when the hydrocarbon column accumulates deeper than the spill point and is juxtaposed to a different fluid across the fault. There are six areas along the fault plane where Tarbert sands are juxtaposed across the fault (Figure 5.13), with four of the juxtaposed areas contain different fluids on each side of the fault. One of these areas is where the UT3-3 sands are self-juxtaposed. This area contains gas in Askja and water and/or oil in Askja East. An ODT 3 258 m is used for Askja East, and the juxtaposed area is located deeper than the ODT resulting in a maximum 68 m contact difference and a minimum sealed column of 18 m. The across fault pressure difference between the gas and water is ~12 bars. The oil in the lower reservoir in Askja E is juxtaposed to both gas and water in the upper and lower reservoirs of Askja, giving the oil in Askja East a minimum 94 m sealed column. The across fault pressure difference is 14 and 16 bars, and the contact differences are 48 m vs. UT3-3 and 4 m vs. UT2 and UT1 Askja. Gas in the lower Askja reservoir is juxtaposed to water in MT2-1 Askja E. The across fault pressure difference is 13 bars, and the sealed column is 2 m. The remaining Tarbert-Tarbert juxtapositions and juxtapositions against the Ness Formation are water-bearing. Three juxtapositions have hydrocarbons in the sands on both sides of the fault. The difference in fluid contacts in the UT3-3 self-juxtaposed area is a maximum of 48 m. The GWC at Askja is located deeper than the shallowest point giving the fluid an 18 m minimum sealed column (overfill). The oil in UT2/UT1 Askja East is juxtaposed to gas in both the upper and lower compartment in Askja with fluid contact differences of 4 and 68 m. The oil has a 94 m minimum seal.

The difference in throw along the fault plane results in a variety of SGR values (Figure 5.15). The SGR values are displayed where sands with good reservoir properties are juxtaposed across the fault and the areas where the Ness Formation is juxtaposed to Tarbert sands and where Ness is juxtaposed to Ness. The sands in the Ness Formation have not been individually interpreted. Instead, SGR values are highlighted for the entire plane where Tarbert sands are juxtaposed to Ness and where the Ness Formation is self-juxtaposed. The lowest SGR values are found where the different Tarbert sands are self-juxtaposed and where UT1 Askja is juxtaposed to MT2-1 Askja East. These areas are found to have a minimum SGR value of 12 to 15%.

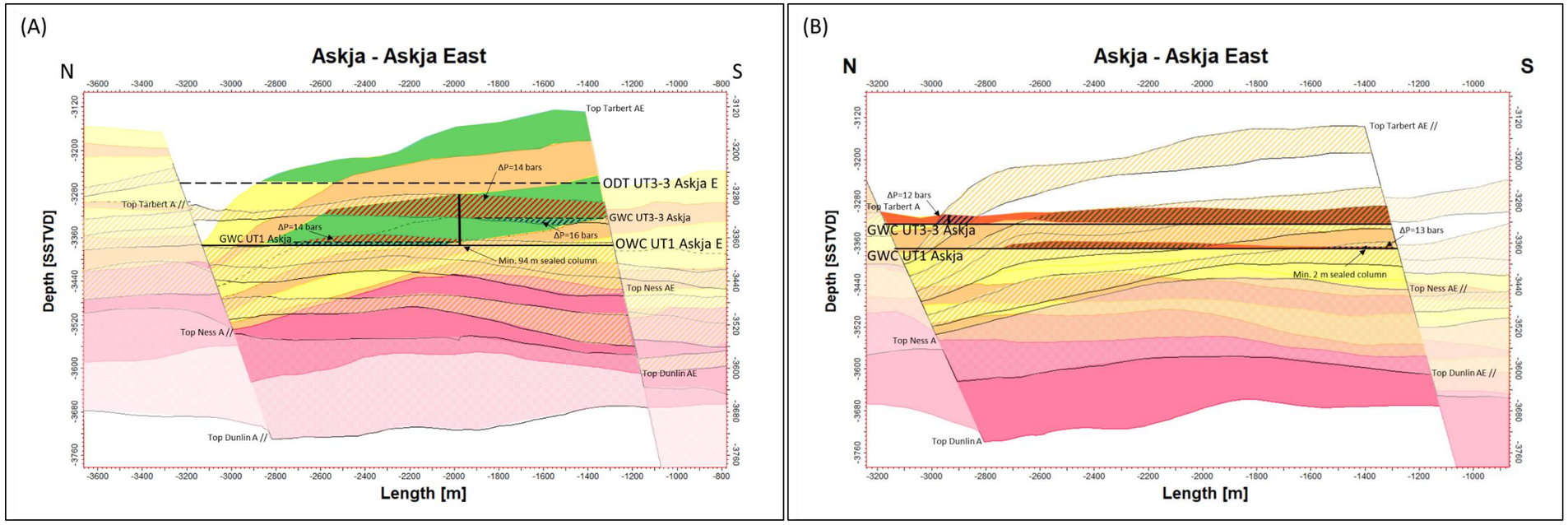

Figure 5.13: Juxtaposition plot of the fault between Askja and Askja East. The upthrown block (Askja East) is in colors, and the downthrown block (Askja) has black outlines where the sands with good reservoir properties have orange slanted lines (A). The downthrown block (Askja) is in colors, and the upthrown block (Askja East) has black outlines (B). Fluid contacts are shown with black horizontal lines. Hydrocarbons in the colored block are shown with a transparent color (gas=red, oil=green), while fluids on the side with black outlines are shown where the fluid is juxtaposed to hydrocarbons across the fault (shown with slanted lines, red=gas, green=oil, and blue=water).

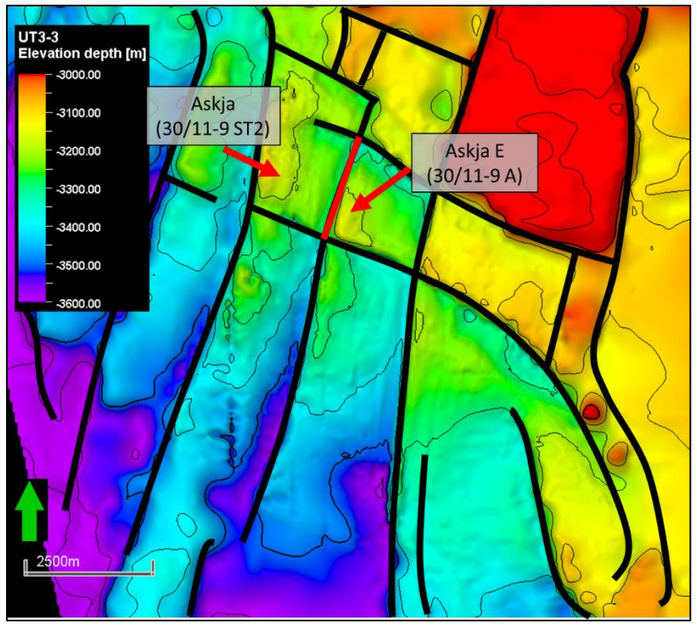

Figure 5.14: Top reservoir map of the Askja area. The red line separating the Askja and Askja East structures is the fault presented in Figures 5.13 and 5.15.

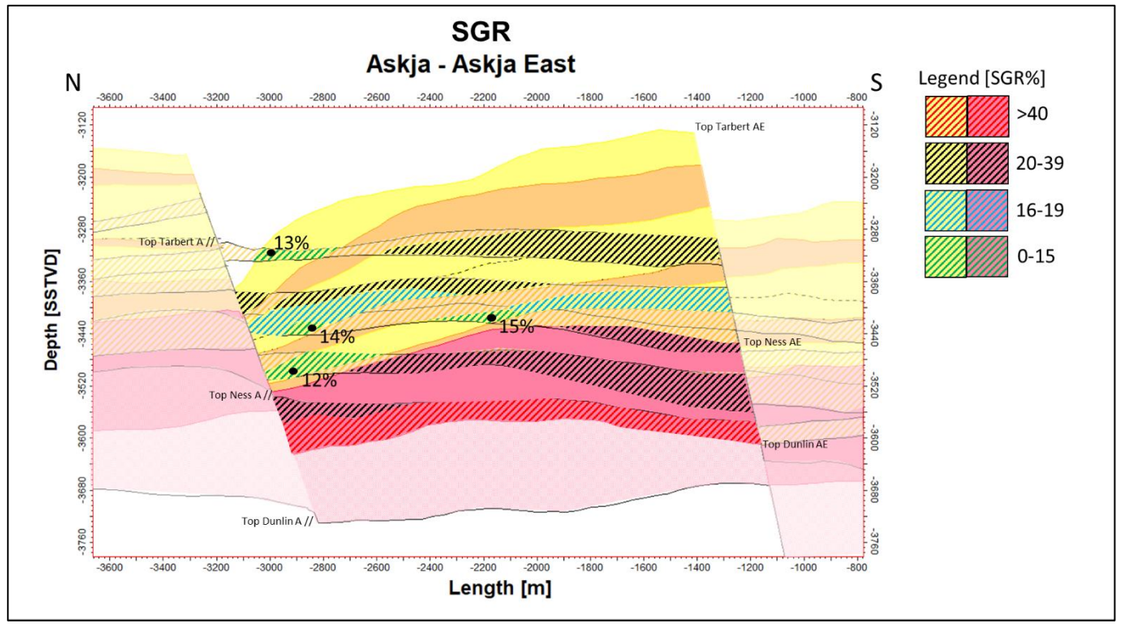

Figure 5.15: SGR plot where the SGR values are displayed where sands with good reservoir properties in the Tarbert Formation are juxtaposed against each other and Tarbert sands vs. Ness Formation and Ness Formation vs. Ness formation. SGR is color-coded in the ranges 0-15%, 16-19%, 20-39% and >40%.

5.2.7 Askja East–Askja Southeast

The fault separating Askja East and Askja Southeast is a WNW-ESE striking normal fault with a dip direction towards SSW. The fault has a throw of 120-150 m, where Askja Southeast is the downthrown block (Figure 5.10 and 5.18). Wells have been drilled in both the upthrown block (30/11-9 A) and the downthrown block (30/11-12 S). Both the wells proved oil in UT3-3 and UT2/UT1. The pressure data from wells -9A and -12S shows similar pressures but no shared fluid gradients or contacts (Figure 5.16).

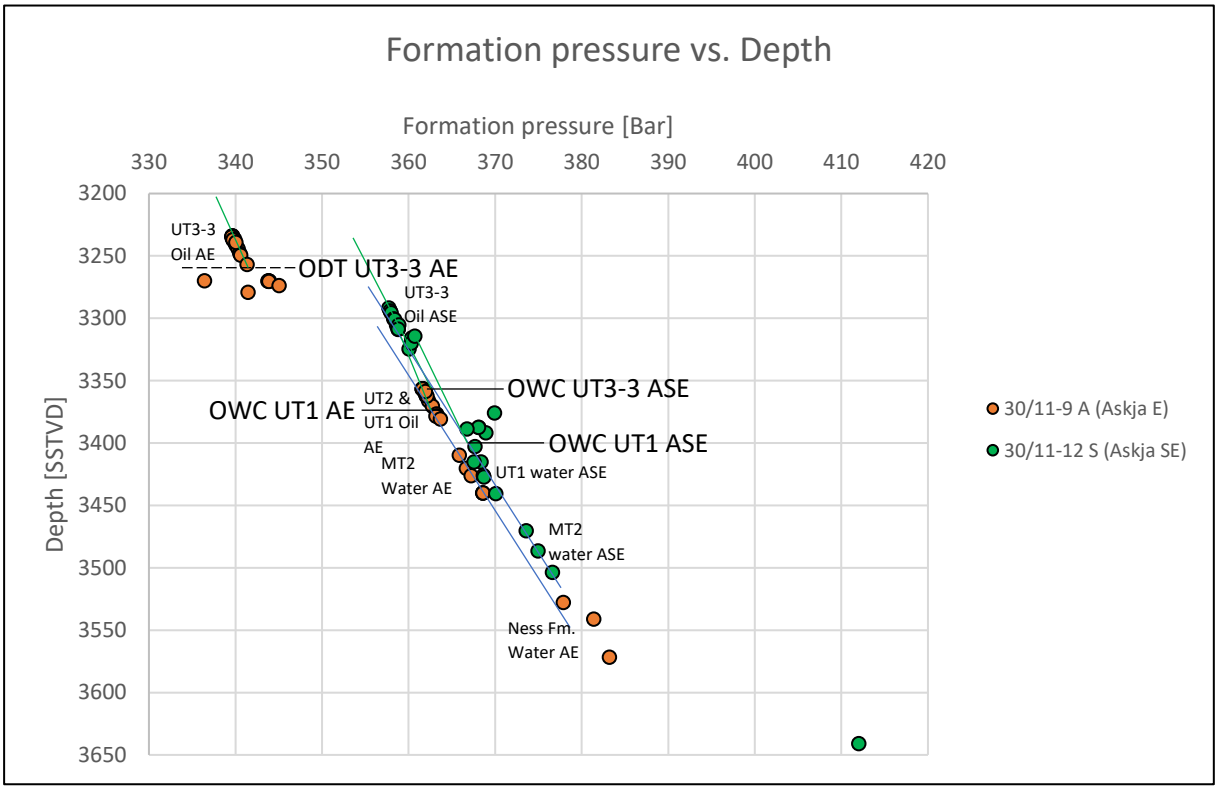

Figure 5.16: Formation Pressure vs. Depth. Pressure data from wells -9A(orange) and -12S(green) are plotted with fluid gradients (green=oil, blue=water) and fluid contacts.

Five juxtaposed areas are observed along the fault plane in the 3 264-3 508 m depth interval (Figure 5.17). The shallowest juxtaposed area is between the UT3-3 reservoir in Askja Southeast and the UT2/UT1 reservoir sands in Askja East, where both reservoirs contain oil and water in the juxtaposed area. The difference between the OWCs is 14 m, where the OWC at Askja East is the deepest, resulting in the oil at Askja East being juxtaposed to both oil and water. The blocks are tilted towards the east resulting in a 110 m column where the oil at Askja East is juxtaposed to fluids at Askja Southeast, where 93 m is oil juxtaposed to oil. The pressure difference between the oils is ~1 bar. The second juxtaposition containing hydrocarbons is between UT2/UT1 Askja Southeast oil and MT2-1 Askja East water with a minimum 44 m

sealed column (overfilled column). The across pressure difference between the two fluids is 3 bars. The fault throw has a span of 120–160 m resulting in a more homogenous SGR value along the fault plane in contrast to the Askja–Askja East fault. The minimum SGR values in the juxtaposed areas range from 15 to 27%. The lowest value is found in the middle of the fault plane, where UT2/UT1 is juxtaposed to MT2-1.

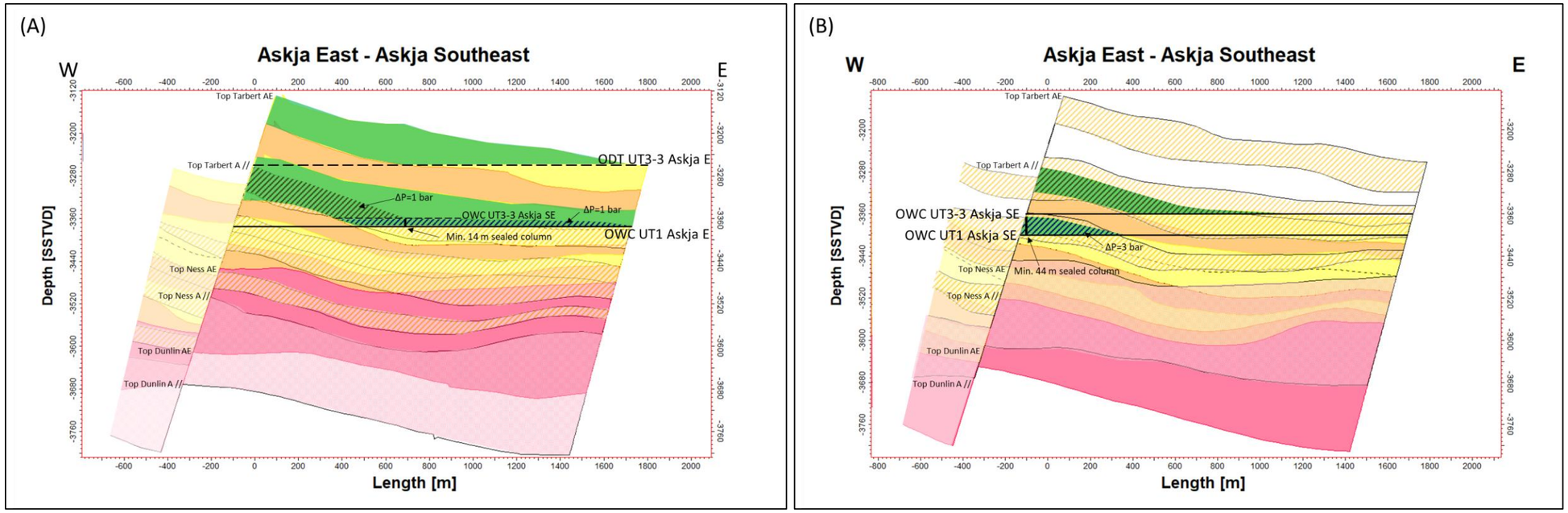

Figure 5.17: Juxtaposition plot of the fault between Askja East and Askja Southeast. The upthrown block (Askja E) is in colors, and the downthrown block (Askja SE) has black outlines where the sands with good reservoir properties have orange slanted lines (A). The downthrown block (Askja SE) is in colors, and the upthrown block (Askja E) has black outlines (B). Fluid contacts are shown with black horizontal lines. Oil in the colored block is shown with a transparent green color, while fluids on the side with black outlines are shown where the fluid is juxtaposed to hydrocarbons across the fault (shown with slanted lines).

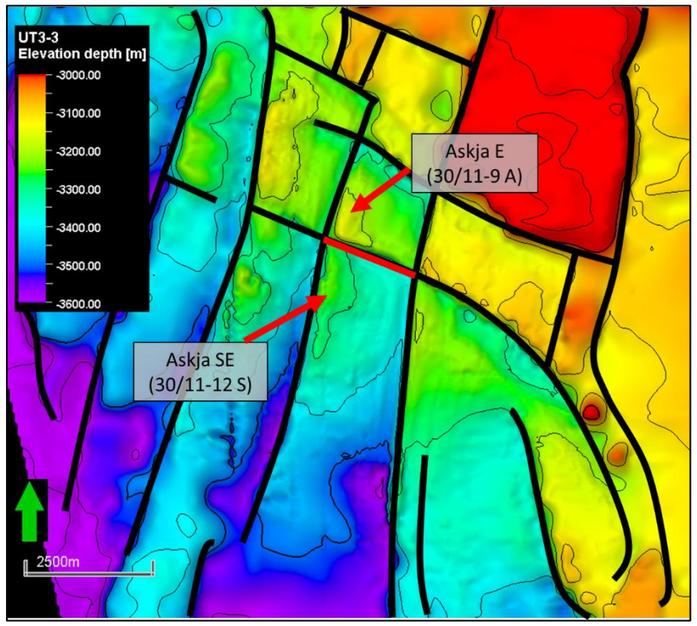

Figure 5.18: Top reservoir map of the Askja area. The red line separating the Askja East and Askja Southeast structures is the fault presented in Figures 5.17 and 5.19.

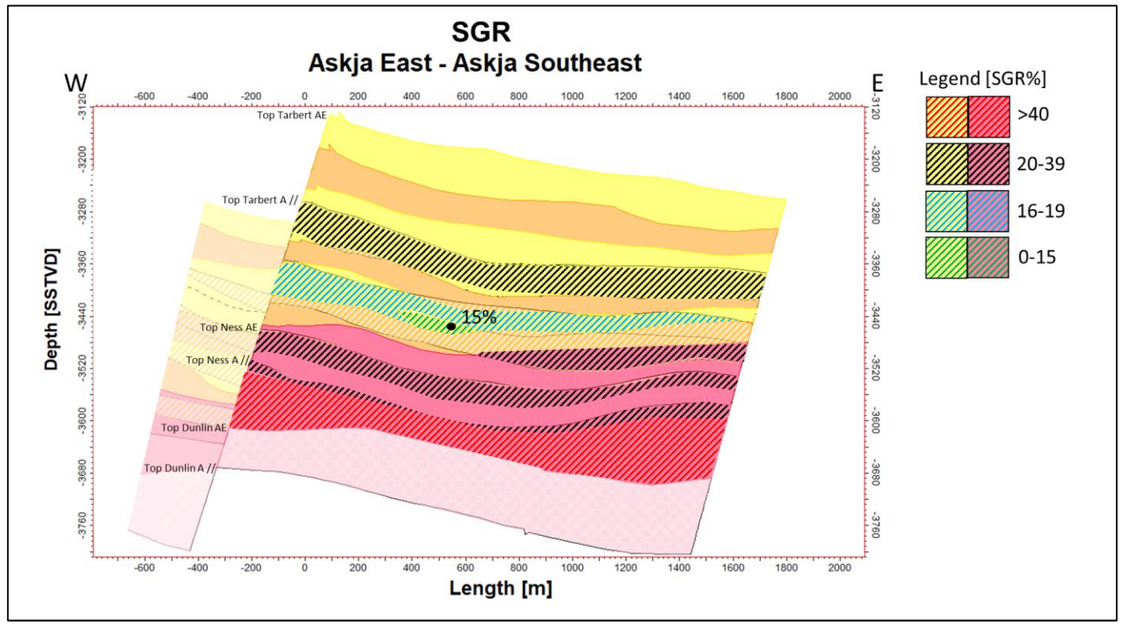

Figure 5.19: SGR plot where the SGR values are displayed where sands with good reservoir properties in the Tarbert Formation are juxtaposed against each other and Tarbert sands vs. Ness Formation and Ness Formation vs. Ness formation. SGR is color-coded in the ranges 0-15%, 16-19%, 20-39% and >40%.

5.2.8 Askja Southeast–Madam Felle

The fault separating Askja Southeast and Madam Felle is an NNE-SSW striking normal fault with a dip direction towards WNW. Wells has been drilled in both the upthrown block (30/11-11 S) and the downthrown block (30/11-12 S). Oil is found in UT3-3 at Madam Felle and is likely controlled by spill towards the southeast (Figure 5.10 and 5.20). Oil accumulates in both UT3-3 and UT2/UT1 Askja Southeast, but the hydrocarbons do not reach the depth where the reservoir sands are in contact with the fault plane.

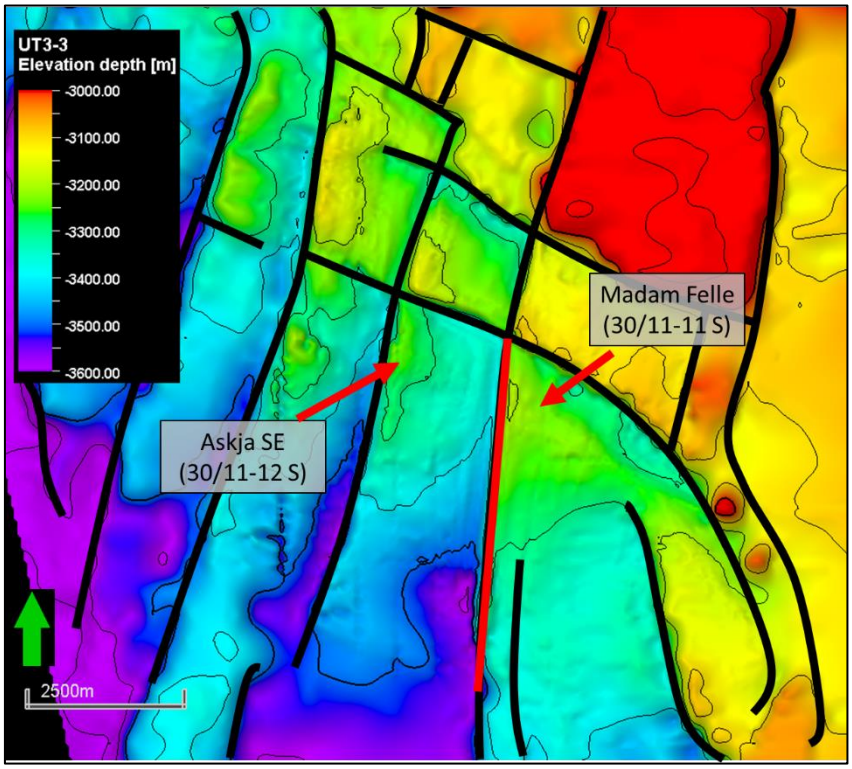

Figure 5.20: Map view of Top Brent. The fault separating Askja Southeast and Madam Felle is shown in red.

The results show six areas along the fault plane where Tarbert and Ness sands are juxtaposed across the fault (Figure 5.21). All the observed juxtaposed areas are water-filled, and the across fault pressure difference is ~16 bars (Figure 5.22). The calculated SGR values are high, ranging from 36 to 53%.

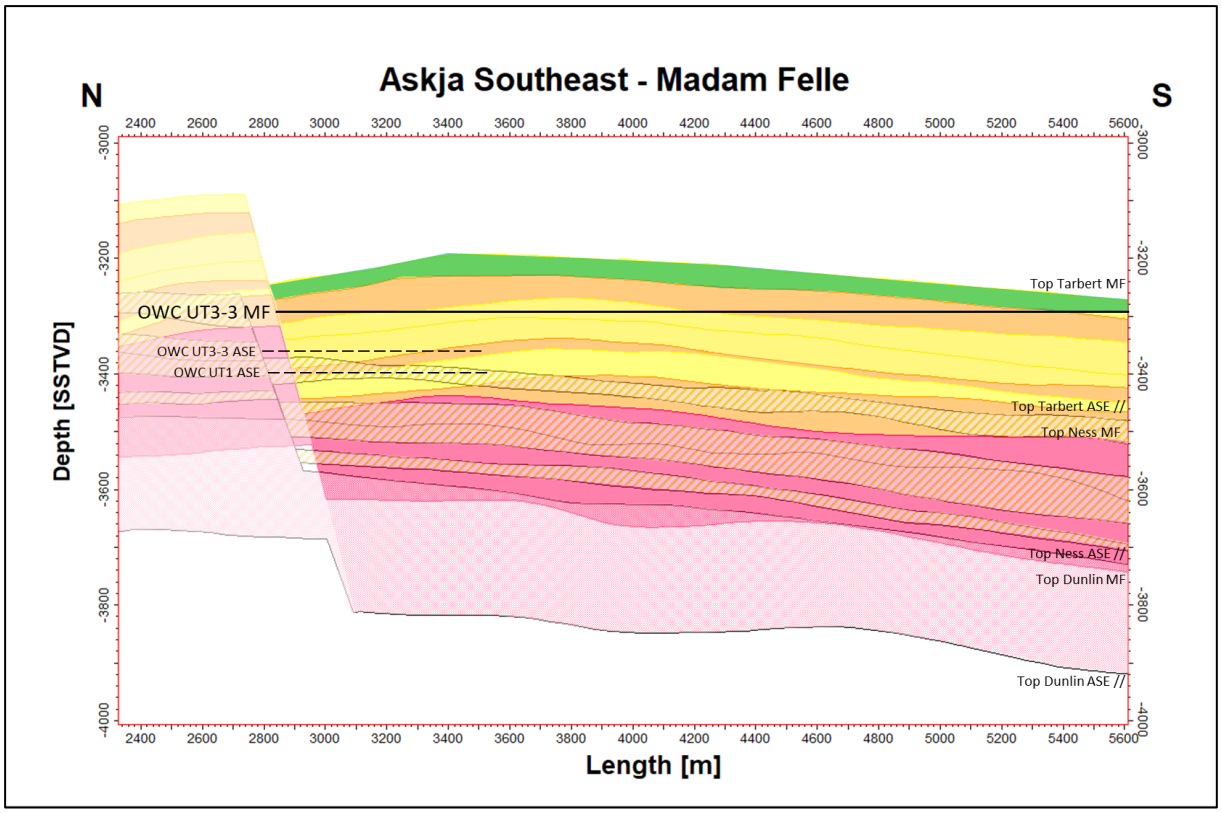

Figure 5.21: Juxtaposition plot of the fault between Askja Southeast and Madam Felle. The upthrown block (Madam Felle) is shown in colors, and the downthrown block (Askja Southeast) is shown with black outlines, where the sands with good reservoir properties are shown with orange slanted lines. Fluid contacts are shown with black lines. Oil in the colored block is shown with a transparent green color.

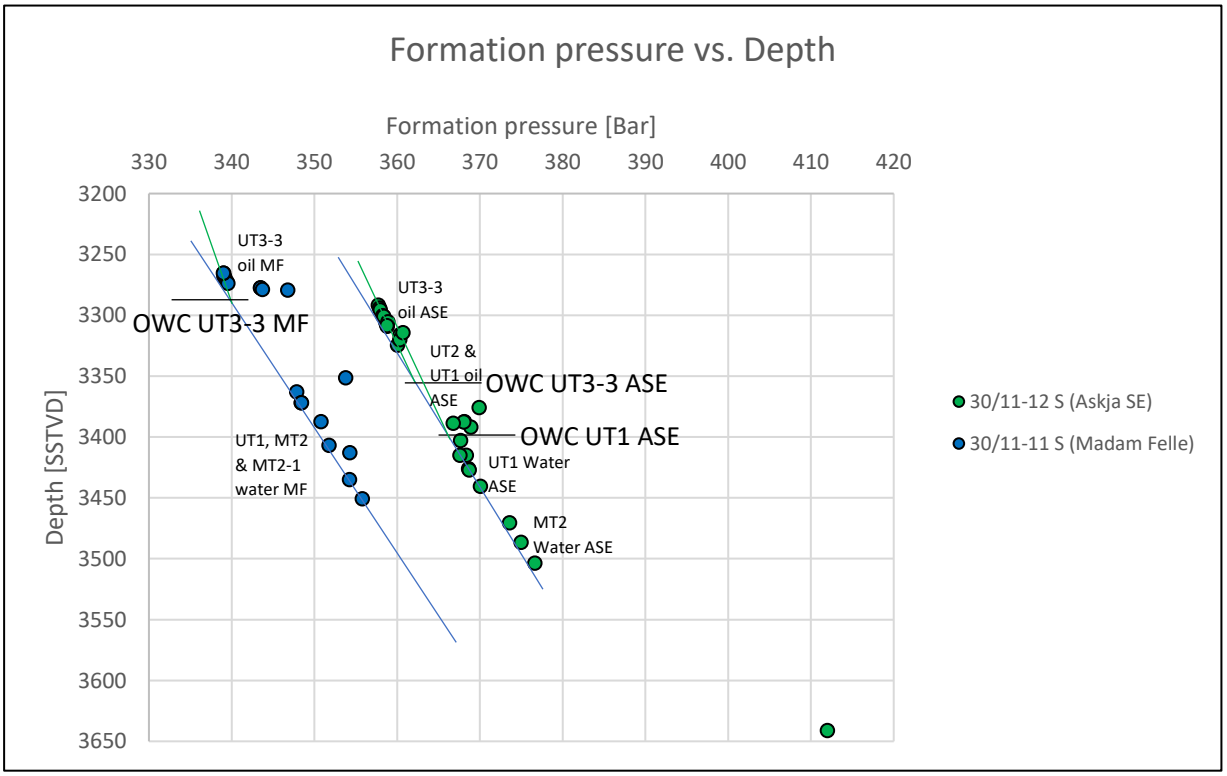

Figure 5.22: Formation pressure vs. depth. Pressure data from wells –11S (blue) and -12S (green) are plotted with fluid gradients (green=oil, blue=water) and fluid contacts.

5.3 Central Area

The Central area is located in the middle of the study area, north of Askja and east of Krafla (Figure 5.23). The area is at a shallower depth than the two other areas and consists of wells -13 (Beerenberg), -14 (Slemmestad), and -14B (Haraldsplass). Gas is proven in UT3-3 and UT2 in the three structures, and oil is proven in UT1 Haraldsplass (Figure 5.24). Well -5 has been drilled in the block between Beerenberg and Askja, and pressure data from this well show no communication with the wells in the Central area (Figure 5.25). Four faults will be presented in this subchapter: the fault between Slemmestad and Haraldsplass, the fault between Haraldsplass and Beerenberg, and the two faults separating Slemmestad and Haraldsplass and the fault blocks to the north. The latter fault is included due to vertical decrease in formation pressure in UT1 and MT2-1 Slemmestad (Figure 5.25).

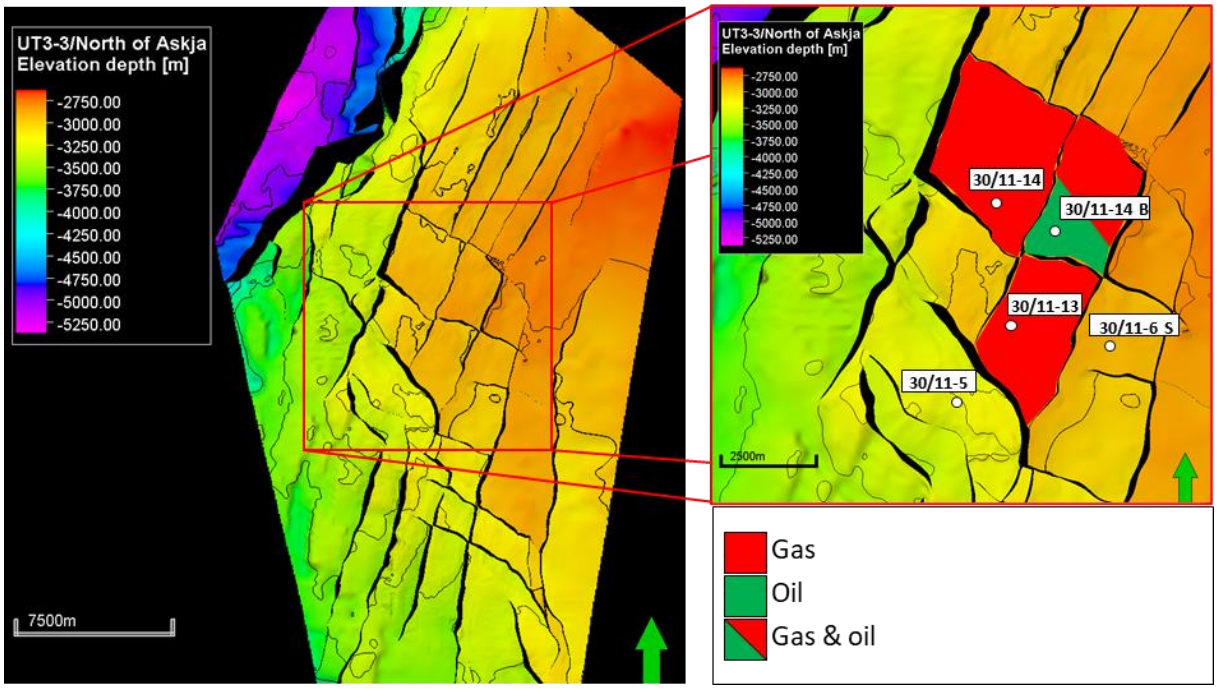

Figure 5.23: Map view of Top Brent Group and the location of the Central area. The wells are shown together with the encountered hydrocarbons.

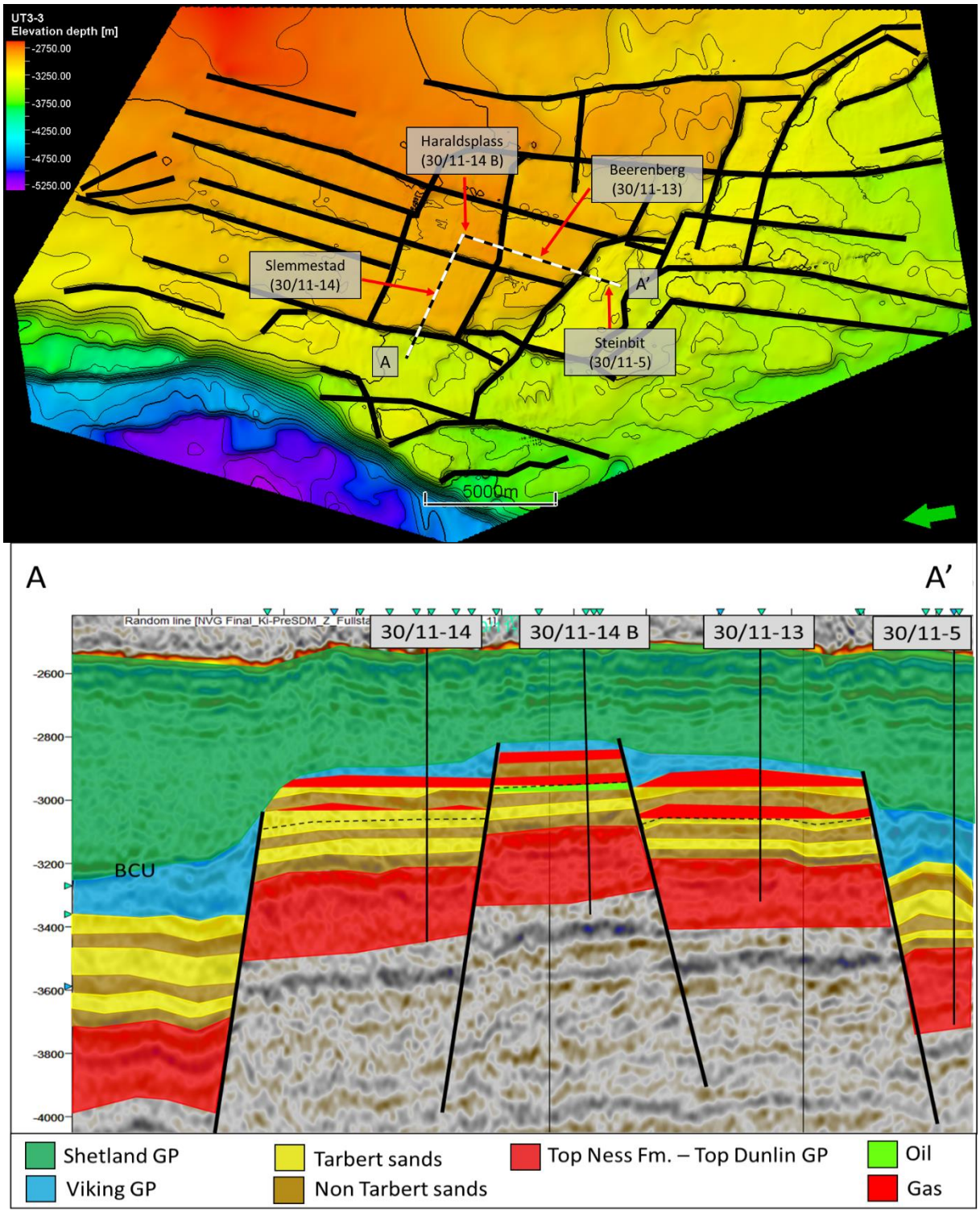

Figure 5.24: Cross-section of Steinbit, Beerenberg, Haraldsplass, and Slemmestad. The zones with good reservoir properties in the Tarbert Formation are shown in yellow. Red in the Tarbert Formation is gas, and green in the Trabert Formation represents oil.

Formation pressures from wells -5, -13, -14, and 14B shows that the three wells in the Central area have a similar pressure regime, with two exceptions. Pressure data from UT1 and MT2-1 in well -14 shows lower pressures than the deeper and shallower layers, where the pressures in MT2-1 follow the hydrostatic gradient (Figure 5.25). The data shows no shared fluid contacts. Two GWCs are found in Haraldsplass, one at 2 883 m for UT3-3 and 2 931 m for UT2, and an OWC at 2 959 for UT1. Beerenberg has two GWCs, one at 2 955 for UT3-3 and one at 3 058 for UT2. Slemmestad has two GWCs, one at 2 949 m for UT3-3 and one at 3 005 m for UT2.

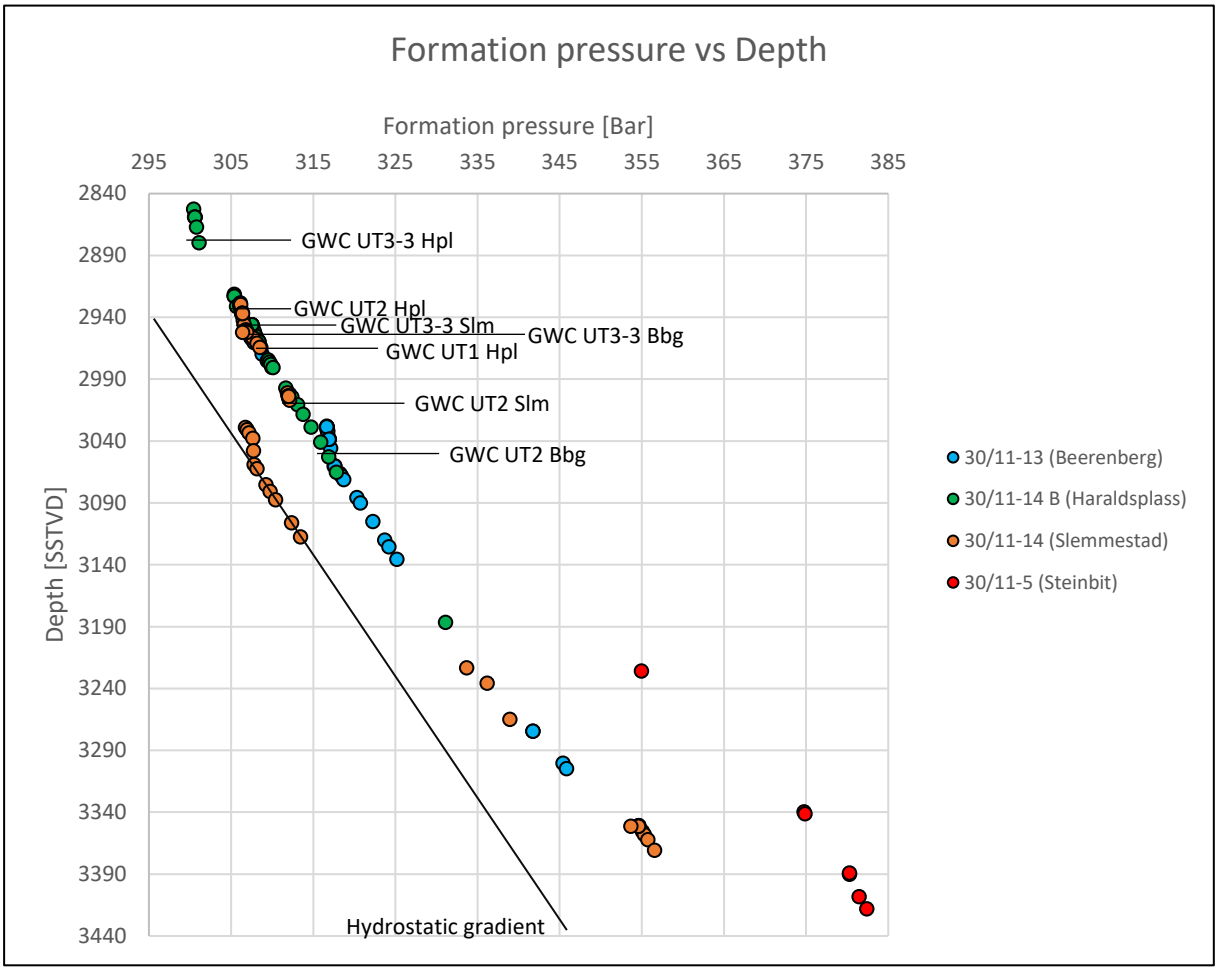

Figure 5.25: Formation pressure from three wells in the Central area and the well in Steinbit. Fluid contacts are shown as horizontal black lines.

5.3.1 Beerenberg

Well 30/11-13 was drilled into the Beerenberg structure in 2016 to test the hydrocarbon potential in two reservoir units within the Tarbert Formation (NPD, 2021). The well encountered gas in two levels in the top part of the formation with GWC at 2 955 m and 3 058 m (SSTVD), which are the same contact depths used in this study. Some gas responses were seen in the Ness Formation with no oil shows.

5.3.2 Slemmestad

Well 30/11-14 was drilled in 2016 to test the Slemmestad prospect to prove hydrocarbons in the Tarbert and Ness Formations (NPD, 2021). The well encountered two gas intervals in the upper Tarbert Formation with GWC at 2 948 m and 3 005 m depth (SSTVD) which correlates with the interpreted fluid contacts in this study. Gas responses were found in the Ness Formation.

5.3.3 Haraldsplass

Well 30/11-14 B is a sidetrack to well 30/11-14 and was drilled into the Haraldsplass prospect in 2016. The objective was to prove hydrocarbon in the Tarbert and Ness Formations (NPD, 2021). The well encountered hydrocarbons in three different reservoir intervals in the Tarbert Formation with two gas-condensate intervals and one oil interval. Gas responses were observed in the Ness and Etive Formations.

5.3.4 Brontes

The Brontes structure is located east of Beerenberg and was drilled by the 30/11-6 S well in 2004 to prove hydrocarbon within the upper and middle Tarbert Formation (NPD, 2021). The second objective was to investigate the remaining Brent Group ant the lower Heather Formation. The well did not prove any commercial hydrocarbons, although oil shows were found in the upper and middle Tarbert Formation. The best reservoir zone in the structure was found to be the upper parts of middle Tarbert.

A summary of the wells, structures, fluid contacts and pressures in the Central area is shown in table 5.2.

Table 5.2: Summary of the wells, structures, reservoir unit, fluid contacts, pressure measurements, and overpressure in Brotes and the Central area.

Well	Structure	Reservoir unit (SSTVD)	GWC/ OWC	Pressure point (SSTVD)	Fluid	P.P. (Bar)	O.P. (Bar)
30/11-6 S	Brontes	MT2-1		3 176.7	Water	330	9.86
30/11-13	Beerenberg	UT3-3	2 955	2 953.49	Gas	307.262	9.61
		UT2	3 058	3 045.74	Gas	317.141	10.1
		UT3-3		2 980.26	Water	309.946	9.6
30/11-14	Slemmestad	UT3-3	2 949	2 945.97	Gas	306.618	9.73
		UT2	3 005	3 005.02	Gas	312.005	9.16
		UT3-3		2 952.06	Water	307.009	9.51
		UT1		3 037.80	Water	307.645	0.86
		MT2-1		3 075.28	Water	309.256	-0.66
30/11-14 B	Haraldsplass	UT3-3	2 883	2 879.64	Gas	301.123	10.91
		UT2	2 931	2 921.24	Gas	305.35	10.95
		UT1	2 959	2 958.25	Oil	308.231	10.1
		MT2-1		3 028.72	Water	314.729	9.5

5.3.5 Haraldsplass-Beerenberg

The fault separating Haraldsplass and Beerenberg is an ESE-WNW striking normal fault with an SSW direction (Figure 5.24 and 5.27). The fault has a throw of ~90-160 m measured at sand-sand juxtapositions. Wells has been drilled in both the upthrown block (30/11-14 B) and the downthrown block (30/11-13). Both wells encountered gas in UT3-3 and UT2, whereas Haraldsplass contain oil in UT1. Pressure data from wells -13 and -14B show a similar pressure regime, but the two wells do not share any fluid gradients or fluid contacts (Figure 5.25). The pressure difference between the two water gradients is ~0.5 bars.

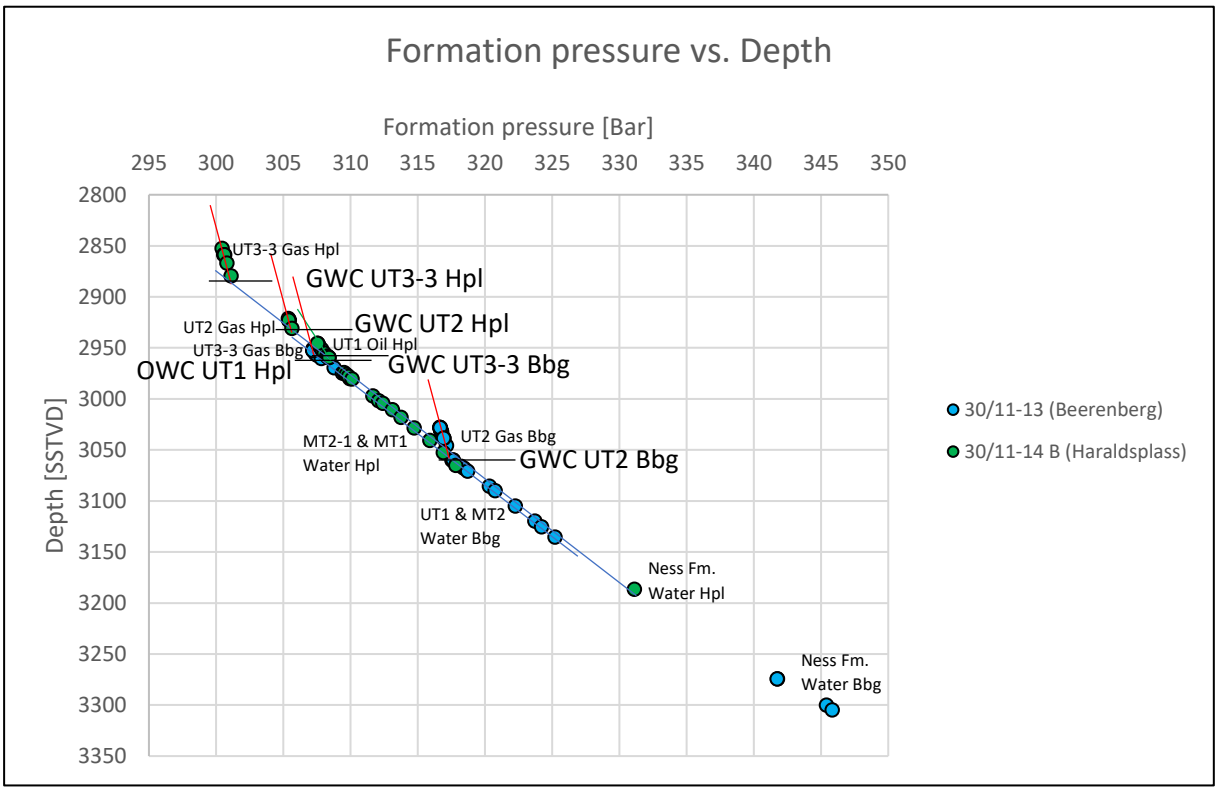

Figure 5.25: Formation pressure vs depth. Pressure data from wells -13 (blue) and -14B (green) are plotted with fluid gradients (red=gas, green=oil, blue=water) and fluid contacts.

There are six areas along the fault plane where Tarbert and Ness sands are juxtaposed across the fault (Figure 5.26). The shallowest juxtaposition is between UT3-3 Beerenberg and UT1 Haraldsplass. Both segments contain hydrocarbon, but none of them reach the depth where the sands are juxtaposed. The second juxtaposed area is between UT2 Beerenberg and MT2-1 Haraldsplass. The pressure difference between the gas in Beerenberg and water in Haraldsplass is 0.5 bars. The column from the shallowest point of the juxtaposed area and down to the GWC in UT2 Beerenberg is 34 m. The minimum SGR values were found to be 27-49% (Figure 5.28).

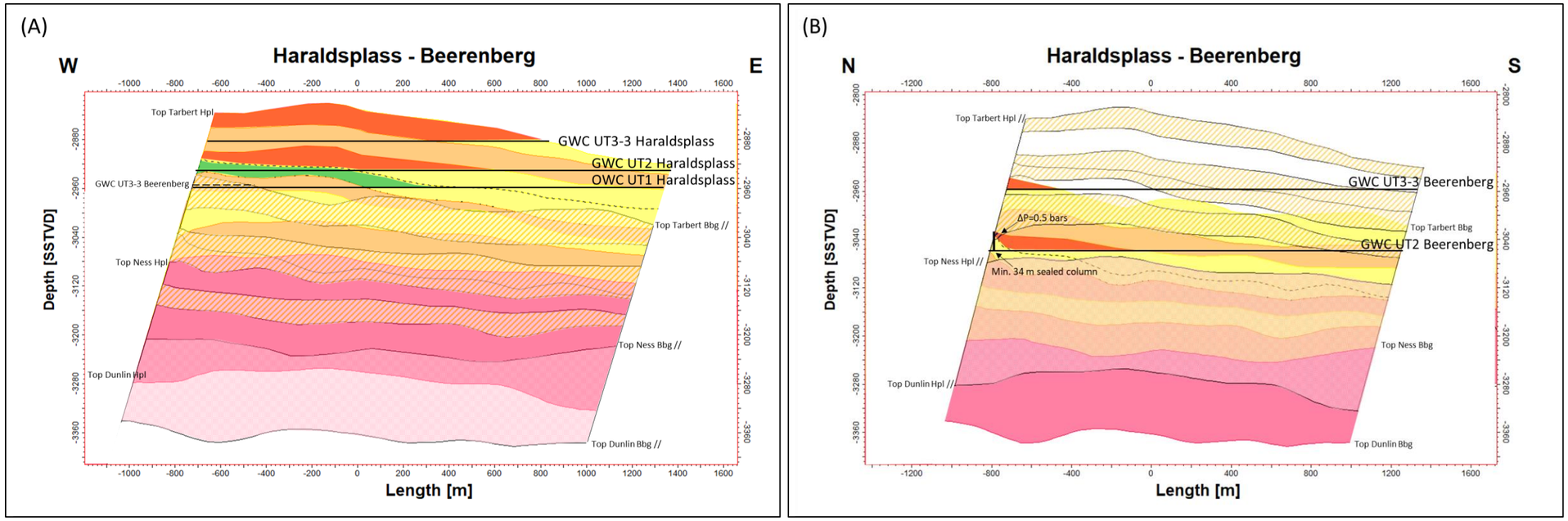

Figure 5.26: Juxtaposition plot of the fault between Haraldsplass and Beerenberg. The upthrown block (Haraldsplass) is in colors, and the downthrown block (Beerenberg) has black outlines where the sands with good reservoir properties have orange slanted lines (A). The downthrown block (Beerenberg) is in colors, and the upthrown block (Haraldsplass) has black outlines (B). Fluid contacts are shown with black horizontal lines. Hydrocarbons in the colored block are shown with a transparent color (gas=red, oil=green), while fluids on the side with black outlines are shown where the fluid is juxtaposed to hydrocarbons across the fault (shown with slanted lines).

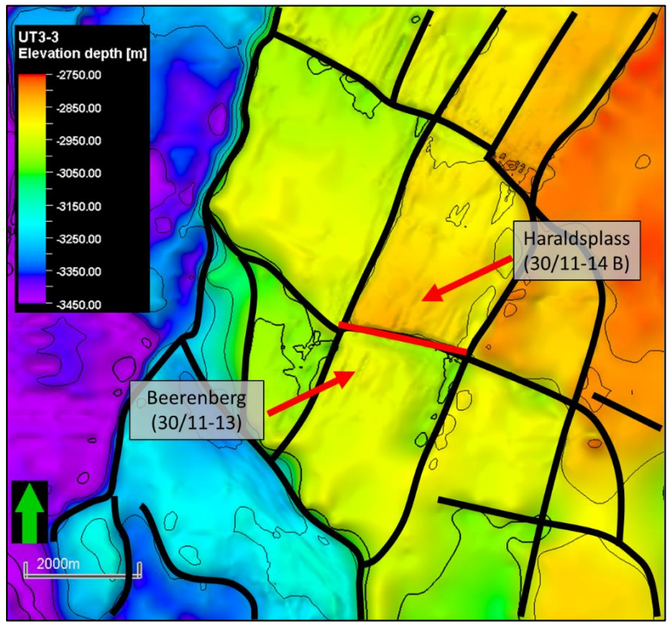

Figure 5.27: Top reservoir map of the Central area. The red line separating the Beerenberg and Haraldsplass structures is the fault presented in Figures 5.26 and 5.28.

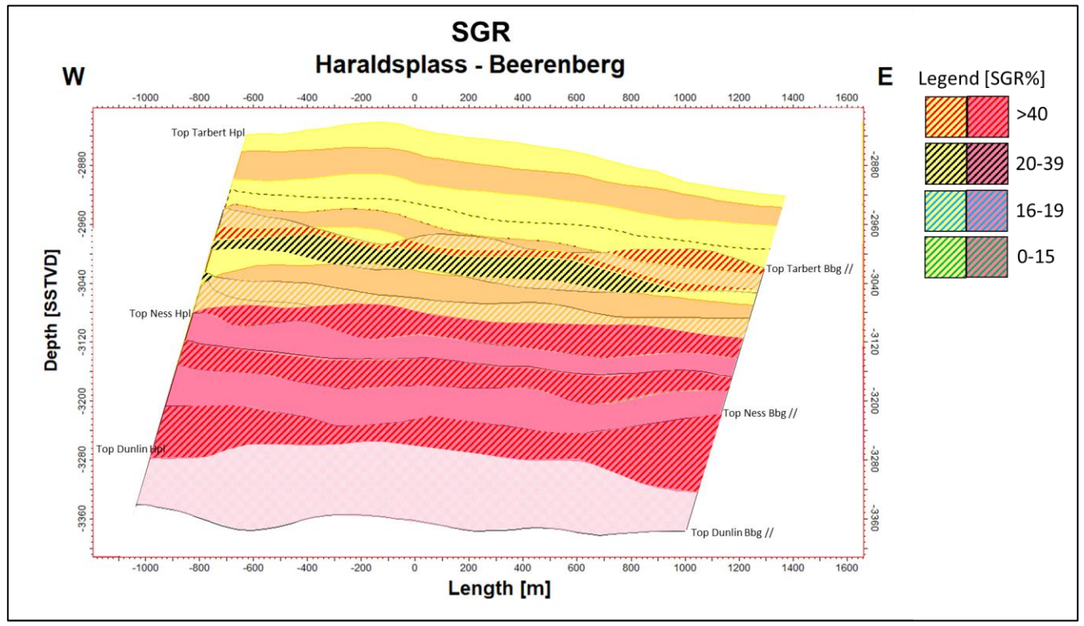

Figure 5.28: SGR plot where the SGR values are displayed where sands with good reservoir properties in the Tarbert Formation are juxtaposed against each other and Tarbert sands vs. Ness Formation and Ness Formation vs. Ness formation. SGR is color-coded in the ranges 0-15%, 16-19%, 20-39% and >40%.

5.3.6 Haraldsplass-Slemmestad

The Haraldsplass-Slemmestad fault is an NNE-SSW striking normal fault with a dip towards WNW, separating Slemmestad to the west and Haraldsplass to the east (Figure 5.24 and 5.31). The fault has a throw of 80–130 m measured at sand-sand juxtapositions. Wells have been drilled in both the upthrown (30/11-14 B) and the downthrown block (30/11-14). Both wells encountered gas in UT3-3 and UT2. Well -14B also encountered oil in UT1. Formation pressure data from wells -14 and -14B are presented in figure 5.29. The water gradient for Slemmestad down to UT1 shows a 0.5 bar lower pressure gradient than the water gradient for Haraldsplass. Formation pressures in UT1 and MT2-1 Slemmestad have lower pressures than the rest of the well.

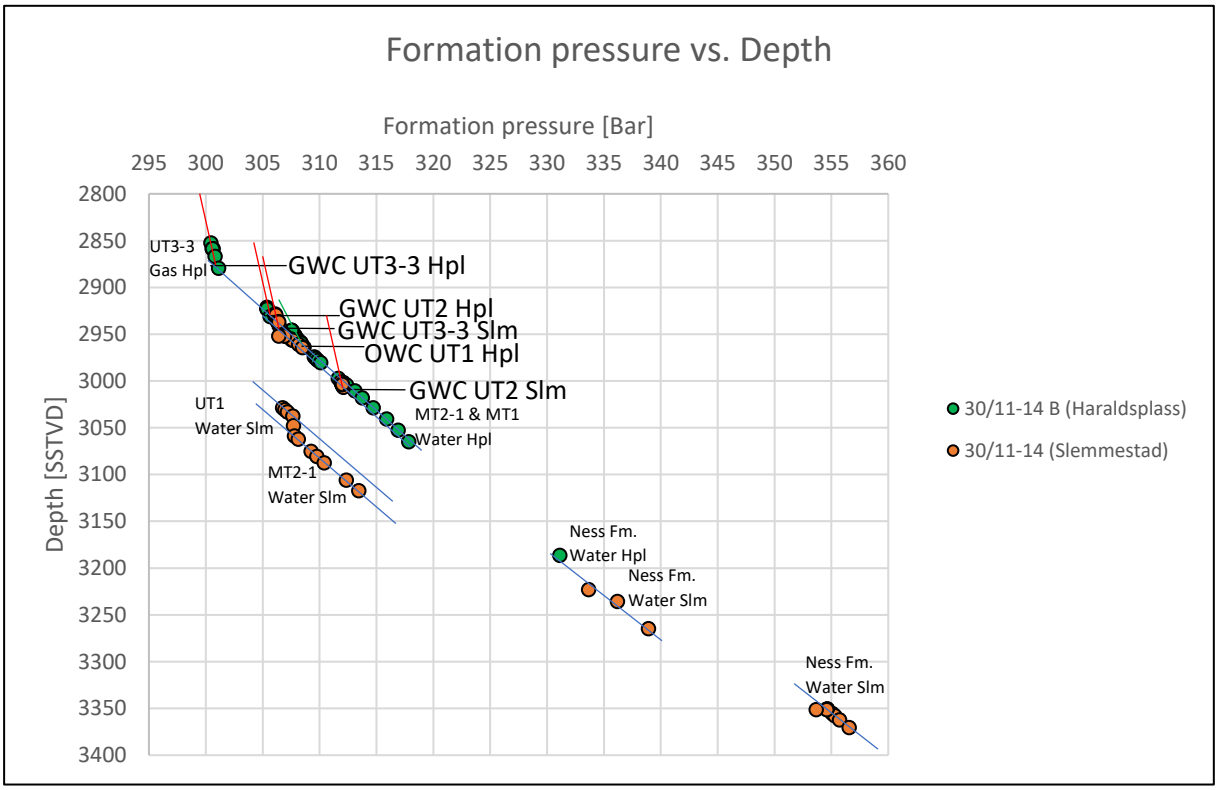

Figure 5.29: Formation pressure vs depth. Pressure data from wells -14 (orange) and -14B (green) are plotted with fluid gradients (red=gas, green=oil, blue=water) and fluid contacts.

Seven Tarbert and Ness juxtapositions are observed, with three of them containing hydrocarbon on either one or both sides of the fault (Figure 5.30).

The gas in UT3-3 Slemmestad is juxtaposed to water in UT2 with an across fault pressure difference of 0.5 bars. The fluid contact difference between the fluid contacts in the two juxtaposed segments is 18 m. The gas at Slemmestad has a minimum 9 m sealed column. The fluid contact difference between UT1 Haraldsplass and UT3-3 Slemmestad is 10 m resulting in

the oil in UT1 Haraldsplass being juxtaposed to gas and water. The oil has a minimum of 17 m sealed column, and the across pressure difference is 0.5 bars. Gas in UT2 Slemmestad is juxtaposed to water in MT2-1 Haraldsplass, resulting in a minimum of 10 m sealed column.

The juxtaposed area with the lowest minimum SGR is MT2-1 Haralsaplass vs. UT1 Slemmestad, with a value of 26%. UT3-3 Slemmestad gas is juxtaposed to UT2 and UT1 with SGR values above 40% (Figure 5.32).

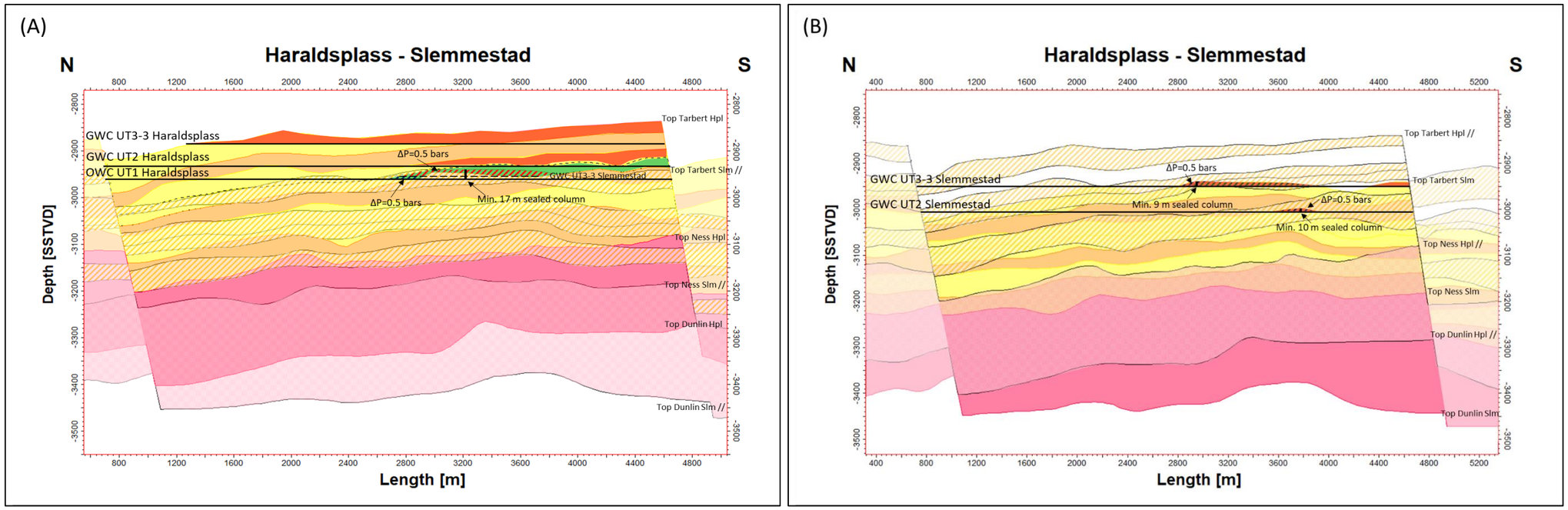

Figure 5.30: Juxtaposition plot of the fault between Haraldsplass and Slemmestad. The upthrown block (Haraldsplass) is in colors, and the downthrown block (Slemmestad) has black outlines where the sands with good reservoir properties have orange slanted lines (A). The downthrown block (Slemmestad) is in colors, and the upthrown block (Haraldsplass) has black outlines (B). Fluid contacts are shown with black horizontal lines. Hydrocarbons in the colored block are shown with a transparent color (gas=red, oil=green), while fluids on the side with black outlines are shown where the fluid is juxtaposed to hydrocarbons across the fault (shown with slanted lines).

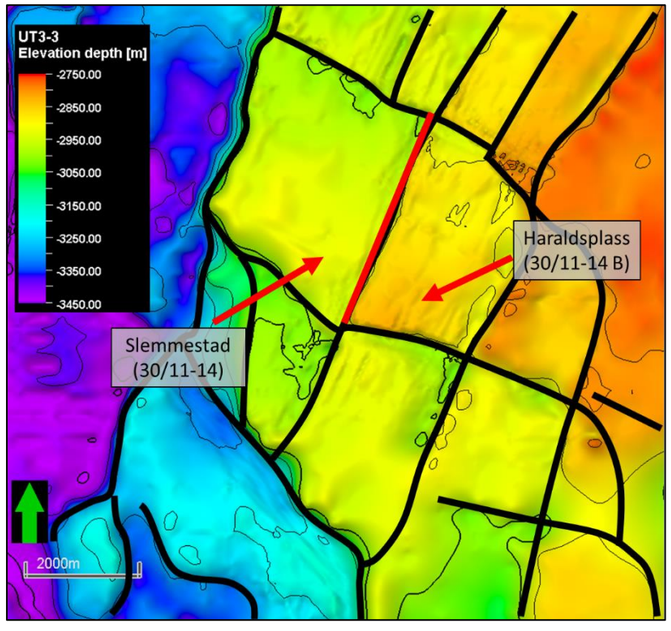

Figure 5.31: Top reservoir map of the Central area. The red line separating the Slemmestad and Haraldsplass structures is the fault presented in Figures 5.30 and 5.32.

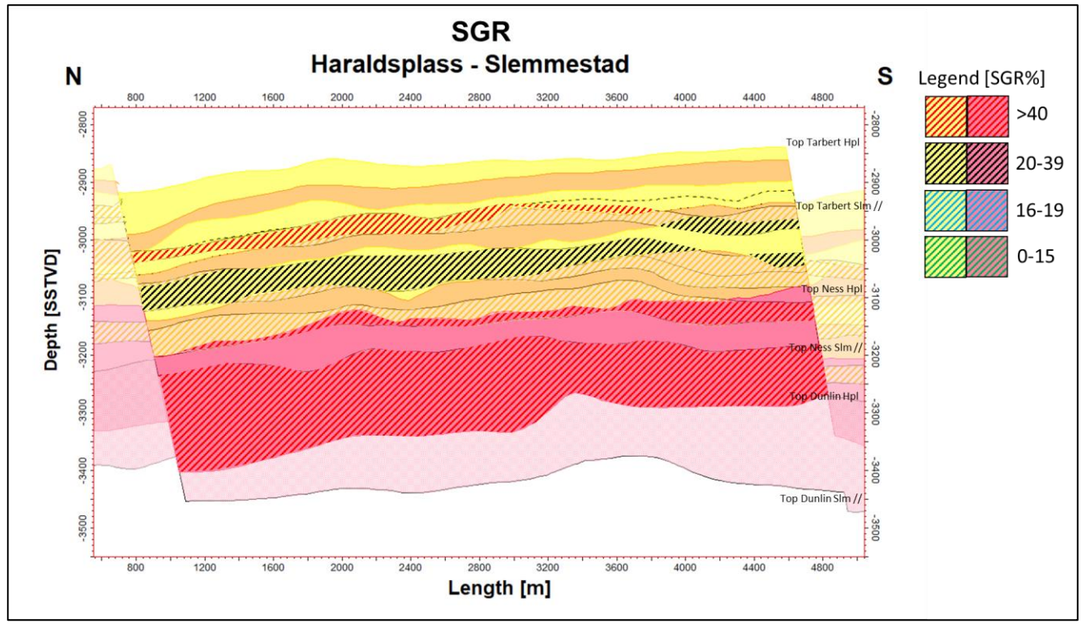

Figure 5.32: SGR plot where the SGR values are displayed where sands with good reservoir properties in the Tarbert Formation are juxtaposed against each other and Tarbert sands vs. Ness Formation and Ness Formation vs. Ness formation. SGR is color-coded in the ranges 0-15%, 16-19%, 20-39% and >40%.

5.3.7 Northern Slemmestad and Haraldsplass faults

The fault north of Slemmestad is analyzed due to the pressure decrease in UT1 and MT2-1 in well 30/11-14. The two faults separate Slemmestad and Haraldsplass and the fault blocks to the north, where one of the blocks leads to the Stjerne structure (Figure 5.34).

The hydrocarbons in Slemmestad and Haraldsplass are interpreted not to reach the depth where the sands are situated against the fault plane (Figure 5.33A). UT1 and MT2-1 Slemmestad have lower pressures than the rest of the well, and these segments are both juxtaposed to MT2-1 across the fault. An SGR value of 28% is found in the area where UT1 is juxtaposed to MT2-1 (Figure 5.33B). The lowest SGR value along the fault plane is between the MT2-1 Slemmestad and MT2-1 to the north. The lowest SGR value where MT2-1 is self-juxtaposed were found to be 12%; the lowest value observed in the study, together with the self-juxtaposed MT2-1 area between Askja and Askja East.

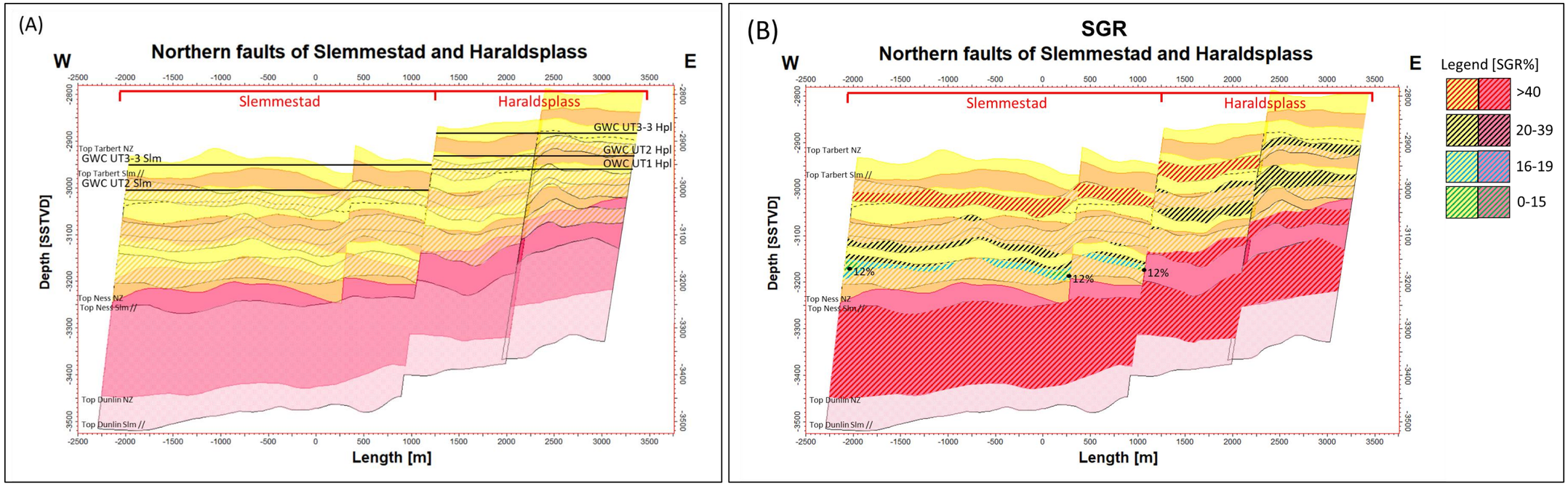

Figure 5.33: Juxtaposition plot of the two faults between Haraldsplass and Slemmestad and the fault blocks to the north (NZ). Upthrown blocks (northern zones) are shown in colors, and the downthrown blocks (Slemmestad and Haraldsplass) are shown with black outlines, where the sands with good reservoir properties are shown with orange slanted lines (A). SGR plot where the SGR values are shown where sands with good reservoir properties in the Tarbert Formation are juxtaposed against each other and Tarbert sands vs. Ness Formation and Ness Formation vs. Ness formation. SGR is color-coded in the ranges 0-15%, 16-19%, 20-39% and >40% (B).

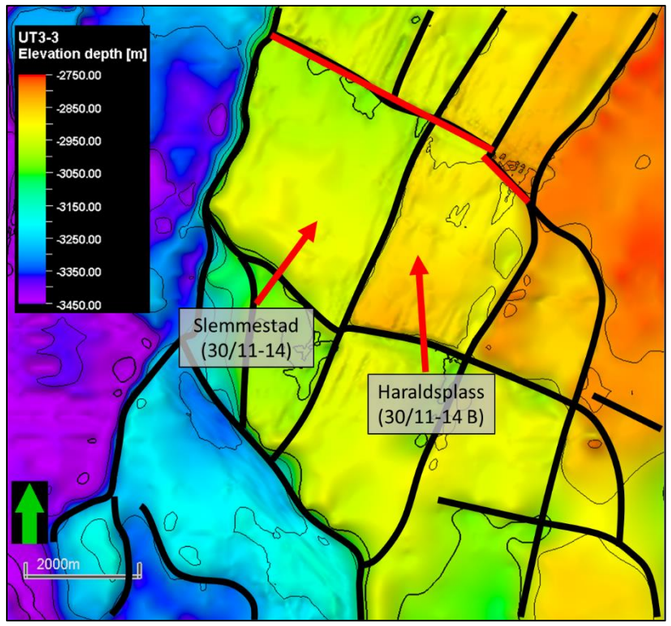

Figure 5.34: Top reservoir map of the Central area. The red line separating the Haraldsplass and Slemmestad structures from the northern zones are the faults presented in Figure 5.33.

5.4 Krafla Area

The Krafla area is located at the western edge of the study area. The area consists of three fault blocks and four wells: Krafla North (30/11-10), Krafla West (30/11-8 A), and Krafla Main (30/11-8 S and 30/11-10 A) (Figure 5.35). The sands with good reservoir properties are UT3-3, UT1, MT2, and MT2-1. Krafla Main and Krafla North have oil in the lower sands, while Krafla West has oil in UT3-3 and gas in the lower sands. The area does not follow the Askja and Central area fault strike and dip trends. Krafla Main is a horst structure and is the upthrown block located between Krafla North and Krafla West. Erosion has affected the area, especially Krafla Main, where UT3-3 and UT3-2 have partially been eroded. A cross-section going through the three structures is presented in Figure 5.36.

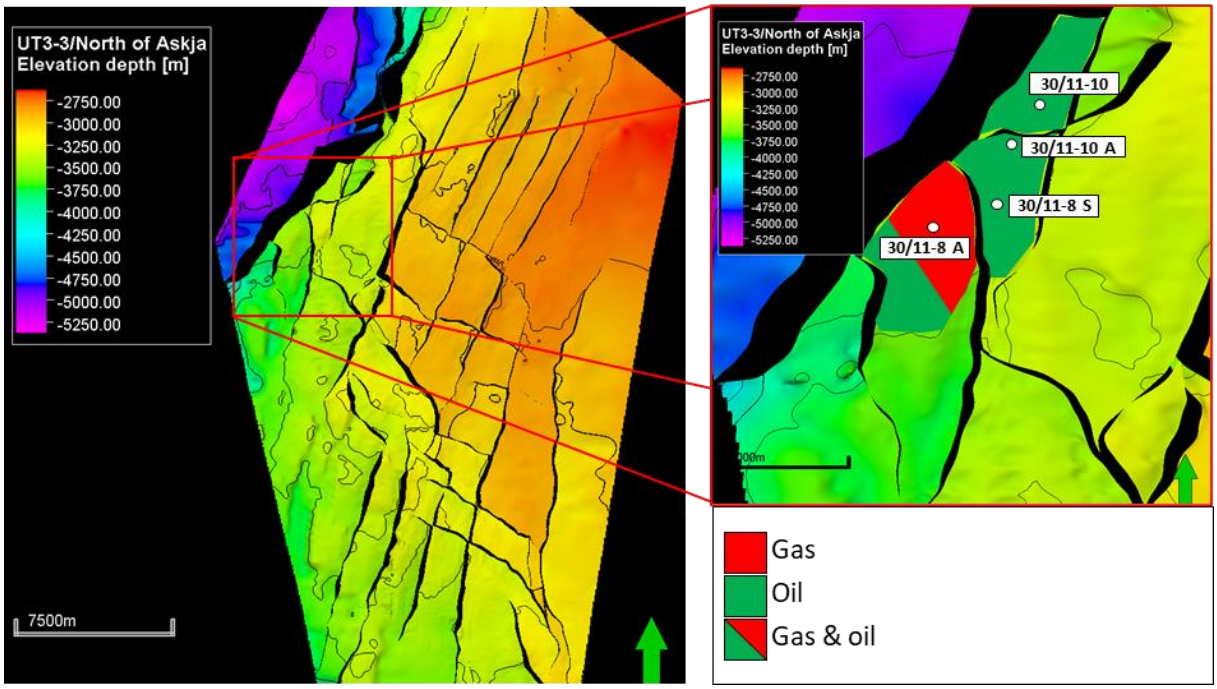

Figure 5.35: Map view of Top Brent Group and the location of the Krafla area. The wells are shown together with the encountered hydrocarbons.

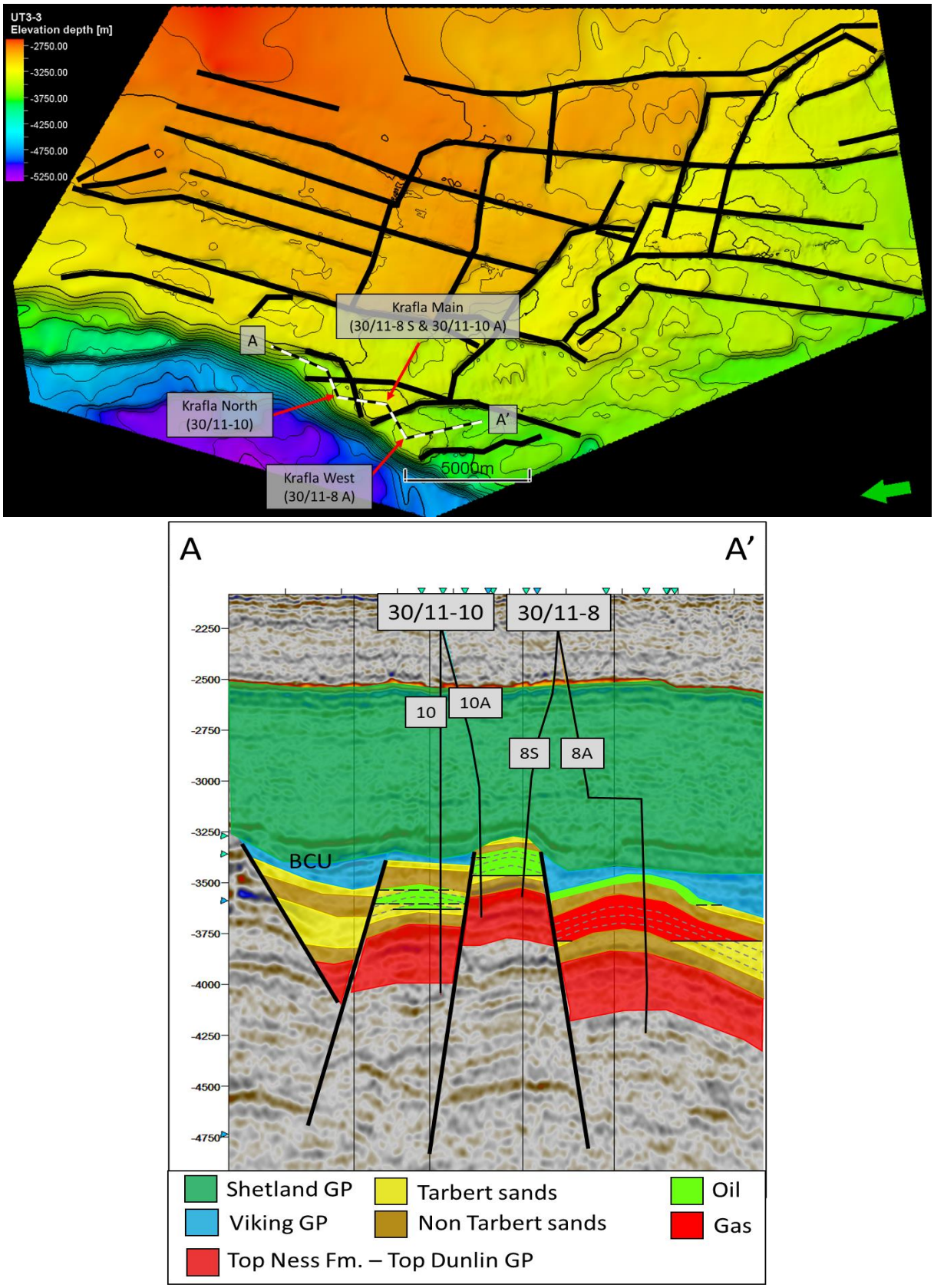

Figure 5.36: Cross-section of Krafla North, Krafla Main, and Krafla West. The zones with good reservoir properties in the Tarbert Formation are shown in yellow. Red in the Tarbert Formation is gas, and green in the Trabert Formation represents oil.

Formation pressures from the four wells are presented in figure 5.37. None of the fluid contacts are estimated to have the same depth. Well -8A is drilled in Krafla West, which is the deepest block. The well has an ODT 3 599 m and a GWC at 3 770 m depth. Wells -8S and -10A are both drilled in the Krafla Main horst. The two wells are interpreted to have the same pressure regimes with the same fluid gradients and fluid contacts. Oil is proven in UT1-2 in both wells. UT1-2 in well -8S is filled with oil, while -10A has both oil and water. A WUT 3 383 m is used for UT1-2. The oil in UT1-1, MT2, and MT2-1 are interpreted to have the same oil gradient. The oil gradient crosses a water gradient found from pressures in MT2-1 at 3 473 m depth. The oil in well -10 is proven to be accumulating in segments UT1-2, UT1-1, MT2, and MT2-1. The oils have three pressure regimes, where the shallowest oil is in UT1-2 with the highest formation pressures and an ODT 3 532 m. The middle oil is in UT1-1 and MT2 with an ODT 3 603 m. Water is found at 3 639 m depth, resulting in an OWC at 3 636 m for the oil in MT2-1.

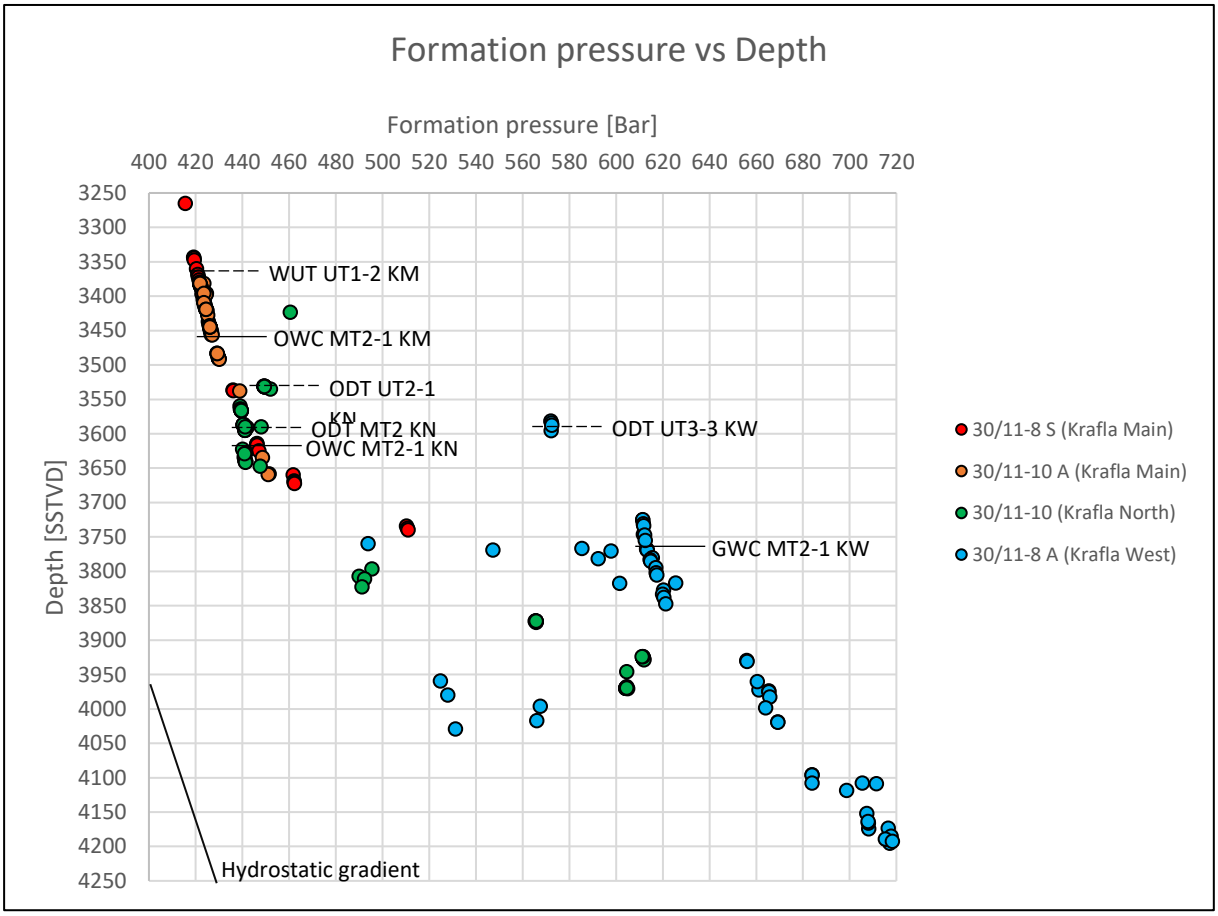

Figure 5.37: Formation pressure from four wells in the Krafla area. Fluid contacts are shown as black horizontal lines, and WUT and ODTs are shown as black dashed lines. ODT is used for UT1-2 and MT2 Krafla North and UT3-3 Krafla West. A WUT is used for UT1-2 Krafla Main.

5.4.1 Krafla North

The Krafla North structure is located on the edge of the sub-basin towards the Viking Graben. Well 30/11-10 was drilled in the structure in 2014 to prove commercial hydrocarbons within the Tarbert, Ness, and Etive Formations (NPD, 2021). The well proved oil in Tarbert (UT1-2, UT1-1, MT2 and MT2-1) and the Etive Formations and rich gas-condensate in the Ness Formation. NPD gives an OWC at 3 636 m depth (SSTVD), the same as the OWC used in this study. The MT2 segment is interpreted to have good reservoir properties, but parts of the zone contain asphaltenes or tar plugging porosity partly or entirely. The well penetrated two sands in Lower Ness with gas condensate. It is interpreted that the structure contains three hydrocarbon accumulations within three reservoir segments: UT1-2, UT1-1&MT2, and MT2-1.

5.4.2 Krafla Main

Two wells have been drilled in the Krafla horst structure. These wells are 30/11-8 S and 30/11-10 A. The block is constrained by four normal faults dipping away from the horst structure. The -8S well was drilled in 2011 with the main objective of proving commercial hydrocarbon accumulation in the upper and middle Tarbert Formation and the Ness and Etive Formations (NPD, 2021). The well encountered oil shows in the upper parts of the Heather Formation, oil in the upper and middle Tarbert Formation, and condensate in parts of the Ness Formation. The well found no fluid contacts. The -10 A well was drilled in 2014 as an appraisal well. The main objective was to reduce uncertainty in oil-in-place and to verify communication with Krafla North. NPD gives an OWC at 3 478 m depth (SSTVD) which is 5 m deeper than the contact used in this study.

5.4.3 Krafla West

Krafla west is located southwest of the Krafla Main horst and is the only structure in the study area with oil in the upper reservoir and gas in the lower reservoir. The fluids are greatly overpressured with approximately 210 to 234 bars higher than the hydrostatic pressure gradient. The hydrocarbon potential of the Krafla West structure was investigated by well 30/11-8 A in 2011. The well encountered oil in the Intra-Heather Formation with an ODT 3 602 m (SSTVD) and did not encounter The Tarbert Formation until a depth of 3 690 m (SSTVD) with the upper and middle Tarbert Formation containing condensate with a fluid contact at 3 769 m depth (SSTVD) (NPD, 2021). These observations do not correlate with the well data acquired from

Equinor ASA. The Tarbert Formation starts at a depth of 3 576 m SSTVD, meaning that the Intra-Heather oil is interpreted as UT3-3 oil with an ODT 3 599 m. The Ness and Etive Formations were both water-bearing.

A summary of the wells, structures, fluid contacts and pressures in the Krafla area is shown in table 5.3.

Table 5.3: Summary of the wells, structures, reservoir unit, fluid contacts, pressure measurements, and overpressure in the Krafla area.

Well	Structure	Reservoir unit (SSTVD)	OWC/ GWC/ ODT*/ WUT**	Pressure point (SSTVD)	Fluid	P.P. (Bar)	O.P. (Bar)
30/11-8 A	Krafla W	UT3-3	3 599*	3 595.26	Oil	572.27	209.95
		UT1-2 – MT2-1	3 770	3 746.29	Gas	611.74	234.2
		MT2-1		3 837	Water	620.41	233.72
30/11-8 S	Krafla M	UT1-2	N/A	3 344	Oil	419.15	82.15
		UT1-1 – MT2-1	N/A	3 445	Oil	426.25	79.07
30/11-10 A	Krafla M	UT1-2	3 383**				
		UT1-1 – MT2-1	3 473	3 456	Oil	427.06	78.77
		MT2-1		3 491.77	Water	430.06	78.17
30/11-10	Krafla N	UT1-2	3 532*	3 530	Oil	449.47	93.72
		UT1-1 – MT2	3 603*	3 595	Oil	441.05	78.75
		MT2-1	3 636	3 613	Oil	441.18	77.07
		MT2-1		3 638	Water	441.39	74.76

5.4.4 Krafla Main–Krafla North

The Krafla Main–Krafla North fault is an E-W striking normal fault with a northward dip direction separating Krafla Main (KM) in the south from Krafla North (KN) in the north (Figure 5.36 and 5.). The fault has a throw of ~100–170 m measured at sand-sand juxtapositions. Wells have been drilled in both the upthrown block (30/11-10 A & 30/11-8 S) and the downthrown block (30/11-10). UT3-3 and UT3-2 are partially eroded, and no hydrocarbons are found in UT3-3. Krafla Main is interpreted to contain two oils, and Krafla North is interpreted to contain three oils. The structures do not share any fluid gradients or fluid contacts (Figure 5.38). The results show one juxtaposed area between Tarbert sands across the fault (Figure 5.39). This juxtaposed area is between MT2 KM and UT3-3 KN and is filled with oil in KM and water in KN. The column from the top of the juxtaposed area and down to the OWC in KM is 68 m. The formation pressure difference across the fault in this area is 35 bars. However, the pressure data from UT3-3 KN is supercharged.

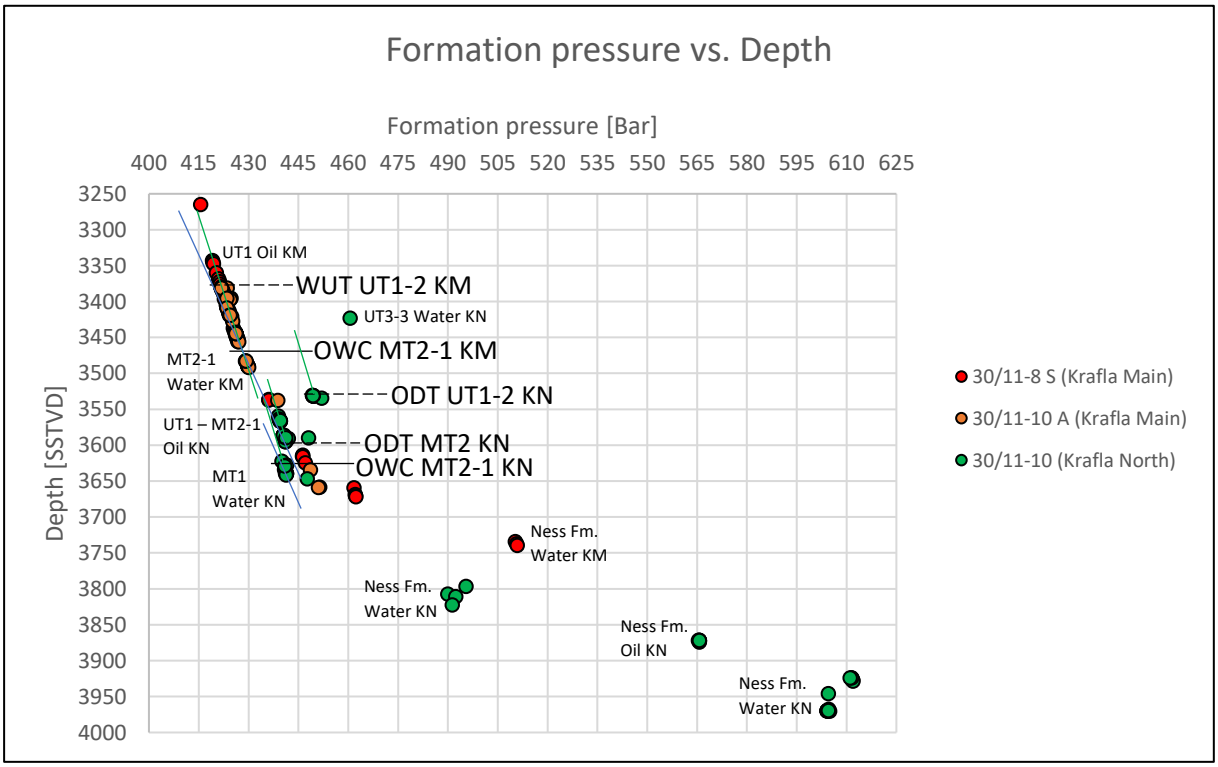

Figure 5.38: Formation pressure vs depth. Pressure data from wells –8S (red), -10A (orange) and -10 (green) are plotted with fluid gradients (green=oil, blue=water) and fluid contacts.

The minimum SGR values from the juxtaposed areas range from 36% to 48% (Figure 5.41).

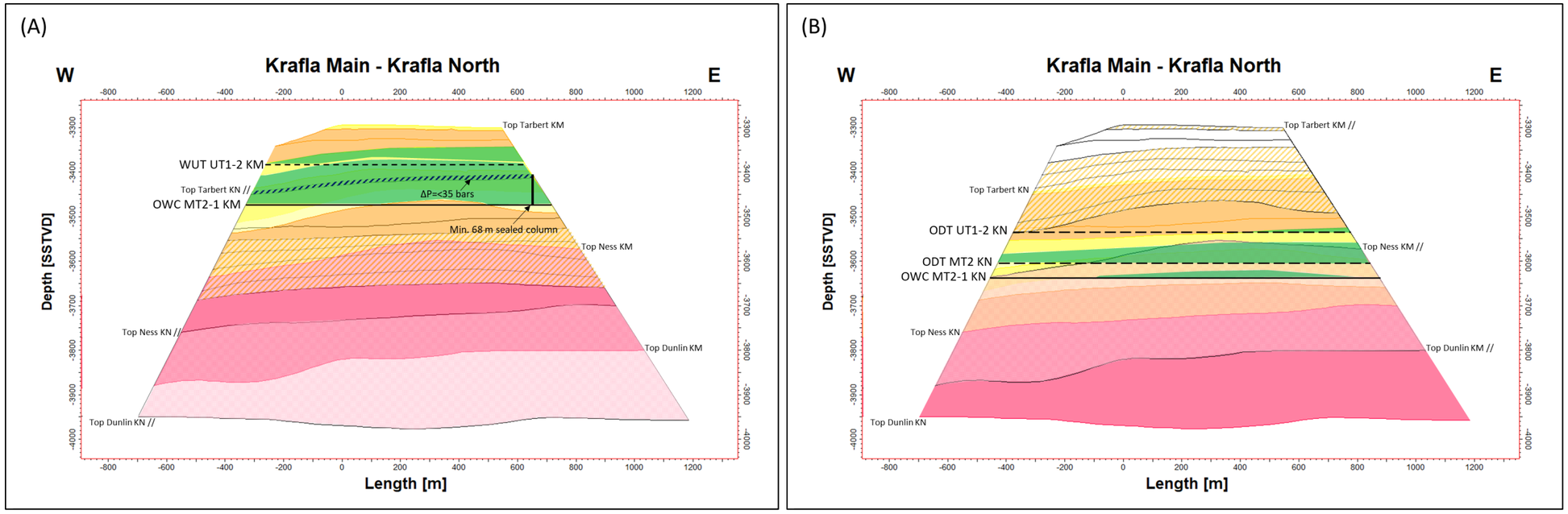

Figure 5.39: Juxtaposition plot of the fault between Krafla Main and Krafla North. The upthrown block (Krafla Main) is shown in colors, and the downthrown block (Krafla North) is shown with black outlines where the sands with good reservoir properties are shown with orange slanted lines (A). The downthrown block (Krafla North) is shown in colors, and the upthrown block (Krafla Main) is shown with black outlines (B). Fluid contacts are shown with black lines. Hydrocarbons in the colored block are shown with a transparent color (green=oil), while fluids in the side with black outlines are only shown where they are juxtaposed to hydrocarbons across the fault (shown with slanted lines).

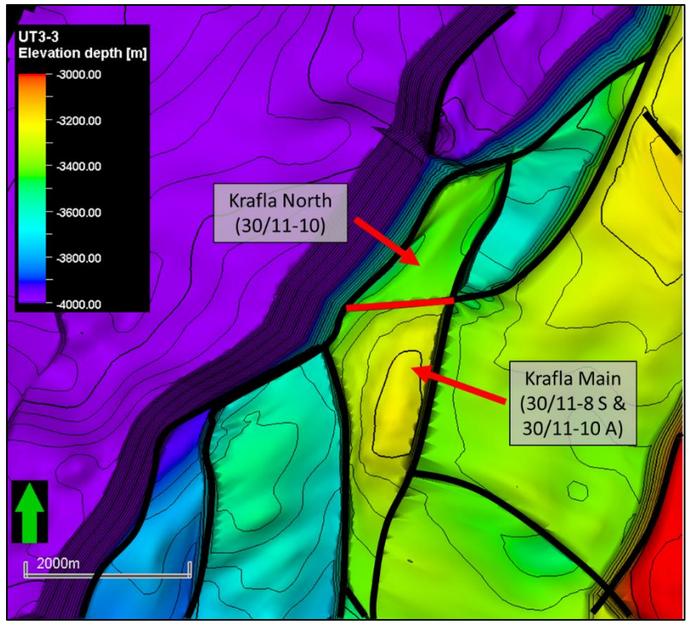

Figure 5.40: Top Brent horizon in the Krafla area. The red line separating the Krafla Main and Krafla North structures is the fault presented in Figures 5.39 and 5.41.

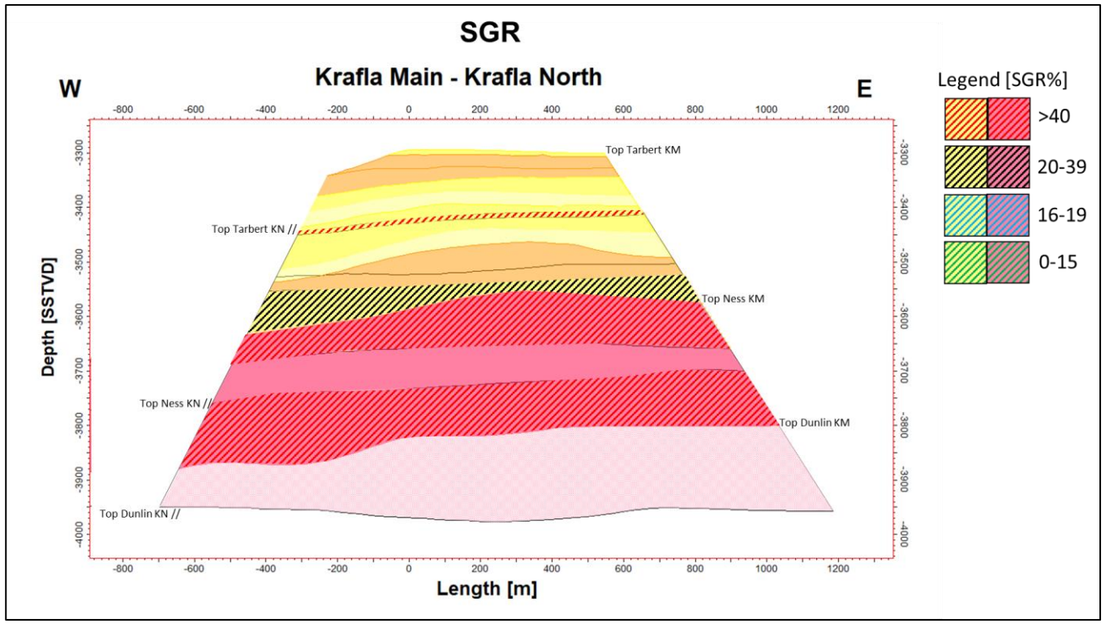

Figure 5.41: SGR plot where the SGR values are displayed where sands with good reservoir properties in the Tarbert Formation are juxtaposed against each other and, the Tarbert sands vs. Ness Formation and the Ness Formation vs. Ness Formation. SGR is color-coded in the ranges 0-15%, 16-19%, 20-39% and >40%.

5.4.5 Krafla Main–Krafla West

The Krafla Main–Krafla West fault has a general N-S fault strike with a westward dip direction (Figure 5.36 and 5.44). The fault has the largest offset out of the analyzed faults with a minimum throw of 240 m. Wells have been drilled in both the upthrown block (30/11-8 S & 30/11-10 A) and the downthrown block (30/11-8 A). Krafla West is the only fault block with oil in the upper reservoir and gas in the lower reservoir. The formation pressures at Krafla West are significantly higher than the pressures in Krafla Main (Figure 5.42). The two structures do not share any fluid contacts. The results show no juxtapositions between Tarbert sands across the fault plane (Figure 5.43). The oil in UT3-3 KW is juxtaposed to MT1 and the Upper Ness Formation. The formation pressure difference across the fault is ~130 and 125 bars. The gas in the lower reservoir is juxtaposed to Middle Ness in the north with a pressure difference of 145 bars and Lower Ness in the middle of the fault plane with a 100-bar pressure difference. The minimum SGR for the juxtaposed areas was found to have values of 30 to 47% (Figure 5.45).

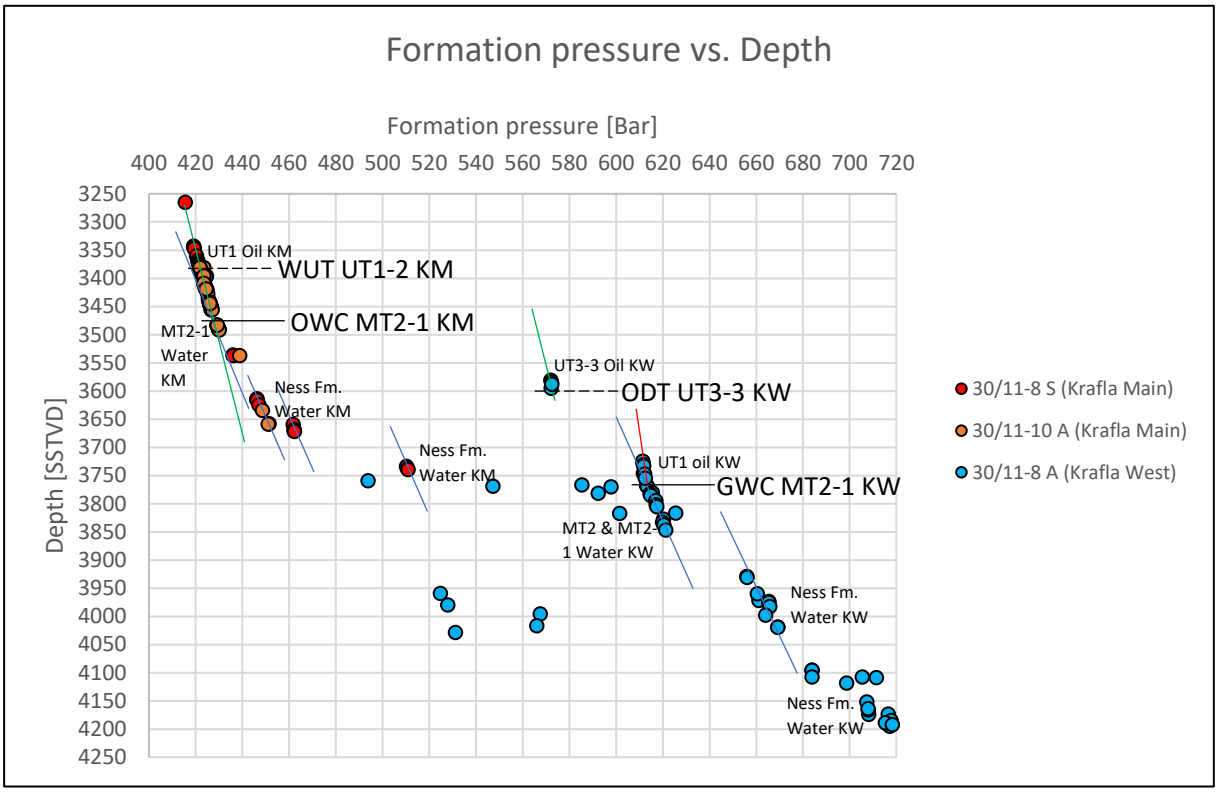

Figure 5.42: Formation pressure vs depth. Pressure data from wells -8A (blue), – 8S (red), and -10A (orange) are plotted with fluid gradients (red=gas, green=oil, blue=water) and fluid contacts.

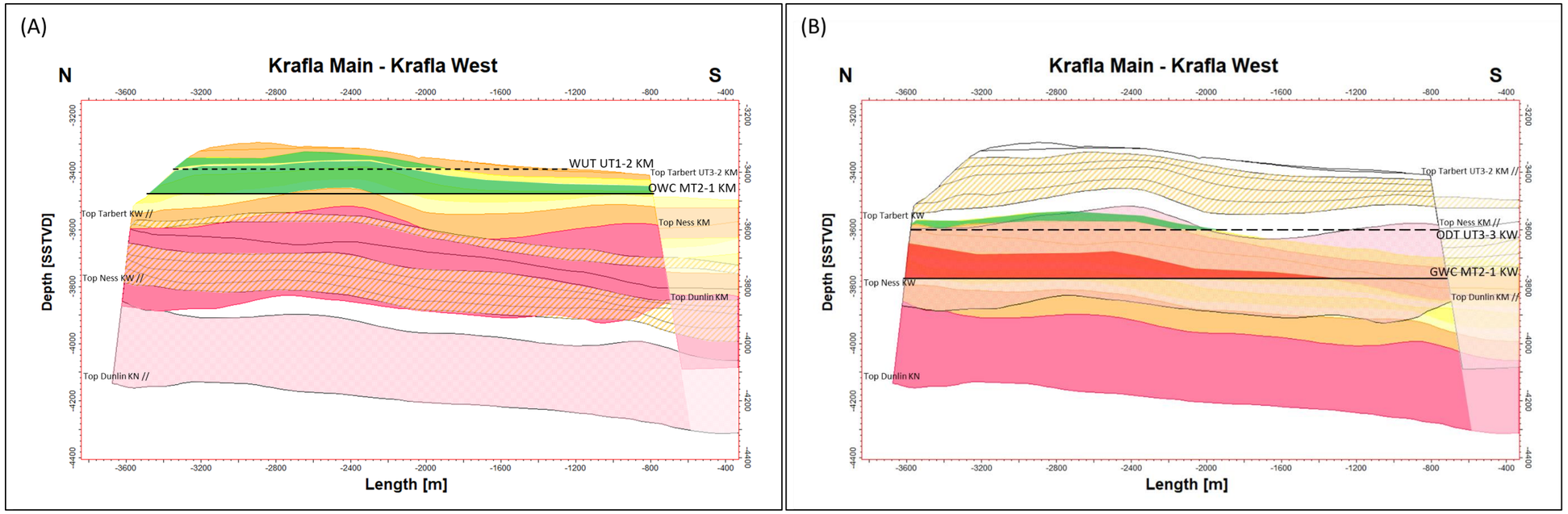

Figure 5.43: Juxtaposition plot of the fault between Krafla Main and Krafla West. The upthrown block (Krafla Main) is shown in colors, and the downthrown block (Krafla West) is shown with black outlines where the sands with good reservoir properties are shown with orange slanted lines (A). The downthrown block (Krafla West) is shown in colors, and the upthrown block (Krafla Main) is shown with black outlines (B). Fluid contacts are shown with black lines. Hydrocarbons in the colored block are shown with a transparent color (gas=red, oil=green), while fluids in the side with black outlines are only shown where they are juxtaposed to hydrocarbons across the fault (shown with slanted lines).

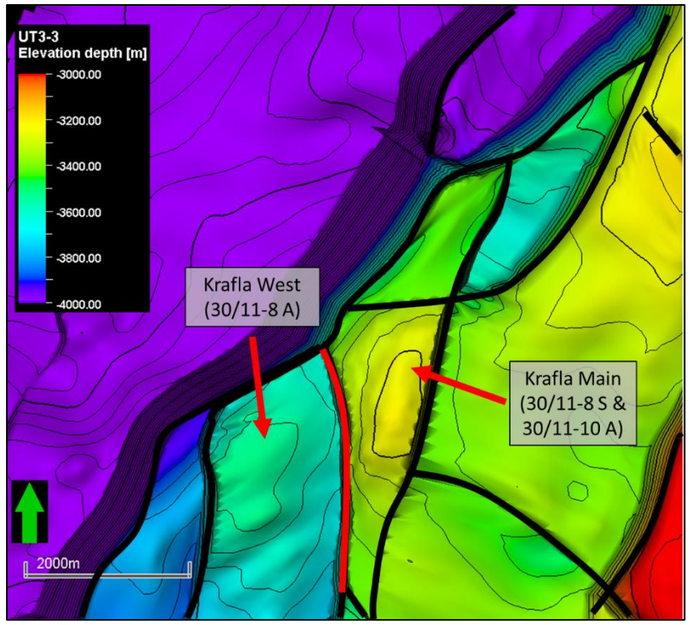

Figure 5.44: Top Brent horizon in the Krafla area. The red line separating the the Krafla Main and Krafla West structures is the fault presented in Figures 5.43 and 5.45.

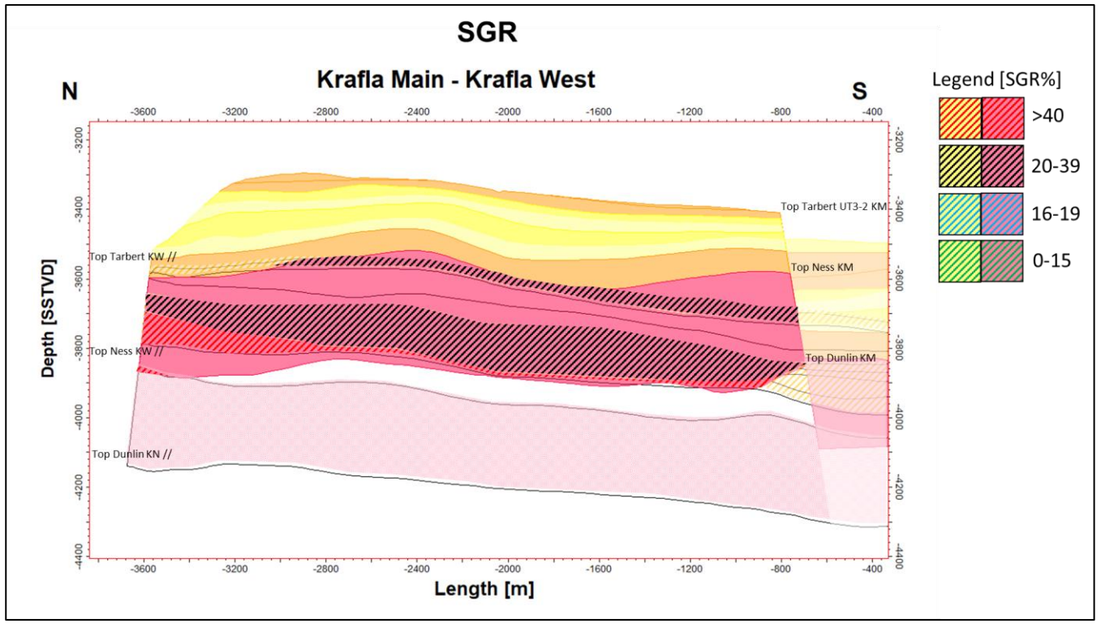

Figure 5.45: SGR plot where the SGR values are displayed where sands with good reservoir properties in the Tarbert Formation are juxtaposed to the Ness Formation and where the Ness Formation are juxtaposed to the Ness Formation. SGR is color-coded in the ranges 0-15%, 16-19%, 20-39% and >40%.

5.5 Stjerne and K structures

The Stjerne and K structures are located north of the main study area. Both the fields contain oil and gas, with fluid contacts shallower than the contacts in the Krafla–Askja area.

5.5.1 Stjerne

The Stjerne structure is located north of the Central area and is situated on the Oseberg Terrace. The structure is constrained by multiple faults, both dipping towards NW and NE. Well 30/9-22 was drilled in 2009 to prove the presence of commercial hydrocarbons in the Tarbert Formation. The well encountered gas in the Heather Formation and both gas and oil in the Tarbert Formation (NPD, 2021). A general interpretation of the structure is presented in Figure 5.46.

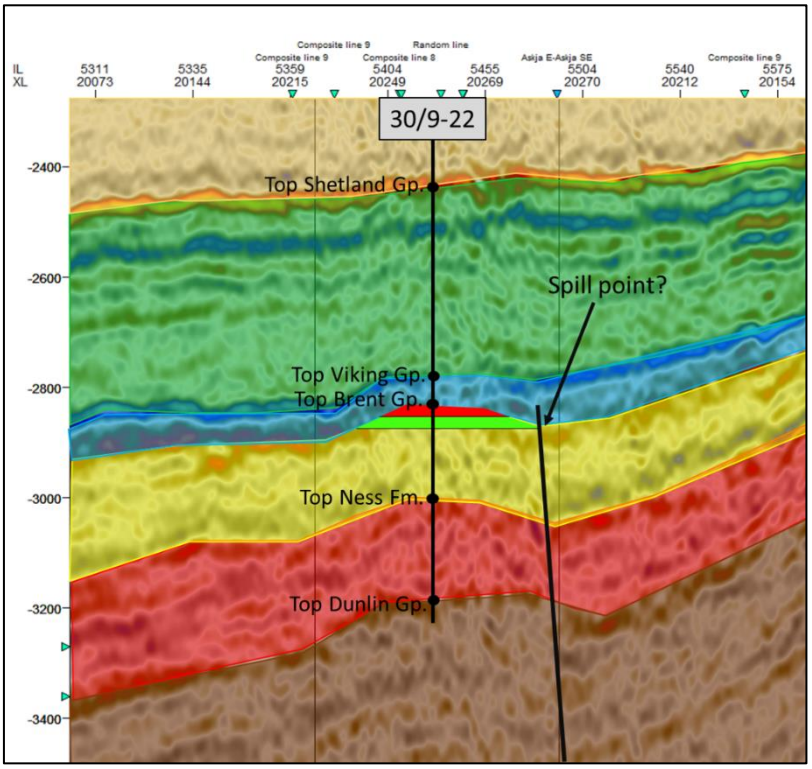

Figure 5.46: Cross-section of the Stjerne structure. The left in the figure is south, and the right-hand side of the figure is east. The Tarbert Formation is shown in yellow.

5.5.2 K structure

The K structure is located at the shallowest interpreted area and was drilled in 1994. The primary objective was to prove hydrocarbon accumulations in the Tarbert Formation and the NORE reservoir. The structure contains gas and oil in the Intra Heather and the Tarbert Formation (NPD, 2021).

Chapter 6 - Discussion

This study aimed to investigate fault sealing in the Krafla-Askja area in the northern North Sea. Parameters such as throw, SGR, spill points, across fault pressure difference, orientation, minimum sealed columns, and contact differences were gathered to investigate possible trends and correlations to predict fault-seal characteristics. One of the objectives of this study was to determine those parameters' importance for controlling fault seals and contact differences where sands with reservoir properties are juxtaposed across the faults. This chapter is divided into two subchapters. Firstly, the results from the fault analyses and uncertainties are discussed. Secondly, a subchapter discussing paleo migration routes, pressure regimes, and present-day fluid contacts.

6.1 Fault seal analysis

Faults can act as both conduits and barriers for fluid flow in the subsurface. Effective stress changes control faulting and fracturing, and changes like these may alter the hydrocarbon column heights. Most hydrocarbon accumulation in the subsurface is trapped by some kind of physical seal which prevents natural buoyancy-related upward migration (Watts, 1987). Wiprut and Zoback (2002) suggest that stress, pressure, and fault orientation appear to be important factors in controlling hydrocarbon leakage and migration in the northern North Sea. A critically stressed fault in the current stress field tends to leak, whereas those not critically stressed are more likely to be sealing. Leakage from a pressure compartment should theoretically happen in the water-bearing zone due to the fluids not having to overcome capillary pressures to leave the compartment.

Fault plane diagrams are a useful method to study fault sealing. These diagrams displays were along the fault plane there possibly are sand-sand juxtapositions and where sands are juxtaposed to impermeable beds. It is important to keep in mind the uncertainties regarding this method. One of the most considerable uncertainties surrounding the result in this study is the seismic interpretation. No clear, continuous horizons within the Tarbert Formation were observed in the seismic data. Thus, a manual interpterion was conducted for all the horizons in the Brent Group. Gas-filled sandstones have a lower acoustic impedance, while water-bearing sandstones have a higher acoustic impedance resulting in horizons varying across the study area. This can result in interpretation errors like a wrong interpretation of horizon tops, bed thicknesses and fault placements. This could result in non-existing sand-sand contacts across the faults being

created and possibly leading to important juxtapositions not being shown. A misinterpreted fault plane would likely influence the calculated shale gouge ratio. If UT3-3 is juxtaposed to UT2, and the poor reservoir zone between the layers was interpreted to be thinner than in reality, it would result in a higher sand-to-shale ratio and thus a lower shale gouge ratio.

Shale gouge ratio was calculated using Vshale curves based on the gamma-ray logs. The Vshale curves range from 0% (being the cleanest sand) to 100% (being the cleanest shale). The curves will vary depending on which values from the gamma-ray log are chosen to represent 0 and 100% shale. The cleanest sands in the study area are found in UT1 shoreface sands, MT2-1 tide-influenced channel/estuarine complex sands, and sands in the Ness Formation. The highest API is found in the offshore Heather shales. The Brent Group is not homogenous across the study area, with the lithology and bed thicknesses varying. The method of creating Vshale logs by picking 0 and 100% could result in different curves depending on the gamma-ray logs. One well might have a clean sand with 15 API, while another well could have the same sand with 30 API. If the logs are picked separately, with 0 being 15 API in one well and 30 API in the other, and 100% is the same in both the wells, then the Vshale curves will be different. This is important to recognize when comparing different studies as the SGR values might not directly correlate. "Moving average" was used for SGR calculation in Petrel. This method takes the Vshale values from the wells and calculates the average Vshale according to the distance from the well. The area between the two wells will have the average value of the two Vshale curves. If the wells are located far from the fault, then there would be greater uncertainty about the lithology at the fault plane. A problem with using the 0-100% shale method is that the shales pick to be 100% shale often are not pure shales. Different methods for calculating SGR will result in different values. There are uncertainties in predicting fault-zone properties, especially when it comes to the proportion of fine-grained material in the fault zone. The highest uncertainty is the methodology used for calculating Vshale curves, as different methods can create different curves. Figure 6.1 is from a study done by Bretan and Yielding (2005), which shows two different Vclay curves and SGR values from the same Brent Group sequence. Curve 1 is the initial Vclay estimate, and curve 2 includes kaolin and mica. When minerals like mica and kaolin are incorporated in calculating Vclay/Vshale curves, it could result in significant differences in SGR values. Another problem is that non-radioactive clays might not be detected by the gamma-ray logs creating uncertainties in the Vshale curves. Non-radioactive minerals are difficult to predict, but both radioactive and non-radioactive clays should be used to get the best curve possible.

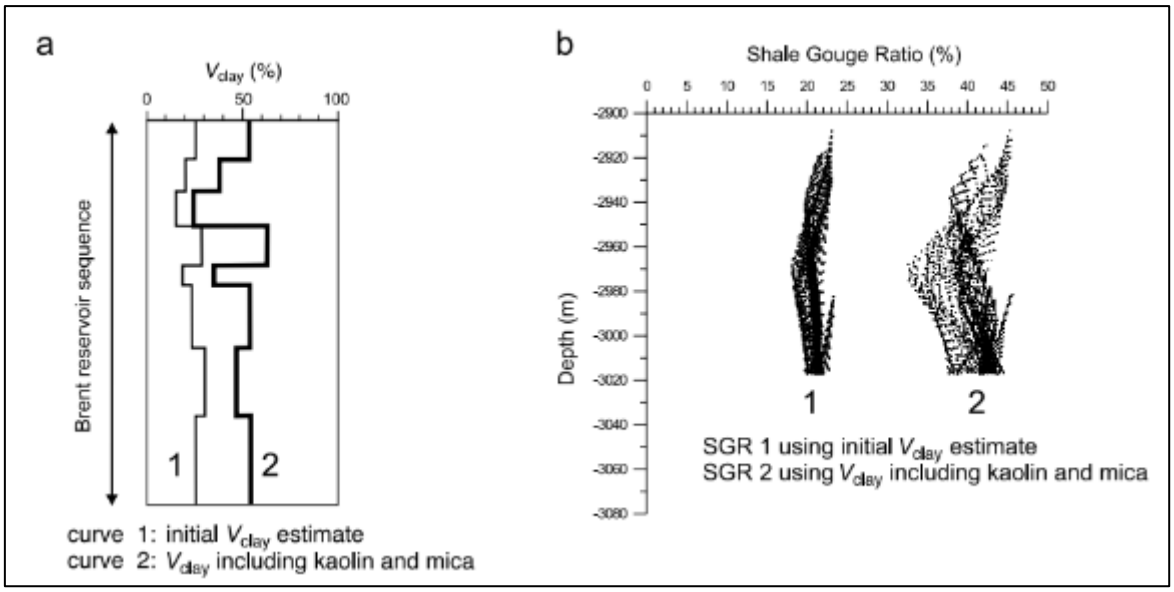

Figure 6.1: Figure showing (a) two different Vclay logs for the same Brent sequence and (b) SGR distribution from reservoir juxtapositions using the Vclay logs (Bretan and Yielding, 2005).

Fristad et al. (1997) did a fault seal study in the Oseberg Sør area. In their analysis, the Vshale was created from an initial petrophysical interpretation of wireline logs. Figure 6.2 shows the weakest points of the fault where the maximum pressure difference for small SGR values occurs. They suggest that no seal is expected at values below 15%. A slight seal with above 1 bar pressure difference or 30 m difference in OWC is expected with values between 15 and 18%. SGR values above 18% give a considerable seal with ~8 bar pressure difference or up to 240 m difference in OWC. The weakest points from the analyzed faults in this study do not follow the same pattern as what Fristad et al. (1997) observed in the Oseberg Sør field. In the Krafla-Askja area, faults with SGR values as low as 12% are observed to hold a pressure difference of 14 bars, and 17% can hold a pressure difference of 27 bars (Figure 6.3).

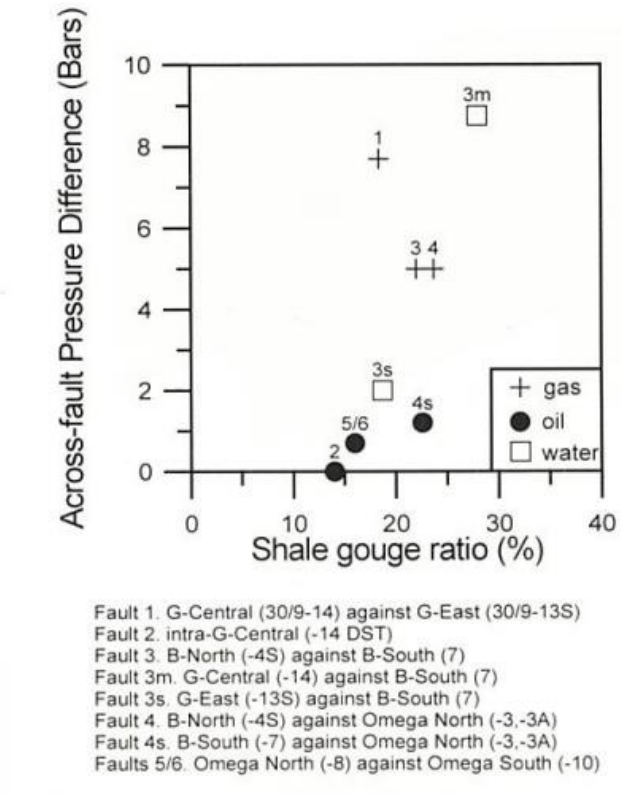

Figure 6.2: Maximum across-fault pressure difference plotted against minimum SGR for six faults in the Oseberg Sør field (Fristad et al., 1997).

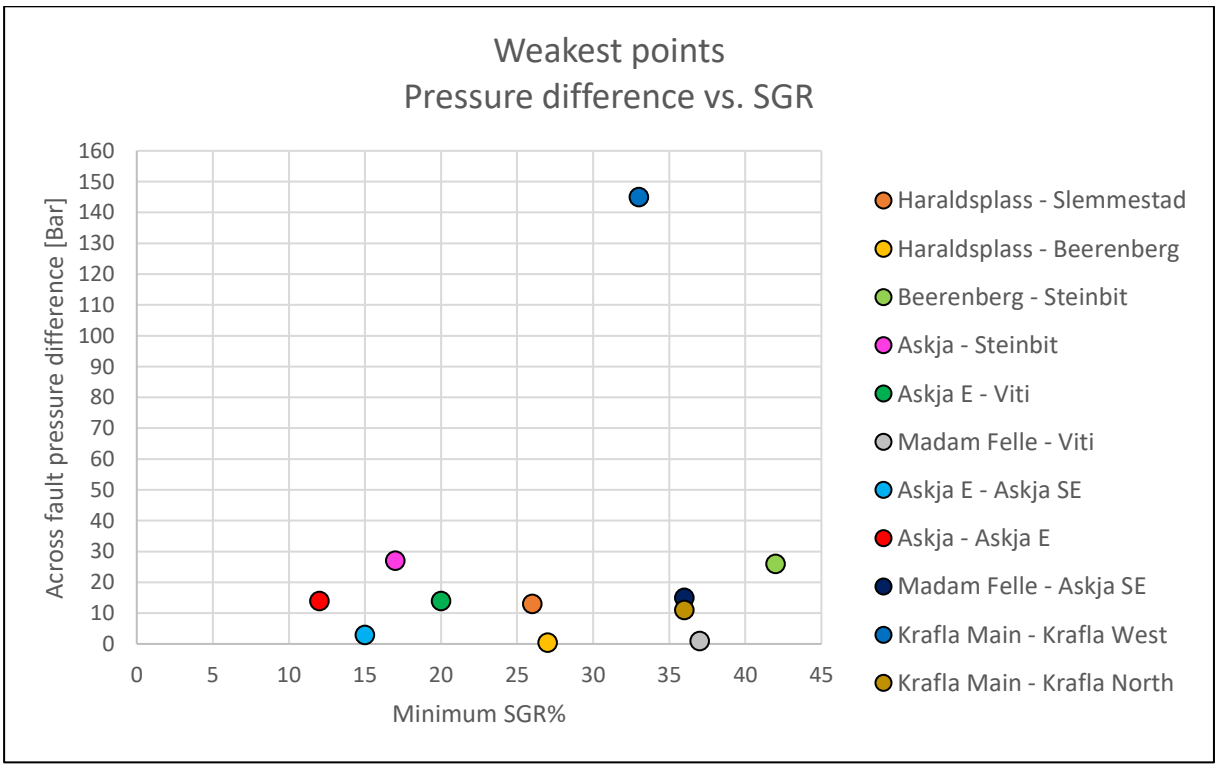

Figure 6.3: Across fault pressure difference vs. minimum SGR plot showing the weakest points from the different faults.

Bretan et al. (2003) did a study where they took the original weakest points from Fristad et al. (1997) and applied different methods for Vshale calculation (Figure 6.4). They incorporated mica and kaolin in their Vshale calculations. The result was higher minimum SGR values for the across fault pressure differences. Fault 1 had an initial SGR value of 18%, but Vshale with mica and kaolin moves the value up to 30% showing that how the Vshale curves are calculated matters greatly. Comparison of published SGR values is difficult due to different methods used to create Vclay. Comparing results from different SGR studies should therefore be done with caution when the methods for Vshale estimation are different or not provided.

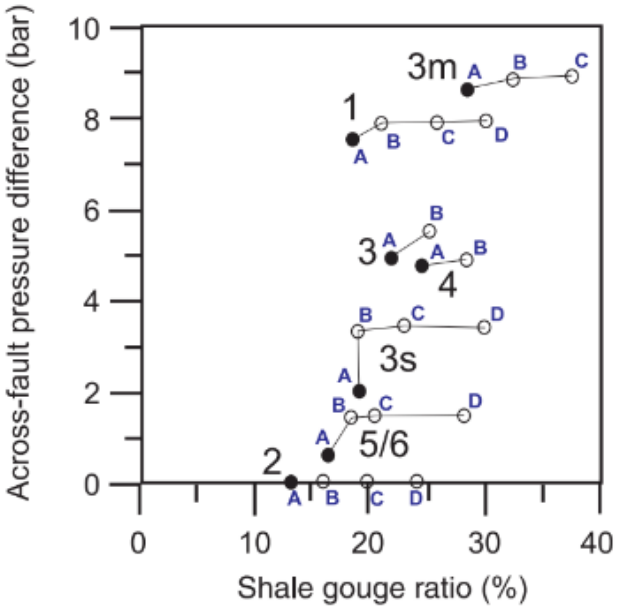

Figure 6.4: Maximum across-fault pressure difference plotted against minimum SGR for six faults in the Oseberg Sør field with different methods for Vshale calculation. 1-6=original values, A=Vshale with no mica, B=Vshale with mica, C=Vshale with mica and kaolin (Bretan et al., 2003, modified from Fristad et al., 1997).

Compartmentalization of the structures can lead to misinterpretation when estimating fluid contacts. Using water gradients from other compartments within a structure could be used when a water gradient is not present in the compartment. Uncertainties do occur when doing this, as this method might not give the correct contact depth. The compartments can be differently pressured or have different fluid densities resulting in different fluid gradients.

Data from 77 juxtapositions across 13 faults were gathered from the Krafla-Askja area. The data are gathered from areas across the faults where Tarbert sands are juxtaposed against Tarbert sands, Tarbert sands against the Ness Formation, and where the Ness Formation is self juxtaposed. The top of the juxtaposed areas (fault spill points) is found in the depth interval of 2 890–3 830 m (Figure 6.5). The Ness Formation is a shaly formation with multiple channel

sands making up different pressure compartments. The sands in the Ness Formation were not individually interpreted. Instead, a rough estimate of Upper, Middle and Lower Ness was used. This could result in wrong values, so data from the Ness juxtapositions should be looked at extra critically. 15 juxtaposed areas where Ness is self-juxtaposed were observed, 25 Tarbert sands vs. the Ness Formation and 37 Tarbert sand vs. Tarbert sand were observed.

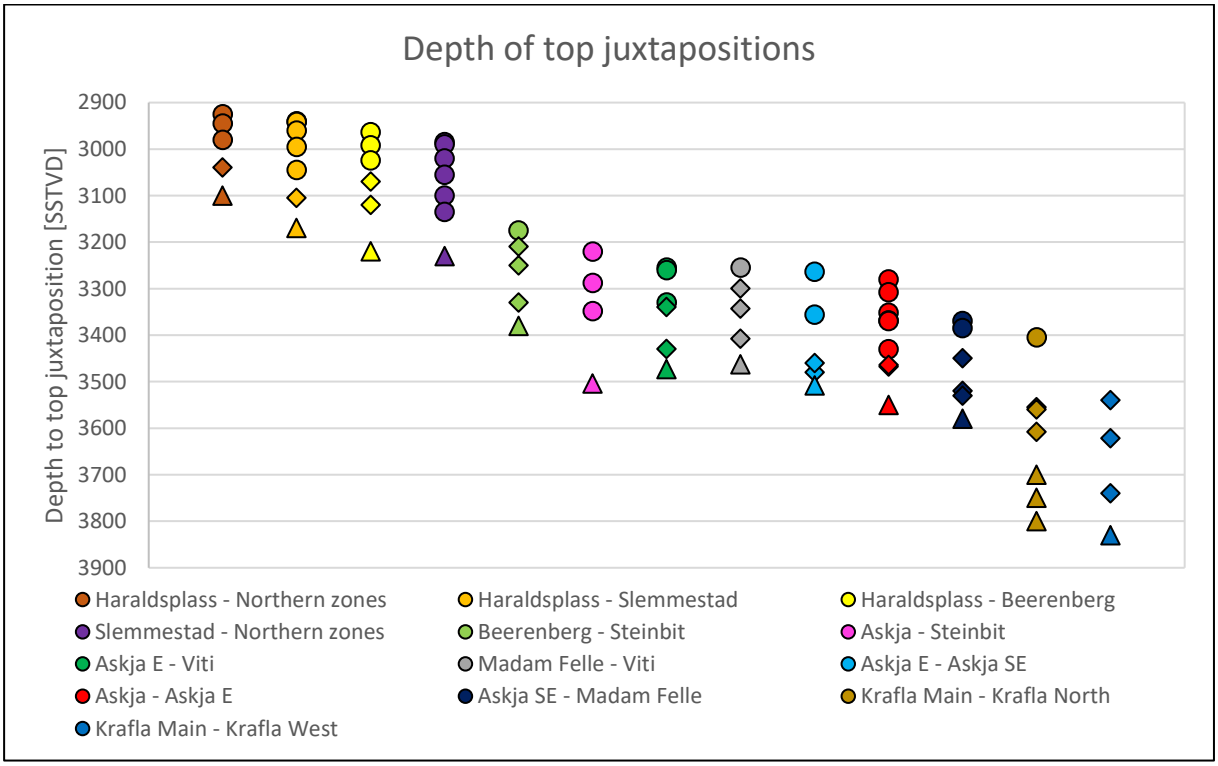

Figure 6.5: Depth to top sand-sand juxtaposition for the 13 analyzed faults. Circles represent Tarbert sands vs. Tarbert sands, diamonds represent Tarbert Sands vs. the Ness Formation, and triangles represent self-juxtaposed Ness sands.

6.1.1 Fault sealing

Fluid contact depths vary within the Krafla-Askja structures, as the area is highly faulted and compartmentalized. Observations from the structures suggest that the supply of hydrocarbons into the reservoirs has been sufficient as the hydrocarbon columns reach deeper than the spill points. 18 sand-sand juxtapositions are observed to have hydrocarbons on either one or both sides of the fault with fluid contacts deeper than the spill points. These are overfilled reservoirs suggesting the fault itself is sealing. A shale gouge ratio was calculated for 11 faults separating different structures with accumulating hydrocarbons and two faults separating Haraldsplass and Slemmestad and the fault block to the north. This was done in order to investigate the correlation between SGR and the sealing capabilities of the faults. The Brent Group is generally quite shaly, and therefore, we might expect any observed sealing behavior to be a consequence either of

juxtaposition or some mechanism of clay smearing (Fristad et al., 1997). The Shale Gouge Ratio (SGR) algorithm takes the average clay content of those beds that have been faulted past any point and treats this as an estimate of upscaled fault-zone composition. When the SGR value is high (above 40-50%), the fault rock is dominated by clay smears. If the Brent Group juxtapositions have less than 15-20% SGR, then the shale smears are discontinuous, and the dominant fault-zone materials are generally unable to provide a recognizable seal (Yielding, 2002; Yielding et al., 2010). The calculated SGR values are shown in Figure 6.6 together with the juxtaposed sands. 45 out of the 77 juxtaposed areas have a minimum SGR value of 20-40%. 33 juxtaposed areas have values above 40% and should thus be dominated by clay smears. The lowest SGR values (values below 20%) are found where Tarbert sands are self-juxtaposed and where UT2/UT2&1 are juxtaposed to MT2-1. Little to no shale has slipped through the intervals where the UT3-3 and MT2-1 reservoir sands are self-juxtaposed. This would result in a lower shale gouge ratio. Gibson (1994) showed that self-juxtaposed sand forms poor fault seals and that significant fault seals are formed when clay smearing can occur down the fault plane . This fits with four of the self-juxtaposed Tarbert sands. However, only one out of the three self-juxtaposed UT3-3 areas has a value below 20%, whereas the two others have a minimum SGR value of 27% and 48%. A possible explanation for the large difference in minimum SGR is likely due to lithological differences (Figure 6.7). The SGR values are calculated using “moving average” in Petrel. This method takes the Vshale values from the wells and calculates the average Vshale according to the distance from the well. This could be an explanation for the vast span in UT3-3 self-juxtaposed SGR values. The lowest of these values are found along the Askja-Askja East fault, with a value of 13%. The two wellbores are relatively close to each other, where -9A is a geologic sidetrack to well -9S. The UT3-3 sands in Askja and Askja East generally have low API resulting in a low SGR value. The UT3-3 self-juxtaposed area with 27% SGR is the fault between Askja and Steinbit. This area has likely a higher SGR than expected for a self-juxtaposition due to Steinbit mostly having an API above 60 and containing finer grains than the UT3-3 self-juxtaposed area between Askja and Askja East. The 48% SGR value is between Slemmestad and the fault block to the north. UT3-3 Slemmestad is not the cleanest sandstone and UT3-3 Stjerne having API above 90. The SGR value at the fault plane is thus likely to be high. The self-juxtaposed UT3-3 area between Askja and Askja East has an across pressure difference of 12 bars and a maximum contact difference of 48 m. The shale smear in this area should be discontinuous; thus, self-juxtaposed membrane seal is the likely seal mechanism. The first-order controls on fault-rock development are the lithologies (clay content) in the faulted sequence and offset of the fault. In areas where there is less shale,

cataclasis and/or diagenesis would have to play a more important role (Fristad et al., 1997). The lowest SGR values are found towards the lower parts of The Tarbert Formations. This is due to the sands in UT1 and MT2-1 being the cleanest sands in the Formation. The juxtaposed areas deeper than ~3.5 km are observed to have SGR values <30%. These are also all Ness juxtaposition which should have higher SGR values due to the amount of clay content. All Tarbert vs. Tarbert juxtapositions are found at depths shallower than 3.5 km, with the shallowest being at 2 890 m and the deepest at 3 468 m depth. Quartz cementation increases significantly at depths exceeding 3 km in the Brent Group (Bjørlykke et al., 1992), with Tarbert juxtaposition being found at shallower and deeper levels.

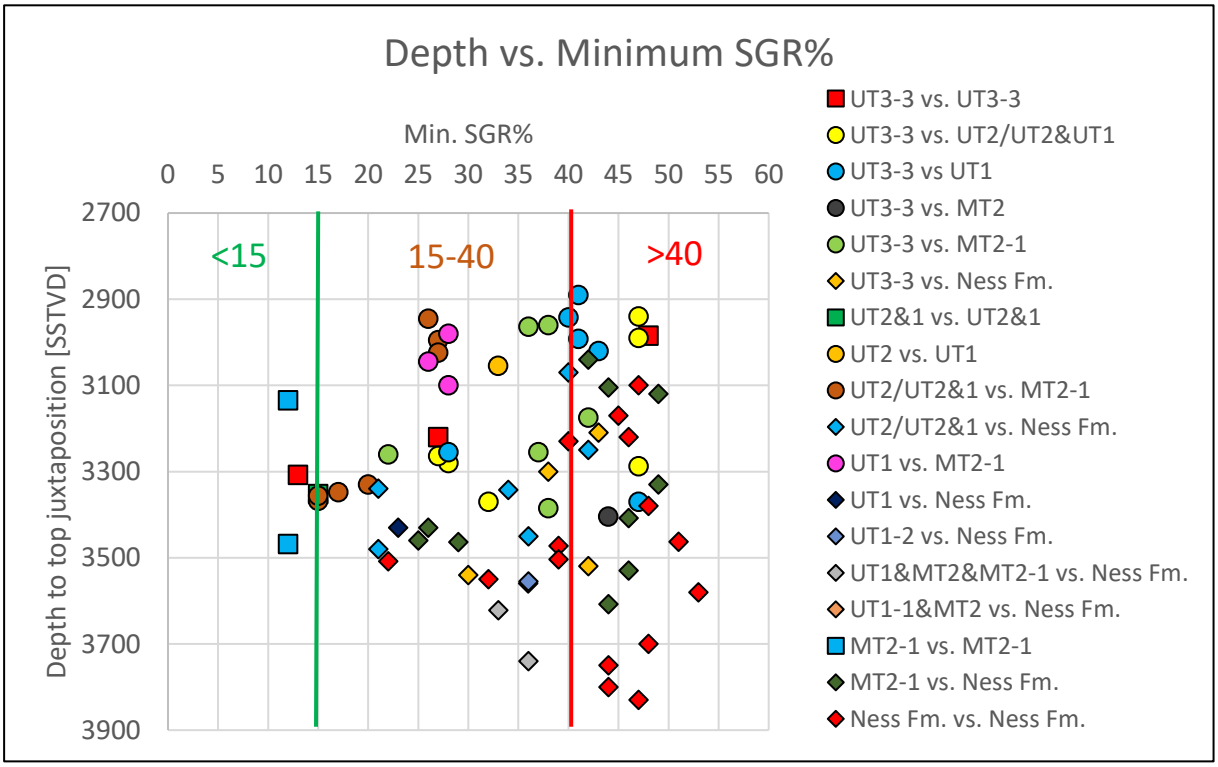

Figure 6.6: Minimum SGR% vs. depth to top sand-sand contacts. Squares represent self-juxtaposed Tarbert sands, circles represent Tarbert sands vs. Tarbert sands, and diamonds represent juxtapositions against the Ness Formation.

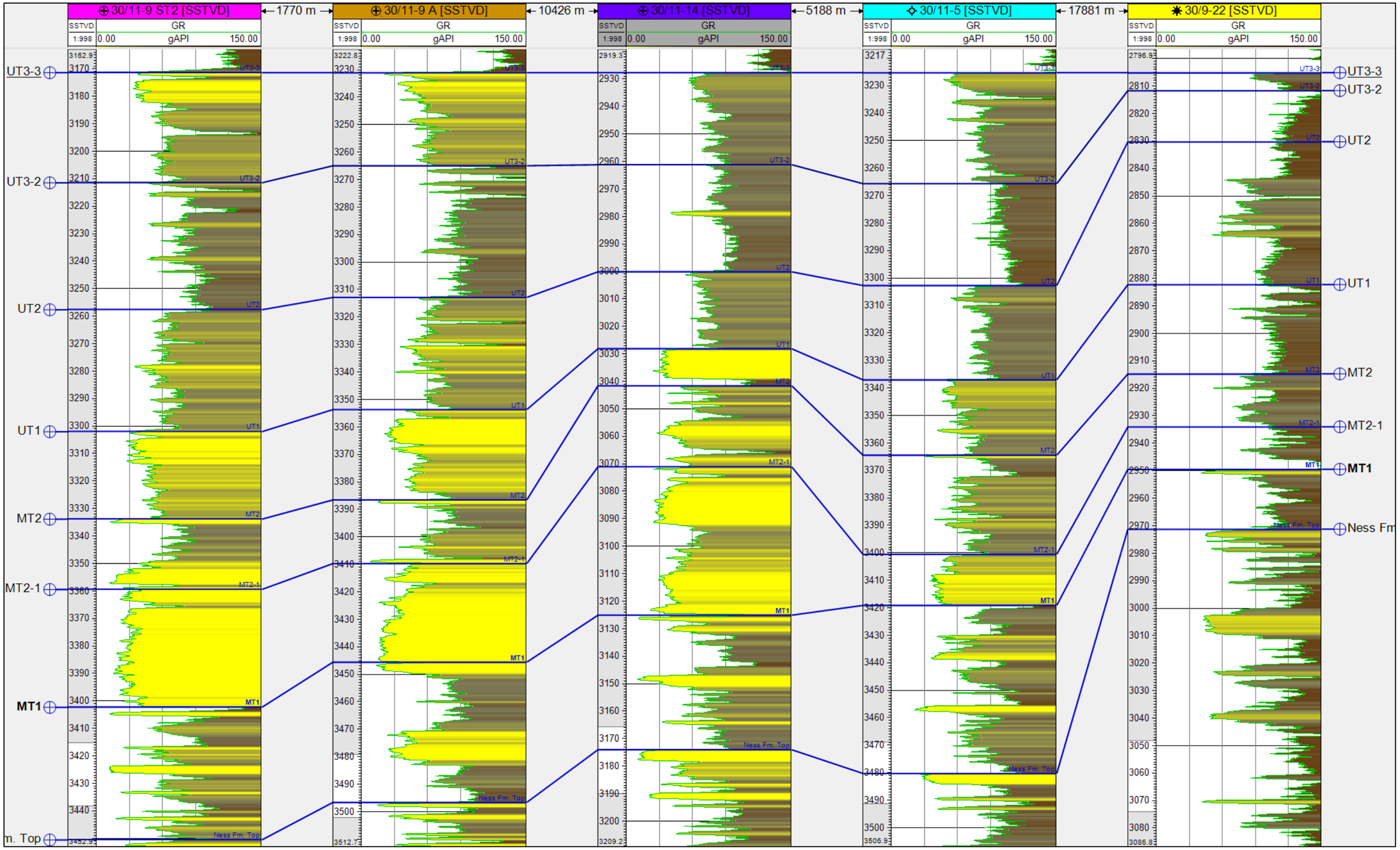

Figure 6.7: Gamma-ray logs from wells 30/11-9 ST2, -9A, -14, -5 and 30/9-22. A lower API value indicates cleaner sand, while a higher API indicates a cleaner shale. Lithology not interpreted in the figure.

Figure 6.8 shows the sealed juxtaposed areas in an across pressure difference vs. minimum SGR plot. The faults are all interpreted to be sealing. With this specific method for calculating SGR values, the results are as follows. An SGR of 12% can hold a pressure difference of 14 bars, a value of 30% can hold a pressure difference of 125 bars, and a value of 33 can hold a pressure difference of 145 bars. A line has been drawn between the three data points suggesting that data points below this line are sealed. Uncertainties do occur as other factors like cementation could play an important role in sealing the fluids. Sealing above this line can occur as the maximum pressure difference that an SGR value could hold is unknown.

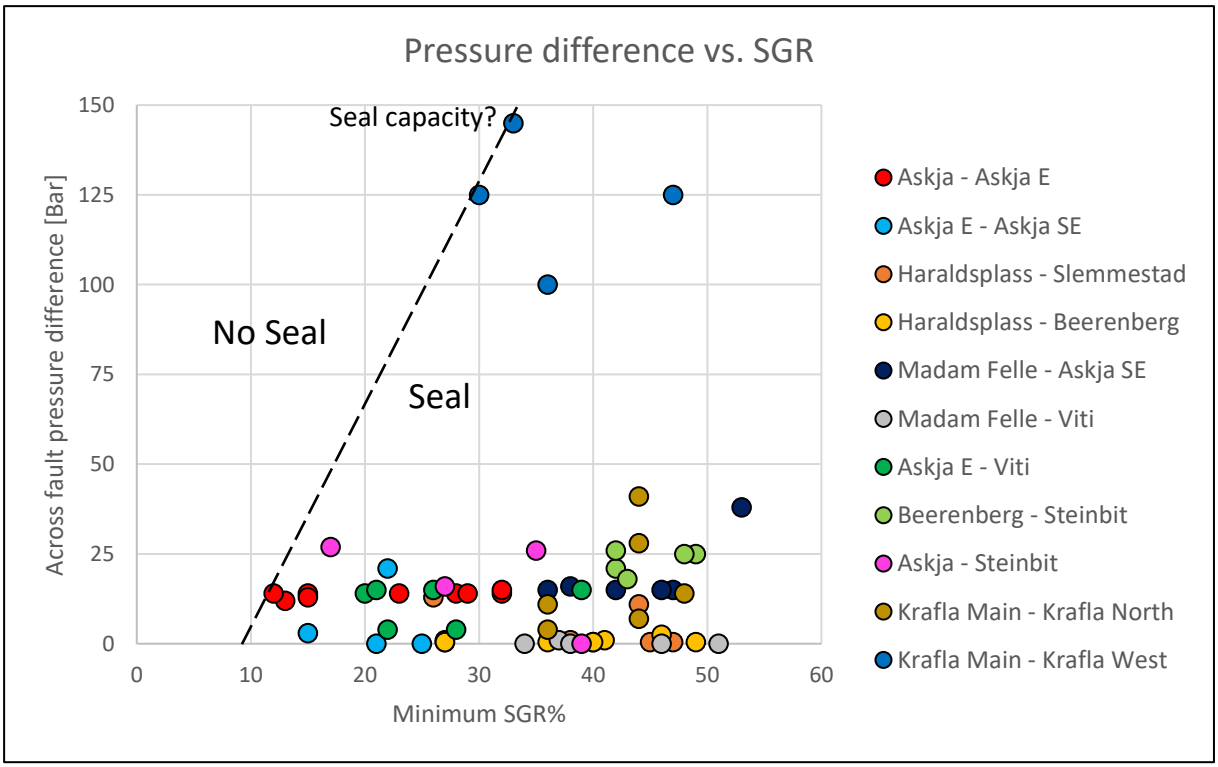

Figure 6.8: Across fault pressure difference vs. minimum SGR.

6.1.2 Fault orientation and present-day stress field

The stress state along the Norwegian Continental shelf has changed several times during Pliocene and Pleistocene due to repeated glacial advances and withdrawals. Increased stress anisotropy could cause trap failure, most likely by fault reactivation (Bolås et al., 2005). Wiprut and Zoback (2000; 2002) suggest that fault reactivation and hydrocarbon leakage in the northern North Sea could be caused by fault orientations nearly optimally oriented for frictional slip in the present-day stress field. Brudy and Kjørholt (2001) observed that the orientation of the maximum horizontal stress in the Oseberg/Troll area has a general E-W orientation (Figure 2.7). Bolås et al. (2005) and Magee et al. (2010) use a $\pm 30^{\circ}$ preferential window from the

maximum horizontal stress orientation. The faults within this window should be critically stressed, making the faults more permeable (Figure 6.9). The faults outside the window should have a higher chance of being held closed due to compression. This correlates with Knotts (1993), suggesting a correlation between fault orientation and sealing, where N-S faults are more commonly sealing than E-W-oriented faults.

Thirteen faults have been analyzed in this study. The faults have been interpreted to have five orientations, with ten of the fault either having an orientation of NNE-SSW parallel to the Viking Graben or WNW-ESE perpendicular to the Viking Graben. Figure 6.9 shows a rose diagram of the faults analyzed in this study together with a $\pm 30^{\circ}$ preferential window for the present-day stress regime. This suggests the WNW-ESE and the E-W oriented faults could be critically stressed and more likely to reactivate in the current stress regime. The locations of the analyzed faults which might be critically stressed in the present-day stress field are shown in Figure 6.10.

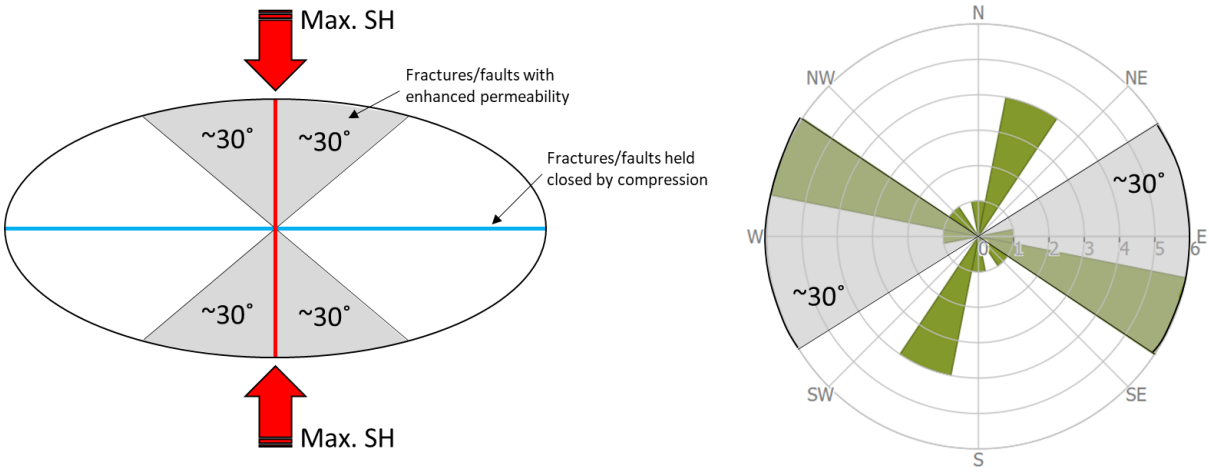

Figure 6.9: Plane strain ellipse illustrating fault orientations with expected permeability. Rose plot shows the orientations of the studied faults with the areas in transparent gray indicating critically stressed faults under an E-W maximum compressive stress.

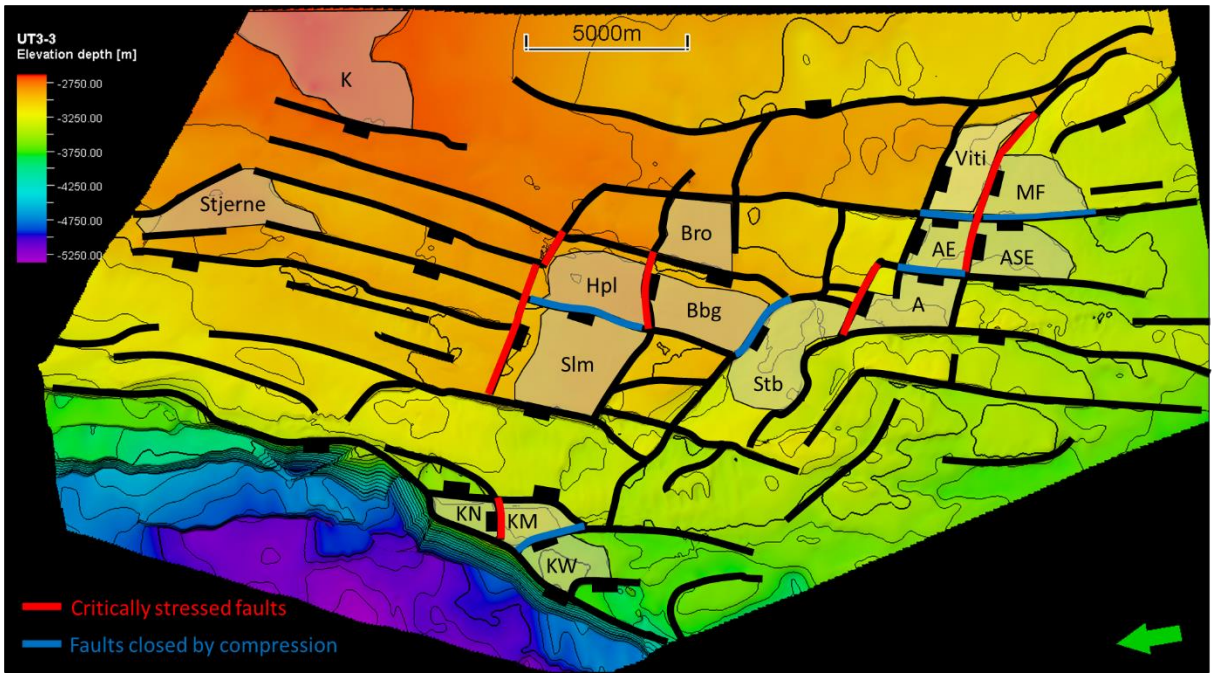

Figure 6.10: Map view of Top Brent with faults shown as black lines and the structures with a transparent gray color. The red lines represent analyzed faults that are critically stressed in the present-day stress field. The blue lines represent analyzed faults that are not critically stressed and are more likely to be closed due to compression.

The critically stressed faults are likely to have been reactivated at a later stage than the non-critically stressed faults. A lower across fault pressure difference could be a result of later fault reactivation. The difference in across fault pressure difference between the critically stressed and non-critically stressed fault is apparent in Figure 6.11. Most of the WNW-ESE striking faults have across fault pressure differences of 0-3 bars with the exception of the Askja-Steinbit fault having pressure differences up to 27 bars. The NNE-SSW striking faults parallel to the Viking Graben have pressure differences generally around 12-16 bars with the exception of the Haraldsplass-Slemmestad fault and the two juxtaposed areas where UT3-3 Askja East is juxtaposed to Viti. The E-W-oriented fault separating Krafla Main and Krafla North should also be critically stressed. The four shallowest juxtaposed areas along the fault have across fault pressure differences of 4-14 bars, possibly indicating a later reactivation than the non-critically stressed faults.

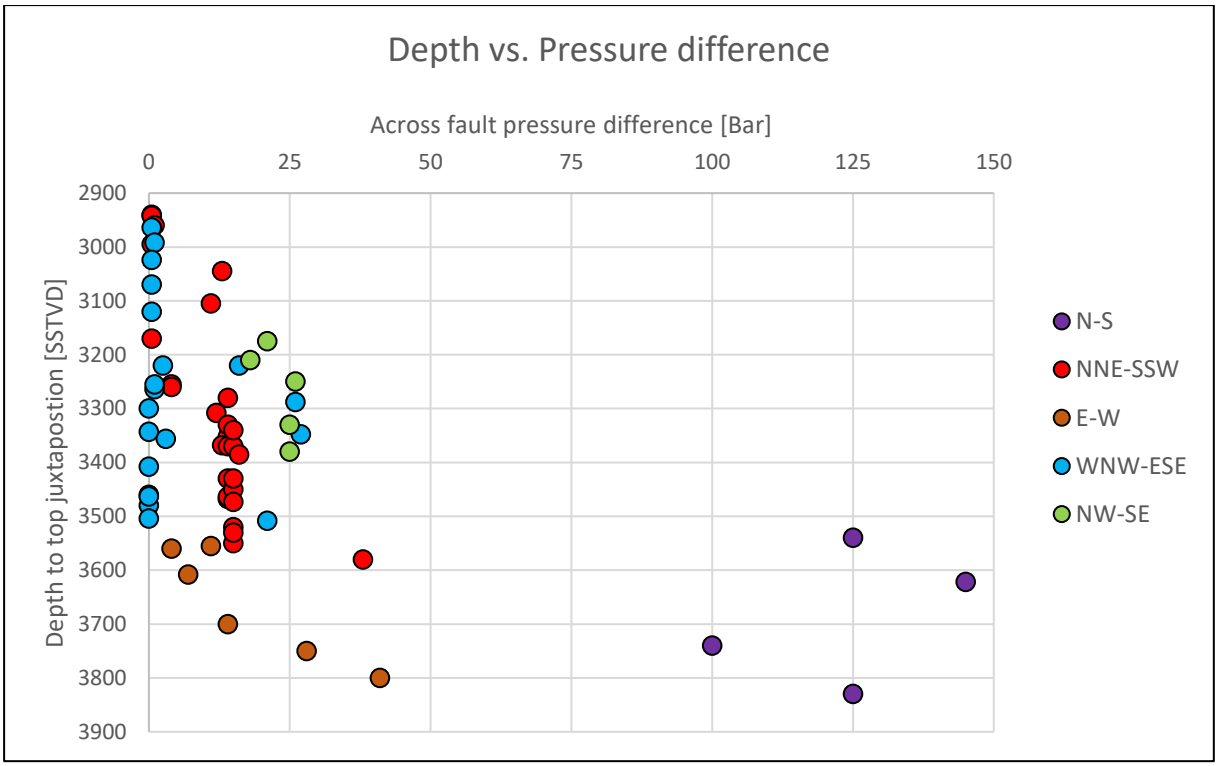

Figure 6.11: Depth to top juxtaposition vs. across fault pressure difference with fault strike orientations.

Formation pressures generally increase horizontally and vertically with depth. Two of the wells used in this study have zones with decreased formation pressures. These being 30/11-10 (Krafla North) and 30/11-14 (Slemmestad) (Figure 6.12). A drop in average reservoir pressure could happen due to depletion during fluid production or fault reactivation, increasing permeability along the fault plane. Four normal faults bound the Slemmestad fault block. The Tarbert Formation is juxtaposed to the Viking Group to the west and share no fluid pressure gradients with Haraldsplass to the east. The most plausible reason for the decreased formation pressure is a reactivation of the northern fault. The pressure decrease is found in UT1 and MT2-1. MT2-1 is self-juxtaposed across the fault, with an SGR of 12% being the lowest SGR value observed together with an MT2-1 self-juxtaposed area between Askja and Askja East. The pressures gradient in UT1 is ~12 bars lower than UT2 and UT3-3. The fault is critically stressed in the present-day stress field, suggesting that a late reactivation could have occurred, releasing pressures in the UT1 and MT2-1 compartments. MT2-1 is normally pressured, following the hydrostatic pressure gradient. The fluids being normally pressured, it having a low SGR value, and the fault is critically stressed could suggest that parts of the fault are open between the MT2-1 sands. Krafla North has formation pressure decreases in both the UT1-1 and MT2-1 compartments (Figure 6.12). UT1-1 is ~12 bars lower than UT1-2 and MT2-1 is ~3 bars lower than UT1-1 and MT2. The Krafla North structure is a down-faulted block with critically

stressed faults to the south and north. The structure does not share any fluid gradients with the Ness Formation in Krafla Main. The decreased formation pressures could have happened due to increased permeability to Ness sands in Krafla Main or the eastern downthrown block.

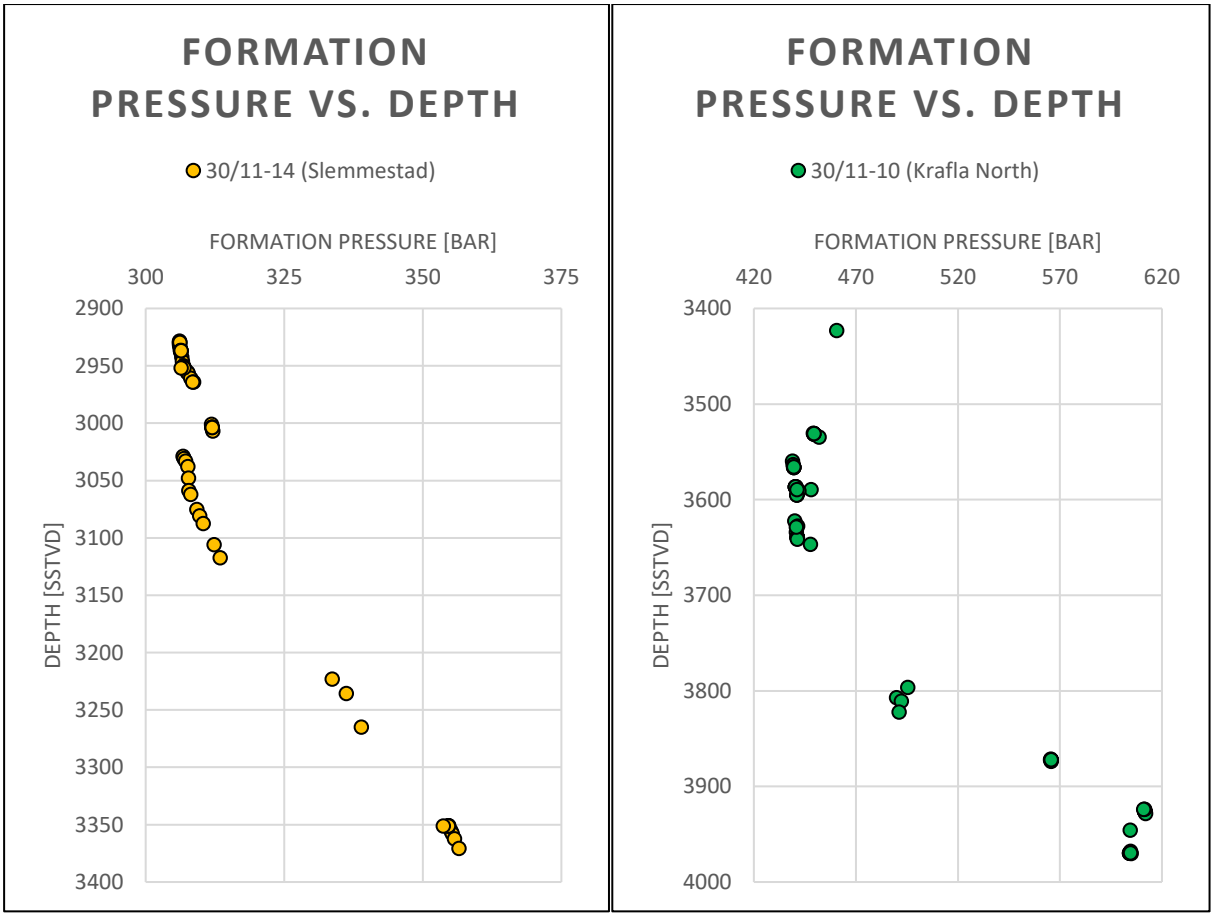

Figure 6.12: Formation pressure vs. depth plots of wells 30/11-10 and 30/11-14.

6.1.3 Fault throw

Shale gouge ratio is dependent on the lithology and throw. The amount of throw at the juxtaposed areas itself should not control the amount of seal. However, if the lithology is similar across the area, we should expect the same juxtapositions, e.g., UT3-3 vs. MT2-1 to have the same SGR at similar throws. Figure 6.13 shows the different juxtaposed areas in a throw vs. minimum SGR plot. The data shows that when the throw in the Brent Group is 150 m or more, the expected minimum SGR value is 30 and higher. Throws above 150 m result in UT3-3 vs. MT2-1 and juxtapositions against Ness. This is only representative of the Brent Group in the study area, whereas another location could have a different lithology and/or thicknesses. Throws less than 150 m show no patterns with minimum SGR values ranging from 12 to 53%. The lowest SGR values are observed in self-juxtaposed Tarbert sands and throws of 80-112 m

between UT2/UT1 and MT2-1, where UT1 and MT2-1 generally are the cleanest sands in the area.

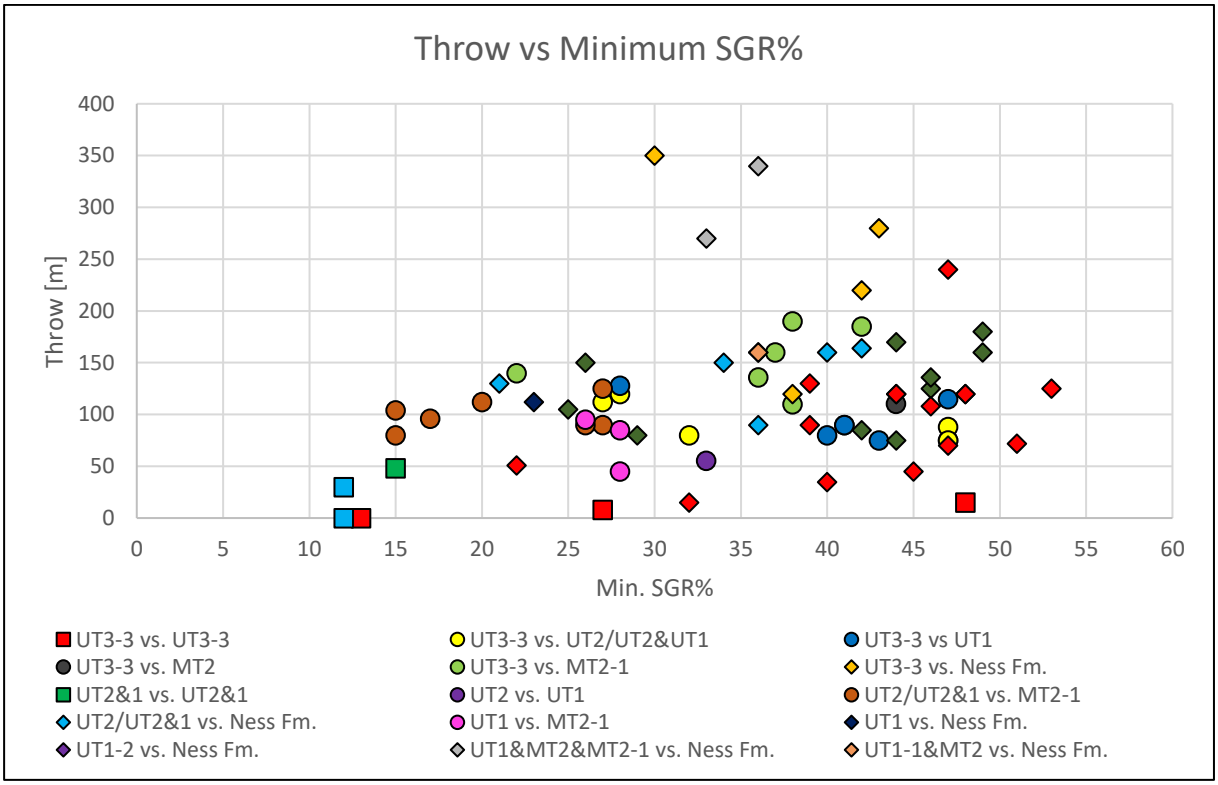

Figure 6.13: Throw vs. minimum SGR% plot highlighting the different juxtaposed areas.

The results suggest no correlation between throw and across fault pressure differences (Figure 6.14). As long as the fault is not critically stressed and slip, then it does not matter how much the reservoir is offset. This correlates with Wiprut and Zoback (2002), who suggests that fault reactivation and hydrocarbon leakage in the northern North Sea appear to be caused by three factors: (1) locally elevated pore pressure due to buoyant hydrocarbons abutting faults, (2) fault orientations that are nearly optimally oriented for frictional slip in the present-day stress filed, and (3) a recent perturbation of the compressional stress associated with postglacial rebound. The fault throws can however, give a good indication of which faults are more likely to leak due to elevated pore pressure and/or being critically stressed. These being faults with small offsets resulting in self-juxtaposing sands with low SGR values, and if a fault has a throw of ~80 to 125 m in the study area, then there is a chance that UT2 or UT1 are juxtaposed to MT2-1, resulting in SGR values below 30% with 4 out of 10 having values of 20 and below in this study.

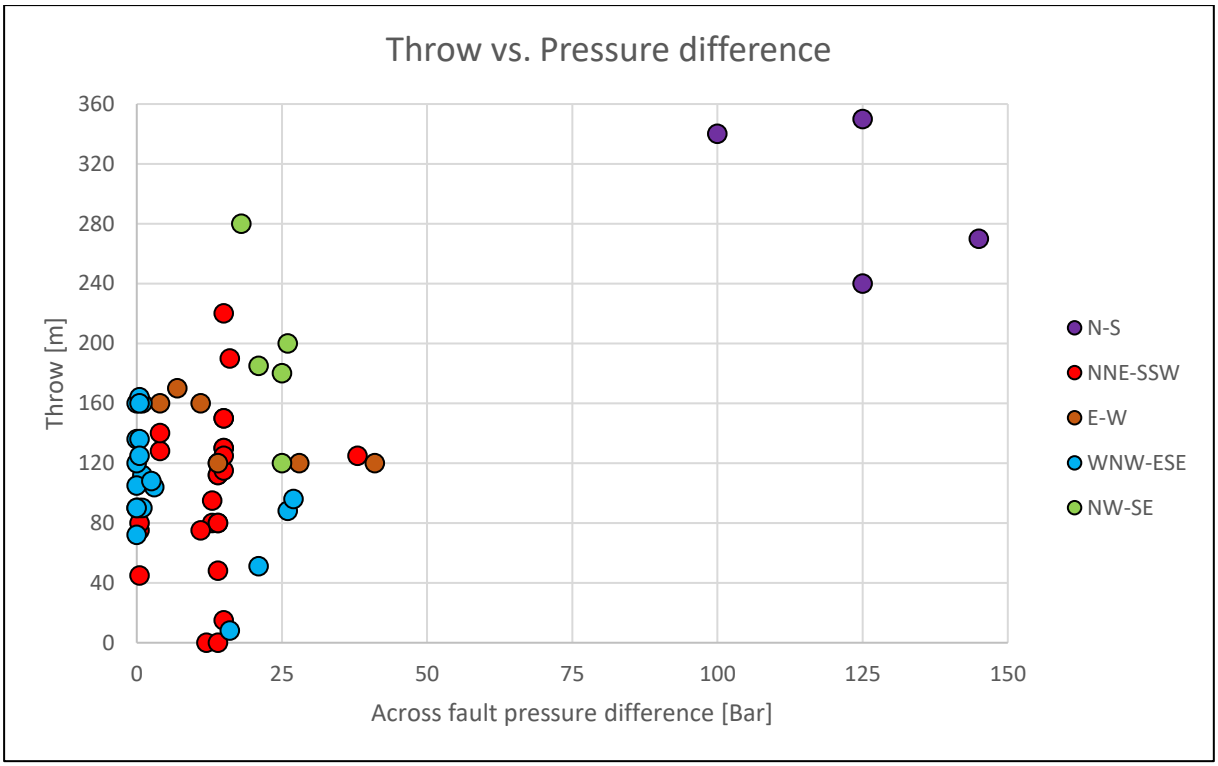

Figure 6.14: Throw vs. across fault pressure difference plot highlighting the fault strike orientations.

6.1.4 Minimum sealed column and fluid contact differences

In several investigated structures, the hydrocarbon columns appear to be controlled by factors other than the depth of the spill points – as the spill points do not coincide with the fluid contacts. One hydrocarbon column is interpreted to be controlled by a structural spill point, being the oil in UT3-3 Madam Felle. The fault plane between Madam Felle and Viti is interpreted to be sealing, resulting in the hydrocarbon column accumulating deeper than the fault spill points. The structural spill point for the Top Brent Group within Madam Felle is found at a depth of 3 291 m, the same depth as the oil-water contact. The minimum sealed column is measured from the top of the juxtapositions (spill point) down to the fluid contact and represents the overfilled column. 18 minimum sealed columns are gathered from the fault analyses. Sealed fluids are defined by one fluid being juxtaposed to a different fluid across the fault. By this definition, the juxtaposed area between UT2 and UT1 Askja East and UT3-3 Askja Southeast only has a sealed column of 14 m, being the difference in the fluid contacts. The total juxtaposed column is 110 m, with 94 m being oil on both sides of the fault. Figure 6.15 is based on the interpreted overfilled structures in fault-related traps and fluid contact difference vs. depth to top juxtapositions (spill points). Overfill due to shale smear is not correlating with depth, resulting in overfilling in the shallowest structures at 2 940 m depth and the deepest at 3 368 m. Sealing due to shale smear looks thus not to be affected by reservoir

depth. Two fluid contact differences were gathered from the Central area, six from the Askja area, and no fluid contact differences were gathered from the Krafla area. One of the contact differences observed is between a GWC at Askja and an ODT Askja East, resulting in this being a maximum value. Eight fluid contact differences, with one being a maximum and one being a minimum, may result in trends not being visible due to the limited data.

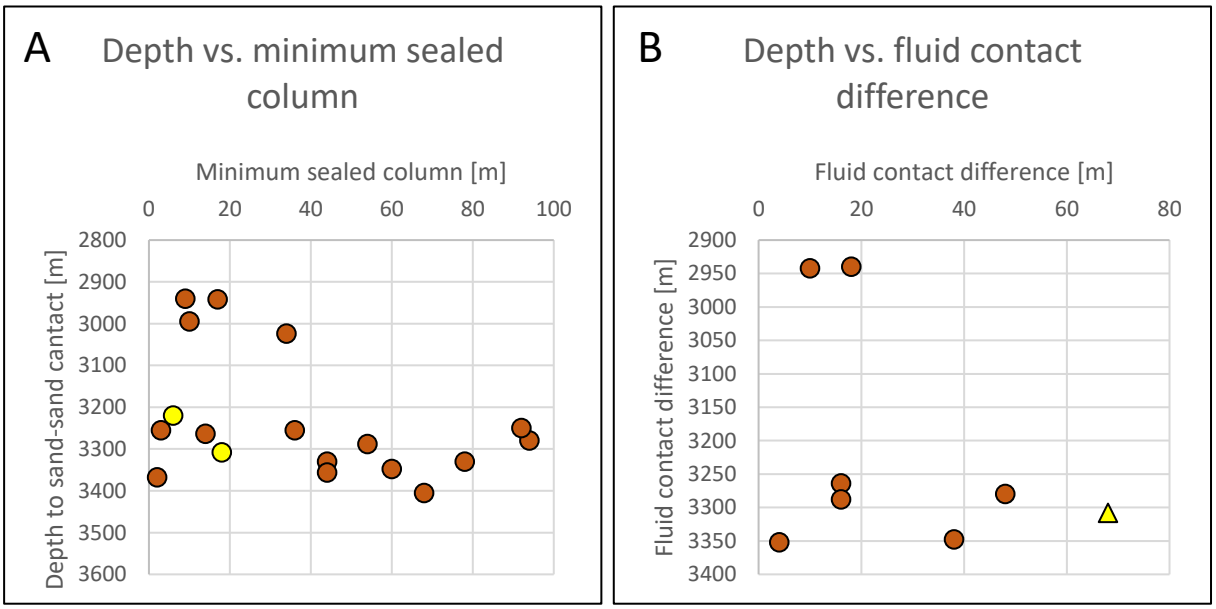

Figure 6.15: Depth to top sand-sand contact vs. minimum sealed column (A) and fluid contact difference (B). Yellow is self-juxtaposed Tarbert sands, and brown is seal by shale smear. Triangle represents GWC vs. ODT.

The minimum sealed columns are plotted against across fault pressure differences and SGR% in Figure 6.16. The data points with higher across fault pressure differences have all a minimum sealed column of over 50 m. However, there should not be a correlation between minimum sealed column and across fault pressure difference. The minimum sealed column represents the hydrocarbon column accumulating in a structure below the spill point and is dependent on throw, lithology, and fluid contact depth. The plots in Figure 6.16 indicates that an SGR value of 28% can hold a 94 m column with 14 bars pressure difference.

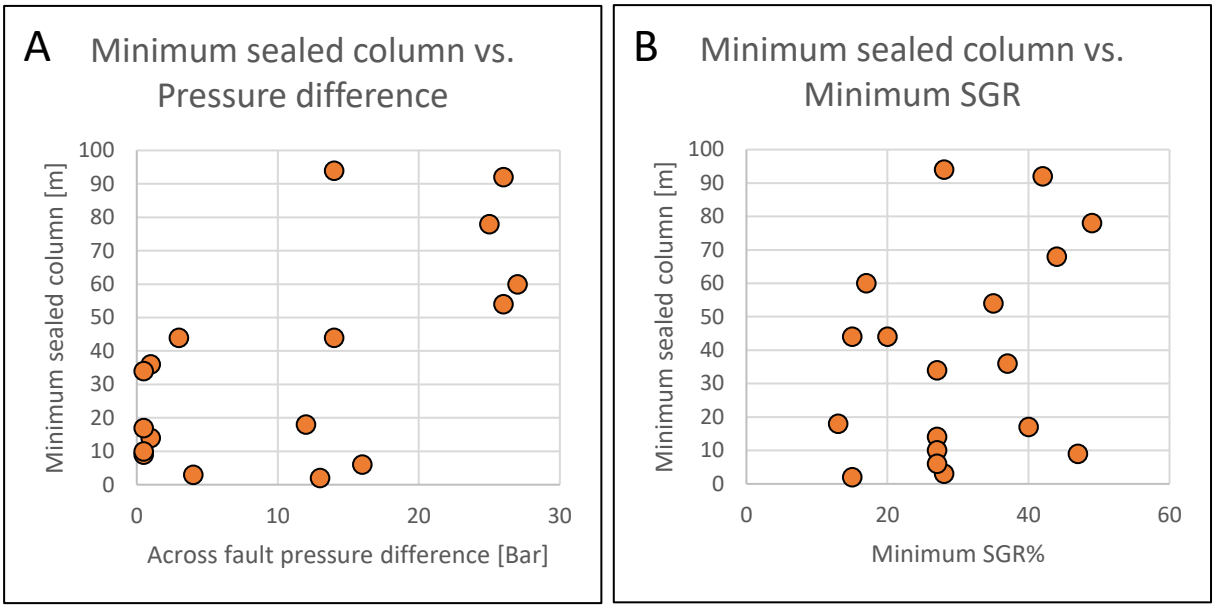

Figure 6.16: Figure showing the minimum seal columns vs. (A) across fault pressure differences and (B) minimum SGR%.

The fluid contact differences are plotted against across fault pressure differences and SGR% in Figure 6.17. None of the parameters were found to control the amount of fluid contact difference. In theory, a higher SGR should be able to hold a larger hydrocarbon column with higher pressures. This was not observed in the area as the data is limited.

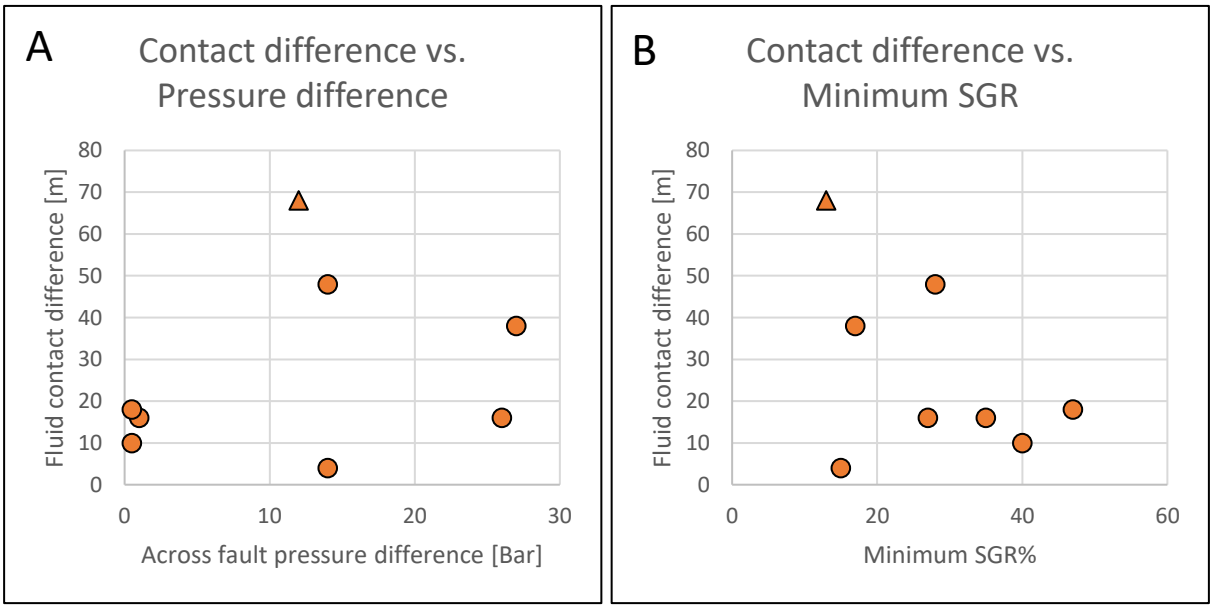

Figure 6.17: Fluid contact difference vs. (A) across fault pressure difference and (B) minimum SGR%. GWC UT3-3 Askja vs. ODT UT3-3 Askja East is represented by a triangle.

6.2 Spill routes, fluid contacts, and pressure regimes

The primary source rock in the northern North Sea is the organic-rich shales of the Upper Jurassic, Draupne Formation. Moretti and Deacon (1995) have calculated that the Draupne Formation enters the oil window at 3 100 m depth and the gas window at 4 000 m depth. Below this depth, generation of gas and cracking of oil into gas will initiate (Goff, 1983). The approximate oil and gas windows for the Draupne Formation are shown on top of the Base Cretaceous Unconformity (Figure 6.18A) and demonstrate the lateral coverage of the Krafla-Askja area. The Heather Formation is situated between the Draupne Formation and the Brent Group. The Heather Formation covers large parts of the Brent Group in the area. Top Tarbert will thus act as base Heather Formation in these areas. Figure 6.18B shows the approximate oil and gas window for the base Heather Formation. The source rock map in Figure 6.18 illustrates that the shallower traps in the Central area, Stjerne, and K, have been dependent on migration from the deeper parts of the area. The Krafla and Askja blocks are situated within the oil window. However, the trapped gas indicates migration from the deeper parts of the Viking Graben. The gas accumulating in the lower reservoir at Krafla West and asphaltenes within the Krafla North structure gas would likely have migrated through the western fault with charge from the basin. The structures, both in the deep and the shallow areas, are filled deeper than the spill points, indicating that migration towards these areas has been efficient. The Askja area is located within the Heather oil window and partially the Draupne oil window (Figure 6.18). The gas accumulating in Askja is likely to have migrated from the deeper Viking Graben to the west. The Central area is located shallower than the Draupne and Heather gas and oil windows. Compartmentalization, pressure differences, different fluids, and fluid-contact depths make the paleo migration history complicated.

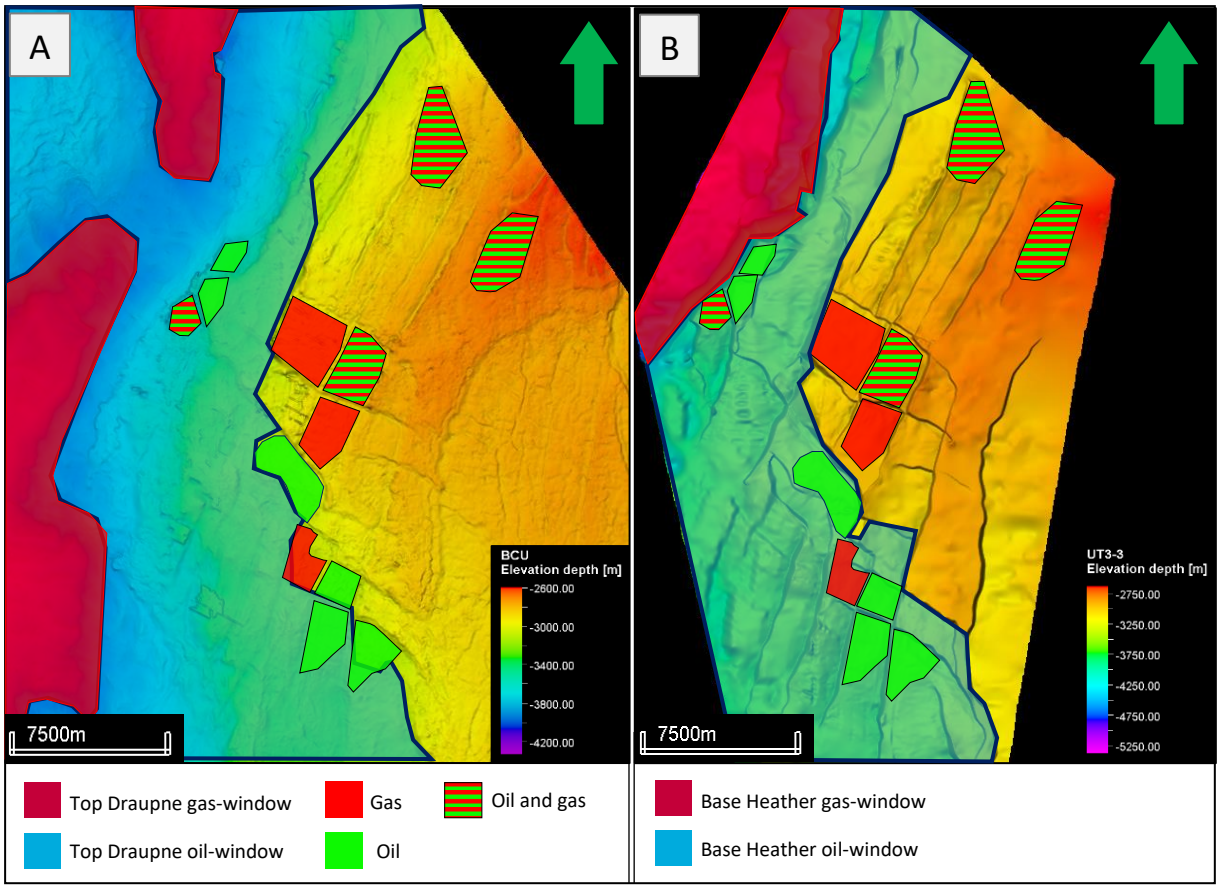

Figure 6.18: (A) Regional Base Cretaceous surface map with the approximate location of the Draupne oil and gas windows. The non-reservoir areas marked in red represents the area where the Draupne Formation is in the gas/condensate window, and the blue areas represent where the Draupne Formation is in the oil window. These intervals are based on calculations from Moretti and Deacon (1995), where the oil window range from 3 100 – 4 000 m, while the gas window is the areas deeper than 4 000 m. (B) Map of Top Brent Group with the oil and gas windows for the Heather Formation. The intervals are based on the same depth calculations as for the Draupne Formation.

None of the main study area structures were found to contain gas and oil within the same compartment. Hydrocarbon columns deeper than the structural spill points suggest hydrocarbon charge to the structures after sealing. When a trap is at its final stage in the fill-spill model, a GWC is situated at the spill point. The Askja structure is gas-filled likely charged from the Viking Graben. The structure is overfilled with gas causing the oil to spill up-dip from the shallowest spill point at the trap. That would either be towards the north or Askja East. This spill likely took place northwards due to the shallowest spill point for the structure is found to the north and the WNW-ESE striking fault between Askja and Steinbit being critically stressed in the present-day stress field.

Oil is proven in the Haraldsplass, Stjerne, and K structures, which are situated at a shallower depth than the Draupne and Heather oil windows. The Askja East and Askja Southeast structures are both generally in the same pressure regime, having the same amount of overpressure. These pressures are not shared by any of the other structures in the area. Both of the structures contain oil, with the juxtaposed oil having a 14 m difference in OWCs. It is likely that these two structures have worked as one structure in the past. This is not the case today, with the structures having different fluid contacts and pressures. Gas will accumulate on top of the oil columns due to buoyancy forces and result in a GOC. This is not seen in the area. This could be a cause of non-existing or insufficient gas charge to the oil structures. The NNE-SSW striking fault between Askja and Askja East could have worked as a barrier for migrating gas resulting in northeastern migration along the NNE-SSW striking faults parallel to the Viking Graben. This could be why gas is proven in the Central area, Stjerne and K, and not at Askja East, Askja Southeast, or Madam Felle.

Both the Stjerne and Madam Felle structures are interpreted to be filled to a structural spill point. The fault separating Madam Felle and Viti is interpreted to be sealed, and the hydrocarbon accumulates further down to a spill point to the east. The fault separating the Madam Felle structure from Viti and a fault southeast of the hydrocarbons has created a relay ramp that controls the structure's fluid contact. The hydrocarbons would likely travel up the relay ramp and accumulate elsewhere (the migration route from Madam Felle is not mapped in this study). Stjerne is interpreted to be a filled structure. The spilling hydrocarbons would likely spill into the K structure due to Stjerne spilling on the eastern side and K being situated shallower than Stjerne with a shallower fluid contact.

Parts of the northern Slemmestad fault could possibly be open. Slemmestad were found to have formation pressure decreases in the water phase in both the UT1 and MT2-1 compartments. The pressures in MT2-1 are normally pressured following the hydrostatic gradient. The water could thus be in communication with fluids outside the Slemmestad fault block. The throw of the fault is small, resulting in MT2-1 being self-juxtaposed. UT1 and MT2-1 are the cleanest sands at Slemmestad, and the SGR calculations done by Petrel have shown an SGR% value as low as 12% being the lowest value out of the analyzed faults. The gas' in Slemmestad does not reach the depth of the UT1 or MT2-1 juxtapositions. The possible opening at the fault plane does not control the fluid contacts at Slemmestad.

Figure 6.19 shows the deepest fluid contact in the Tarbert Formation for each of the structures. The general shallowing follows the bathymetry of the Tarbert Formation, with the fluid contacts generally shallowing to the north and the east apart from the Krafla Main horst and Steinbit. The Central area, Stjerne, and K are not situated within the Draupne and Heather gas or oil windows (Figure 6.18) and have thus been dependent on hydrocarbon migration. Formation pressure decreases, and asphaltenes in the Krasfla North structure suggest that migration has taken place in the area. The hydrocarbons are likely to have migrated northward and could possibly be trapped by the faults to the north.

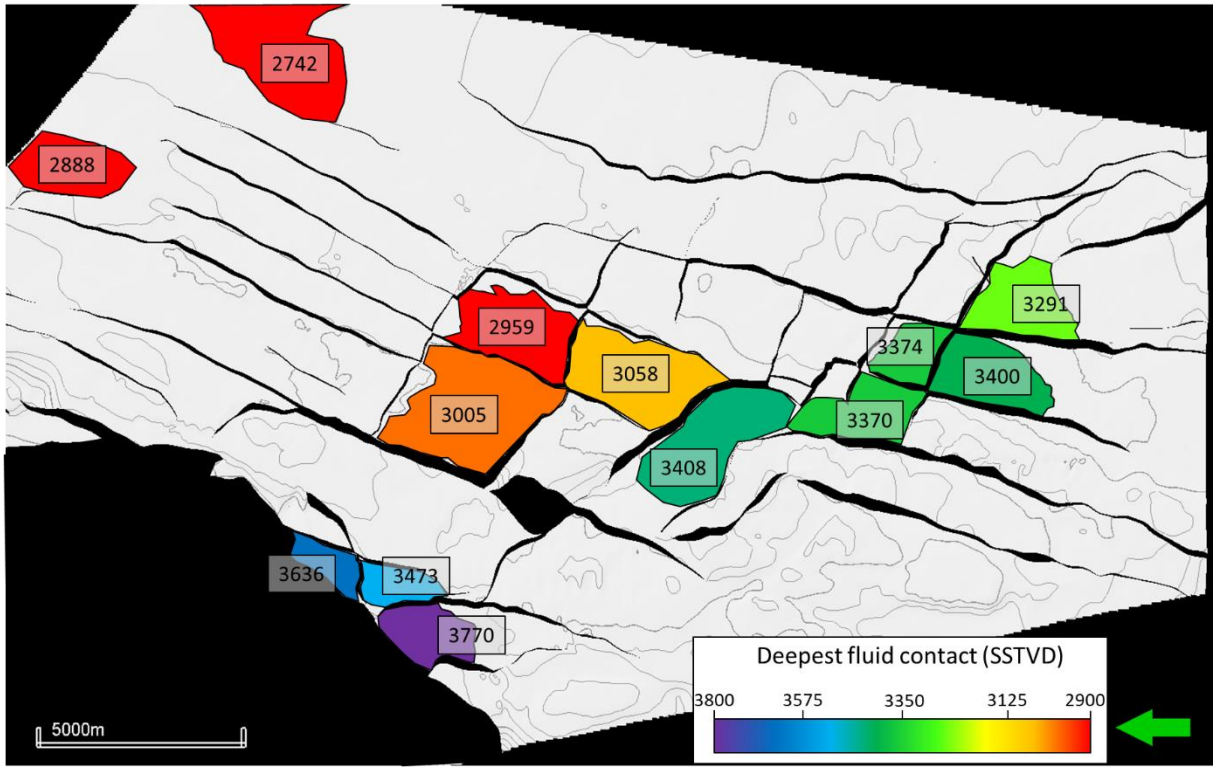

Figure 6.19: Map of the deepest fluid contact at each of the structures superimposed onto the Top Brent Group horizon.

Chapter 7 - Conclusion

This study aimed to investigate fault sealing in the Krafla-Askja area in the northern North Sea. Detailed mapping of the analyzed faults and the hydrocarbon-bearing structures have been conducted with fluid contacts, pressure data, and shale gouge ratio calculation being utilized to get an understanding of the fault sealing in the area. The main conclusions are as follows:

- The Krafla-Askja area is heavily faulted with the structures being compartmentalized, varying in lateral communication. The structures contain overpressured fluids, with structures containing multiple hydrocarbon-water contacts. Fill-spill routes in this area are suggested to be closed at the present day.
- Lateral variations of formation pressure in various structures are believed to result from lateral impermeable barriers caused by sealing faults.
- Spill point analysis of 13 faults has been mapped in the Krafla-Askja area where 76 sand-sand juxtapositions are believed to be sealing and one juxtaposed area between Slemmestad and the northern blocks possibly being open.
- The structural spill point at Madam Felle is interpreted to control the oil-water contact. Only the fluid contacts at the Madam Felle and Stjerne structures are believed to be controlled by a structural spill point.
- Laterally sealing faults, predominantly shale smear and juxtapositions seal controls the hydrocarbon-water contacts in the overfilled structures. Cementation is thought to play an important role in self-juxtaposed zones and where UT2/UT2&1 are juxtaposed to MT2-1.
- WNW-ESE and E-W oriented faults perpendicular to the Viking Graben are critically stressed in the present-day stress field and are thought to be reactivated more recently than the non-critically stressed faults resulting in a lower across fault pressure difference.
- Juxtaposed areas deeper than 3 500 m were observed to have an SGR value of 30% and higher. At this depth, the analyzed juxtapositions are between Tarbert sands and the Ness Formation and self-juxtaposed Ness sands.
- Fault throws above 150 m in the Krafla-Askja area were observed to have SGR values above 30%. Throws below 150 m were found to have SGR values ranging from 12% all the way to 53%.

- The overpressured gas' in Krafla West and the upper Askja reservoir, and the closer to hydrostatic gas' in the Central area and the lower Askja reservoir could result from a reduced supply of gas into the shallower area. This is suggested to be related to the closing of migration routes caused by cementation and sealing faults. Due to the Central area being situated shallower than the oil and gas windows for the Draupne and Heather Formations and the asphaltenes in MT2 Krafla North suggests that hydrocarbon migration has previously occurred in the area.

7.1 Proposal and further work

There are many uncertainties regarding the interpretation of the spill points and the method for calculating Shale Gouge Ratio. To reduce the uncertainties in a possible future study, the following is suggested:

- Utilization of 3D seismic data with improved quality would result in fewer uncertainties when mapping the different zones within the Tarbert Formation.
- Interpretation of the sands in the Ness Formation is suggested for more accurate data.
- The creation of a Vshale curve with radioactive and non-radioactive clay minerals is suggested to get the most accurate estimation of SGR values possible to map the weakest points along the faults.

References

Allan, U.S. (1989) Model for Hydrocarbon Migration and Entrapment Within Faulted Structures. *AAPG Bulletin*, 73(3), 803-811.

Bartholomew, I.D., Peters, J.M. & Powell, C.M. (1993) Regional structural evolution of the North Sea: oblique slip and the reactivation of basement lineaments. *Petroleum Geology Conference Series*, 4, 1109–1122.

Badley, M.E., Egeberg, T. & Nipen, O. (1984*)* Development of rift basins illustrated by the structural evolution of the Oseberg feature, Block 30/6, offshore Norway. *Journal of the Geological Society*, 141, 639-649.

Barnard, P. & Bastow, M. (1991), Hydrocarbon generation, migration, alteration, entrapment and mixing in the Central and Northern North Sea. *Geological Society of London, Special Publications*, 59, 167-190.

Bjørlykke, K., Nedkvitne, T., Ramm, M. & Saigal, G.C. (1992) Diagenetic processes in the Brent Group (Middle Jurassic) reservoirs of the North Sea: an overview. *Geological Society of London, Special Publications*, 61, 263-287.

Bjørlykke, K. (1999) An overview of factors controlling rates of compaction, fluid generation and flow in sedimentary basins. *Jamtveit, B., and Meakin, P., eds., Growth, Dissolution and Pattern Formation in Geosystems, Kluwer Academic Publishers, The Netherlands*, 381-404.

Bjørlykke, K. (2010) Petroleum Geoscience. Sedimentary Environments to Rock. Physics., chap. Introduction to petroleum geology. Springer Science.

Blatt, H. (1979) Diagenetic processes in sandstones. *The Society of Economic Paleontologist and Mineralogists*, 26, 141-157.

Bolås, H.M.N., & Hermanrud, C. (2003) Hydrocarbon leakage processes and trap retention capacities offshore Norway. *Petroleum Geoscience*, 9(4), 321–332.

Bolås, H.M.N., Hermanrud, C, & Teige, G.M.G. (2005) The Influence of Stress Regimes on Hydrocarbon Leakage. *AAPG Hedberg Series*, 2, 109–123.

Borge, H. (2000) Fault controlled pressure modelling in sedimentary basins. [Ph. D thesis], *Norwegian University of Science and Technology*, p. 156.

Bretan, P., Yielding, G. & Jones, H. (2003) Using calibrated shale gouge ratio to estimate hydrocarbon column heights. *AAPG Bulletin*, 87(3), 397-413.

Bretan, P. & Yielding, G. (2005) Using Buoyancy Pressure Profiles to Assess Uncertainty in Fault Seal Calibration. *AAPG Hedberg Series*, 2, 151-162.

Brudy, M., & Kjørholt, H. (2001) Stress orientation on the Norwegian continental shelf derived from borehole failures observed in high-resolution borehole imaging logs. *Tectonophysics*, 337(1), 65–84.

Buhrig, C. (1989) Geopressured Jurassic reservoirs in the Viking Graben: modelling and geological significance. *Marine and Petroleum Geology*, 6, 31-48.

Chapman, R. E. (1972) Primary migration of petroleum from clay source rocks. AAPG Bulletin, 56, 2185-2191.

Childs, C., Manzocchi, P.A.R., Nell, J.J., Walsh, J.A., Heath, A.E. & Lygren, T.H. (2002) Geological implications of a large pressure difference across a small fault in the Viking Graben. *Norwegian Petroleum Society Special Publications*, 11, 187-201.

Doré, A.G., Lundin, E.R., Jensen, L.N., Birkleand, Ø., Eliassen, P.E. & Fichler, C. (1999) Principal tectonic events in the evolution of the northwest European Atlantic margin. *Geological Society*, 5, 41-61.

Eldholm, O., Thiede, J., & Taylor, E. (1989) Evolution of the Vøring volcanic margin. *Proceedings ODP Scientific Results*, 104, 1033–1065.

Faleide, J. I., Bjørlykke, K., & Gabrielsen, R.H. (2010) Geology of the Norwegian continental shelf. *Petroleum Geoscience*, 467-499.

Fejerskov, M. & Lindholm, C. (2000) Crustal stress in and around Norway: an evaluation of stress-generating mechanisms. *Geological Society, London, Special Publications*, 167, 451-467.

Finkbeiner, T, Zoback, M.D., Flemings, R & Stump, B. (2001) Stress, pore pressure, and dynamically constrained hydrocarbon columns in the South Eugene Island 330 Field, northern Gulf of Mexico. *AAPG Bulletin*, 85(6), 1007-1031.

Fossen, H., Schultz, R.A., Rundhovde, E., Rotevatn, A. & Buckley, S.J. (2010) Fault linkage and graben stepovers in the Canyonlands (Utah) and the North Sea Viking Graben, with implications for hydrocarbon migration and accumulation. *AAPG Bulletin*, 94, 597-613.

Fristad, T., Groth, A., Yielding, G. & Freeman, B. (1997) Quantitative fault seal prediction: a case study from Oseberg Syd. *Norwegian Petroleum Society Special Publication*, 7, 107-124.

Færseth, R. (1996) Interaction of Permo-Triassic and Jurassic extensional fault-blocks during the development of the northern North Sea. *Journal of the Geological Society*, 153, 931-944.

Færseth, R. & Ravnås, R. (1998) Evolution of the Oseberg fault-block in context of the northern North Sea structural framework. *Marine and Petroleum Geology*, 15, 467-490

Færseth, R. B. (2006) Shale smear along large faults: continuity of smear and the fault seal capacity. *Journal of the Geological Society*, 163, 741-751.

Færseth, R.B., Johnsen, E. & Sperrevik, S. (2007) Methodology for risking fault seal capacity: Implications of fault zone architecture. *AAPG bulletin*, 91, 1231-1246.

Gartrell, A., Zhang, Y., Lisk, M. & Dewhurst, D. (2003) Enhanced hydrocarbon leakage at fault intersections: an example from the Timor Sea, Northwest Shelf, Australia. *Journal of Geochemical Exploration*, 78, 361–365.

Gibson, R.G. (1994) Fault-Zone Seals in Siliciclastic Strata of the Columbus Basin, Offshore Trinidad. *AAPG Bulletin*, 78(9), 1372-1385.

Giles, M., Stevenson, S., Martin, S., Cannon, S., Hamilton, P., Marshall, J. & Samways, G. (1992) The reservoir properties and diagenesis of the Brent Group: a regional perspective. *Geological Society of London, Special Publications*, 61, 289-327.

Goff, J. C. (1983) Hydrocarbon generation and migration from Jurassic source rocks in the E Shetland Basin and Viking Graben of the northern North Sea. *Journal of the Geological Society*, 140(3), 445–474.

Grollimund, B. & Zoback, M. D. (2003) Impact of glacially induced stress changes on fault-seal integrity offshore Norway. *AAPG bulletin*, 87(3), 493–506.

Gussow, W. C. (1954) Differential trapping of hydrocarbons, *AAPG*, 1, 4-5.

Helland-Hansen, W., Ashton, M., Lømo, L. & Steel, R. (1992) Advance and retreat of the Brent delta: recent contributions to the depositional model. *Geological Society of London, Special Publications*, 61, 109-127.

Holgate, N. E., Jackson, C. A.-L., Hampson, G. J. & Dreyer, T. (2013) Sedimentology and sequence stratigraphy of the Middle–Upper Jurassic Krossfjord and Fensfjord formations, Troll Field, northern North Sea, *Petroleum Geoscience*, 19, 237-258.

Johnsen, J. R., Rutledal, H. & Nilsen, D. E. (1995) Jurassic reservoirs; field examples from the Oseberg and Troll fields: Horda Platform area. *Norwegian Petroleum Society, Special Publications*, 4, 199-234.

Knipe, R. J. (1992) Faulting processes and fault seal. *Norwegian Petroleum Society Special Publications*, 1, 325-242.

Løseth, T. M., Ryseth, A.E. & Young, M. (2009) Sedimentology and sequence stratigraphy of the middle Jurassic Tarbert Formation, Oseberg South area (northern North Sea). *Basin Research*, 21, 597-619.

Lindsay, N., Murphy, F., Walsh, J. & Watterson, J. (1993) Outcrop studies of shale smears on fault surfaces. *International Association of Sedimentologists, Special Publication*, 15, 113-123.

Magee, T., Buchan, C. & Prosser, J. (2010) The Kujung Formation in Kurnia-1 : A Viable Fractured reservoir play in the south Madura block. *Proceedings, Indonesian Petroleum Association*.

Mearten, L., Gillespie, P. & Pollard, D.D. (2002) Effects of local stress perturbation on secondary fault development. *Journal of Structural Geology*, 24, 145-153.

Moretti, I. & Deacon, K. (1995) Subsidence, maturation and migration history of the Tampen Spur area. *Marine and Petroleum Geology*, 12, 345-375.

Nøttvedt, A., Gabrielsen, R.H. & Steel, R.J. (1995) Tectonostratigraphy and sedimentary architecture of rift basins, with reference to the northern North Sea. *Marine and Petroleum Geology*, 12(8), 881–901.

Neuzil, C.E. & Pollock, D.W. (1983) Erosional unloading and fluid pressures in haudraically "tight" rocks. *J. Geol*, 91(2), 179-193.

NPD (2021) The NPD fact pages and maps, Tech. rept. Norwegian Petroleum directorate. http://npd.no/.

Osborne, M.J. & Swarbrick, R.E. (1997) Mechanisms for generating overpressure in sedimentary basins: a reevaluation. *AAPG Bulletin*, 81, 1023-1041.

Ottesen, D., Batchelor, C.L., Dowdeswell, J.A. & Løseth, H. (2018) Morphology and pattern of Quaternary sedimentation in the North Sea Basin (52–62°N). *Marine and Petroleum Geology, 98, 836-859.*

Phillips, T.B., Fazlikhani, H., Gawthorpe, R.L., Fossen, H., Jakson, C.H.-L., Bell, R.E., Faleide, J.I. & Rotevatn, A. (2019) The Influence of Strucural Inheritance and Multiphase Extension on Rift Development, the Northern North Sea. *Tectonics*, 38, 4099-4126.

Schowalter, T.T. (1979) Mechanics of secondary hydrocarbon migration and entrapment. *AAPG bulletin*, 63, 723-760.

Skogseid, J. (1994) Dimensions of the late Cretaceous–Paleocene northeast Atlantic rift derived from Cenozoic subsidence. *Tectonophysics*, 240, 225–247.

Sollie, O.C.E. (2015) Controls on hydrocarbon column-heights in the north-eastern North Sea. [Master thesis]: *University of Bergen*, p. 118.

Steel, R. (1993) Triassic–Jurassic megasequence stratigraphy in the Northern North Sea: rift to post-rift evolution. *Geological Society of London, Petroleum Geology Conference series*, 4, 299-315.

Surlyk, F. & Ineson, J. (2003) The Jurassic of Denmark and Greenland: Key elements in the reconstruction of the North Atlantic Jurassic rift system. *Geological Survey of Denmark and Greenland Bulletin*, 1, 9-20.

Teige, Gunn M. G., Hermanrud, C., Kløvjan, O. S., Eliassen, P. E., Løseth, H. & Gading, M. (2002) Evaluation of caprock integrity in the western (high-pressured) Haltenbanken area: a case history based on analyses of seismic signatures in overburden rocks. *Norwegian Petroleum Society Special Publications*, 11, 233–242.

Walderhaug, O. (1990*)* A fluid inclusion study of quartz-cemented sandstones from offshore mid-Norway-possible evidence for continued quartz cementation during oil emplacement. *Journal of Sedimentary Research*, 60, 203-210.

Watts, N. (1987) Theoretical aspects of cap-rock and fault seals for single-and two-phase hydrocarbon columns. *Marine and Petroleum Geology*, 4, 274-307.

Whipp, P., Jackson, C., Gawthorpe, R., Dreyer, T. & Quinn, D. (2014) Normal fault array evolution above a reactivated rift fabric; a subsurface example from the northern Horda Platform. *Norwegian North Sea: Basin Research*, 26, 523-549.

Wiprut, D., & Zoback, M.D. (2000) Fault reactivation and fluid flow along a previously dormant normal fault in the northern North Sea. *Geology*, 28, 595-598.

Wiprut, D., & Zoback, M.D. (2002) Fault reactivation, leakage potential, and hydrocarbon column heights in the northern North Sea. *Norwegian Petroleum Society Special Publications*, 11, 203–219.

Yielding, G., Badley, M.E. & Roberts, A.M. (1992) The Structural Evolution of the Brent Province. *Geological Society Special Publications*, 61, 27-43.

Yielding, G., Freeman, B. & Needham, T. (1997) Quantitative fault seal prediction. *Am. Assoc. Pet. Geol. Bull,* 81, 897-917.

Yielding, G. (2002) Shale Gouge Ratio – calibration by geohistory. *Norwegian Petroleum Society Special Publication,* 11, 1-15.

Yielding, G., Bretan, P. & Freeman, B. (2010) Fault seal calibration: a brief review. *Geological Society Special Publications*, 347, 243-255.

Zhiqiang, F. (2013) Primary Migration of Hydrocarbons Through Microfracture Propagation in Petroleum Source Rocks. The *University of Maine*.

Ziegler, P. A. (1992) North-Sea Rift System. *Tectonophysics*, 208, 55-75.

Appendix

Data from fault analysis

Fault	Depth	Sand contacts	Min. SGR	Pressure diff.	Min. sealed column	Fluid contact diff.	Throw	Dip	Orientation
A-AE	3280	UT3-3 vs. UT2&1	28	14	94	48	120	WNW	NNE-SSW
A-AE	3308	UT3-3 vs. UT3-3	13	12	18	68	0	WNW	NNE-SSW
A-AE	3352	UT2&1 vs. UT2&1	15	14		4	48	WNW	NNE-SSW
A-AE	3368	UT2&1 vs. MT2-1	15	13	2		80	WNW	NNE-SSW
A-AE	3370	UT2 vs. UT3-3	32	14			80	WNW	NNE-SSW
A-AE	3468	MT2-1 vs. MT2-1	12	14			0	WNW	NNE-SSW
A-AE	3430	UT1 vs. Ness	23	14			112	WNW	NNE-SSW
A-AE	3464	MT2-1 vs. Ness	29	14			80	WNW	NNE-SSW
A-AE	3550	Ness vs. Ness	32	15			15	WNW	NNE-SSW
AE-Viti	3255	UT3-3 vs. UT1	28	4	3		128	WNW	NNE-SSW
AE-Viti	3260	UT3-3 vs. MT2-1	22	4			140	WNW	NNE-SSW
AE-Viti	3330	UT2 vs. MT2-1	20	14	44		112	WNW	NNE-SSW
AE-Viti	3340	UT2&1 vs. Ness	21	15			130	WNW	NNE-SSW
AE-Viti	3430	MT2-1 vs. Ness	26	15			150	WNW	NNE-SSW
AE-Viti	3473	Ness vs. Ness	39	15			130	WNW	NNE-SSW

AE-ASE	3264	UT2&1 vs. UT3-3	27	1	14	14	112	SSW	WNW-ESE
AE-ASE	3356	MT2-1 vs. UT2&1	15	3	44		104	SSW	WNW-ESE
AE-ASE	3480	Ness vs. UT2&1	21	0			90	SSW	WNW-ESE
AE-ASE	3460	Ness vs. MT2-1	25	0			105	SSW	WNW-ESE
AE-ASE	3508	Ness vs. Ness	22	21			51	SSW	WNW-ESE
MF-ASE	3370	UT1 vs. UT3-3	47	15			115	WNW	NNE-SSW
MF-ASE	3385	MT2-1 vs. UT3-3	38	16			190	WNW	NNE-SSW
MF-ASE	3520	Ness vs. UT3-3	42	15			220	WNW	NNE-SSW
MF-ASE	3450	Ness vs. UT2&1	36	15			150	WNW	NNE-SSW
MF-ASE	3530	Ness vs. MT2-1	46	15			125	WNW	NNE-SSW
MF-ASE	3580	Ness vs. Ness	53	38			125	WNW	NNE-SSW
MF-VITI	3255	UT3-3 vs. MT2-1	37	1	36		160	SSW	WNW-ESE
MF-VITI	3300	UT3-3 vs. Ness	38	0			120	SSW	WNW-ESE
MF-VITI	3343	UT2&1 vs. Ness	34	0			160	SSW	WNW-ESE
MF-VITI	3408	MT2-1 vs. Ness	46	0			136	SSW	WNW-ESE
MF-VITI	3463	Ness vs. Ness	51	0			72	SSW	WNW-ESE
HPL-SLM	2940	UT2 vs. UT3-3	47	0.5	9	18	75	WNW	NNE-SSW
HPL-SLM	2942	UT1 vs. UT3-3	40	0.5	17	10	80	WNW	NNE-SSW
HPL-SLM	2960	MT2-1 vs. UT3-3	38	1			110	WNW	NNE-SSW
HPL-SLM	2995	MT2-1 vs. UT2	27	0.5	10		90	WNW	NNE-SSW
HPL-SLM	3045	MT2-1 vs. UT1	26	13			95	WNW	NNE-SSW

HPL-SLM	3105	Ness vs. MT2-1	44	11			75	WNW	NNE-SSW
HPL-SLM	3170	Ness vs. Ness	45	0.5			45	WNW	NNE-SSW
HPL-BBG	2964	MT2-1 vs. UT3-3	36	0.5			136	SSW	WNW-ESE
HPL-BBG	2992	UT1 vs. UT3-3	41	1			90	SSW	WNW-ESE
HPL-BBG	3024	MT2-1 vs. UT2	27	0.5	34		125	SSW	WNW-ESE
HPL-BBG	3070	Ness vs. UT2&1	40	0.5			164	SSW	WNW-ESE
HPL-BBG	3120	Ness vs MT2-1	49	0.5			160	SSW	WNW-ESE
HPL-BBG	3220	Ness vs. Ness	46	2.5			108	SSW	WNW-ESE
A-ST	3220	UT3-3 vs. UT3-3	27	16	6		8	SSW	WNW-ESE
A-ST	3288	UT3-3 vs. UT2&1	35	26	54	16	88	SSW	WNW-ESE
A-ST	3348	UT2&1 vs. MT2-1	17	27	60	38	96	SSW	WNW-ESE
A-ST	3504	Ness vs. Ness	39	0			90	SSW	WNW-ESE
BBG-ST	3175	MT2-1 vs. UT3-3	42	21			185	SW	NW-SE
BBG-ST	3210	Ness vs. UT3-3	43	18			280	SW	NW-SE
BBG-ST	3250	Ness vs. UT2&1	42	26	92		200	SW	NW-SE
BBG-ST	3330	Ness vs. MT2-1	49	25	78		180	SW	NW-SE
BBG-ST	3380	Ness vs. Ness	48	25			120	SW	NW-SE
KM-KN	3405	MT2 vs. UT3-3	44		68		110	N	E-W
KM-KN	3555	UN vs. UT1-2	36	11			160	N	E-W
KM-KN	3560	UN vs. UT1-1&MT2	36	4			160	N	E-W
KM-KN	3608	UN vs. MT2-1	44	7			170	N	E-W

KM-KN	3700	MN vs. UN	48	14			120	N	E-W
KM-KN	3750	LN vs. UN	44	28			120	N	E-W
KM-KN	3800	LN vs. MN	44	41			120	N	E-W
KM-KW	3540	UN vs. UT3-3	30	125			350	W	N-S
KM-KW	3622	MN vs. UT1/MT2/MT2-1	33	145			270	W	N-S
KM-KW	3740	LN vs. UT1/MT2/MT2-1	36	100			340	W	N-S
KM-KW	3830	LN vs. UN	47	125			240	W	N-S
SLM-NZ	2985	UT3-3 vs. UT3-3	48				15	SSW	WNW-ESE
SLM-NZ	2990	UT3-3 vs. UT2	47				75	SSW	WNW-ESE
SLM-NZ	3020	UT3-3 vs. UT1	43				75	SSW	WNW-ESE
SLM-NZ	3055	UT2 vs. UT1	33				55	SSW	WNW-ESE
SLM-NZ	3100	UT1 vs.MT2-1	28				45	SSW	WNW-ESE
SLM-NZ	3135	MT2-1 vs. MT2-1	12				30	SSW	WNW-ESE
SLM-NZ	3230	Ness vs. Ness	40				35	SSW	WNW-ESE
HPL-NZ	2925	UT3-3 vs. UT2	47				70	SSW	WNW-ESE
HPL-NZ	2890	UT3-3 vs. UT1	41				90	SSW	WNW-ESE
HPL-NZ	2945	UT2 vs. MT2-1	26				90	SSW	WNW-ESE
HPL-NZ	2980	UT1 vs. MT2-1	28				85	SSW	WNW-ESE
HPL-NZ	3040	MT2-1 vs. Ness	42				85	SSW	WNW-ESE

HPL-NZ	3100	Ness vs. Ness	47				70	SSW	WNW-ESE